

Interwell Connectivity and Diagnosis Using Correlation of Production and Injection Rate Data in Hydrocarbon Production

FINAL REPORT

Reporting Period Start Date: June 2003

Reporting Period End Date: March 2007

Principal Authors

Dr. Jerry L. Jensen, TAMU
Dr. Larry W. Lake, UT-Austin
Ali Al-Yousef, UT-Austin
Dan Weber, UT-Austin
Ximing Liang, UT-Austin
Dr. T.F. Edgar, UT-Austin
Nazli Demiroren, TAMU
Danial Kaviani, TAMU

June, 2007

DOE Contract No. DE-FC26-03NT15397

Submitting Organization:

Texas Engineering Experiment Station
Texas A&M University, College Station, TX 77843-3116

Subcontractor: Larry W. Lake
Petroleum and Geosystems Engineering
University of Texas, Austin, TX 78712

DISCLAIMER

“This report was prepared as an account of work sponsored by an agency of the United States Government. Neither the United States Government nor any agency thereof, nor any of their employees, makes any warranty, express or implied, or assumes any legal liability or responsibility for the accuracy, completeness or usefulness of any information, apparatus, product, or process disclosed, or represents that its use would not infringe privately owned rights. Reference herein to any specific commercial product, process, or service by trade name, trademark manufacturer, or otherwise does not necessarily constitute or imply its endorsement, recommendation, or favoring by the United States Government or any agency thereof. The views and opinions of authors expressed herein do not necessarily state or reflect those of the United States Government or any agency thereof.”

ABSTRACT

This report details progress and results on inferring interwell communication from well rate fluctuations. Starting with the procedure of Albertoni and Lake (2003) as a foundation, the goal of the project was to develop further procedures to infer reservoir properties through weights derived from correlations between injection and production rates. A modified method, described in Yousef and others (2006a,b), and herein referred to as the “capacitance model”, is the primary product of this research project. The capacitance model (CM) produces two quantities, λ and τ , for each injector—producer well pair.

For the CM, we have focused on the following items:

1. Methods to estimate λ and τ from simulated and field well rates. The original method uses both non-linear and linear regression and lacks the ability to include constraints on λ and τ . The revised method uses only non-linear regression, permitting constraints to be included as well as accelerating the solution so that problems with large numbers of wells are more tractable.
2. Approaches to integrate λ and τ to improve connectivity evaluations. Interpretations have been developed using Lorenz-style and log-log plots to assess heterogeneity. Testing shows the interpretations can identify whether interwell connectivity is controlled by flow through fractures, high-permeability layers, or due to partial completion of wells. Applications to the South Wason and North Buck Draw Fields show promising results.
3. Optimization of waterflood injection rates using the CM and a power law relationship for watercut to maximize economic return. Tests using simulated data and a range of oil prices show the approach is working.
4. Investigation of methods to increase the robustness of λ and τ estimates. Human interventions, such as workovers, also cause rate fluctuations and can be misinterpreted by the model if bottom hole pressure data are not available. A revised method, called the “segmented capacitance model”, identifies times when production changes might not be caused strictly by water injection changes. Application to data from Monument Butte Field shows encouraging results.

Our results show the CM and its modified forms can be an important tool for waterflood management. We have moved beyond the proof of principle stage to show it can actually be applied to assess connectivity in field situations. Several shortcomings, however, remain to be addressed before the CM can be routinely applied by field operators.

The CM and its modifications analyze well rates in the time domain. We also explored the assessment of interwell connectivity in the spectral domain. We applied conventional methods, based on analyzing passive linear electrical networks, to the analysis of injection and production data. In particular, we assessed the effects of near-wellbore gas on the apparent connectivity. With only oil and water in the system, the results were as expected, giving good connectivity estimates. In the presence of gas, however, the methods could not produce useful estimates of connectivity.

TABLE OF CONTENTS

DISCLAIMER.....	ii
ABSTRACT.....	iii
TABLE OF CONTENTS.....	iv
EXPERIMENTAL.....	v
RESULTS AND DISCUSSION.....	6
PART 1. Capacitance model development and testing	6
PART 2. Reservoir diagnosis using capacitance model parameters	43
PART 3. Waterflood optimization using the capacitance model.....	71
PART 4. Improvements to capacitance model robustness.....	90
PART 5. Spectral analysis of injection and production data.....	121
CONCLUSIONS.....	135
REFERENCES.....	136

EXPERIMENTAL

No experimental procedures were involved in this project.

RESULTS AND DISCUSSION

PART 1. CAPACITANCE MODEL DEVELOPMENT AND TESTING

We present a procedure to quantify communication between vertical wells in a reservoir based on fluctuations in production and injection rates. The proposed procedure provides information about preferential transmissibility trends and the presence of flow barriers. In this section, Part 1, we describe the procedure and show some example applications. Two further applications of the procedure are described in Parts 2 and 3. In Part 4, we revisit the procedure, discussing improvements and further issues to be resolved

Previous work to measure interwell connectivity has used a steady-state (purely resistive) model of interwell communication. Data in that work often had to be filtered to account for compressibility effects and time lags. Even though it was often successful, the filtering required subjective judgment as to the goodness of the interpretation. This work uses a more complicated model that includes capacitance (compressibility) as well as resistive (transmissibility) effects.

The procedure was tested on rates obtained from a numerical flow simulator. It was then applied to a short time-scale data set from an Argentinean field and a large-scale data set from a North Sea field. The simulation results and field applications show that the connectivity between wells is described by model coefficients (weights) that are consistent with known geology, the distance between wells and their relative positions. The developed procedure provides parameters that explicitly indicate the attenuation and time lag between injector and producer pairs in a field without filtering. The new procedure provides a better insight into the well-to-well connectivities for both fields than the purely resistive model.

The new procedure has several additional advantages. It

1. can be applied to fields in which injection wells are shut-in frequently or for long periods of time,
2. allows for application to fields where the rates have a remnant of primary production, and
3. has the capability to incorporate bottom hole pressure data (if available) to enhance the investigation about well connectivity.

1.1 Introduction

Production and injection rates are the most abundant data available in any injection project. Valuable and useful information about interwell connectivity can be obtained from the analysis of these data. The information may be used to optimize subsequent oil recovery by changing injection patterns, assignment of priorities in operations, recompletion of wells, and in-fill drilling.

A variety of methods have been used to compare the rate performance of a producing well with that of the surrounding injectors. Heffer and others (1995) used Spearman rank correlations to relate injector-producer pairs and associated these relations with geomechanics. Refunjol (1996), who also used Spearman analysis to determine preferential flow trends in a reservoir, related injection wells with their adjacent producers and used time lags to find an extreme coefficient value. Sant'Anna Pizarro (1998) validated the Spearman rank technique with numerical simulation and pointed out its advantages and limitations. Panda and Chopra (1998) used artificial neural networks to determine the interaction between injector-producer pairs. Soeriawinata and Kelkar (1999), who also used Spearman rank analysis, suggested a statistical approach to relate injection wells and their adjacent producing wells. They applied superposition

to introduce concepts of constructive and destructive interference. See also the works of Araque-Martinez (1993) and Barros-Griffiths (1998).

Albertoni and Lake (2003), hereinafter termed AL, estimated interwell connectivity based on a linear model with coefficients estimated by multiple linear regression (MLR). The linear model coefficients, or weights, quantitatively indicate the communication between a producer and the injectors in a waterflood. Filters were adopted to account for the time lag between producer and injector.

In this work, as in AL, the reservoir is viewed as a system that converts an input signal (injection) into an output signal (production). However, we use a more complete model that includes capacitance (compressibility) as well as resistive (transmissibility) effects. For each injector-producer pair, two coefficients are determined; one parameter (the weight) quantifies the connectivity, and another (the time constant) quantifies the degree of fluid storage between the wells. This work shows that the new model captures the true attenuation and time lag between injector and producer pairs.

The new procedure resolves several limitations of the previous methods and extends the applications to a wide range of real cases. It can be applied to fields in which wells are shut-in frequently or for long periods of time, it allows for application to fields where the rates have a remnant of primary production, and it has the capability to use bottom hole pressure data (if available) to enhance the investigation about wells connectivity.

The developed technique is first applied to synthetic fields and then to producing fields in Argentina and the North Sea.

1.2 Procedure

Two different approaches are proposed to study interwell connectivity: the balanced capacitance model (BCM), and the unbalanced capacitance model (UCM). The appropriate approach will depend on the type of waterflood and the data to be analyzed. Both approaches are based on material balance, using the total (oil + water + gas) production rates (in reservoir volumes/time) and the injection rates (in reservoir volumes/time) for every well in a waterflood as input data. The well locations are not required. The simplicity of the method and the wide spread availability of production and injection data make this technique potentially a very practical tool.

First, the mathematical development of the capacitance model and the intrinsic (built-in) filters are explained; then both BCM and UCM approaches are addressed.

1.2.1 Mathematical development

The capacitance model is a total mass balance with compressibility. We first consider one injector-producer well pair in a drainage volume. The governed material balance differential equation at reservoir conditions is given by:

$$c_t V_p \frac{d\bar{p}}{dt} = i(t) - q(t) \dots\dots\dots (1)$$

where c_t is the total compressibility; V_p is the drainage pore volume, \bar{p} is the average pressure in V_p ; $i(t)$ is the injection rate and $q(t)$ is the total production rate. This equation states that at any time the net rate of mass depletion from the drainage volume is accounted for by a change in average pressure. The terms on the right of Eq. 1 can be interpreted to be the total rate of the injectors and producers.

Equation 1 is based on the assumptions that the total compressibility of a reservoir is small and constant and there is no fluid transfer out of or into the volume V_p . It can be derived from a spatial integration of the diffusivity equation under the same assumption. View in this manner, our procedure is a form of interference testing, but with rate rather than pressures (Sabet, 1991). With $i(t) = 0$ this equation is used by Walsh and Lake (2003) to describe primary depletion. The equation is also of the form used to describe the flow of electrical current in a resistor-capacitance network (e.g., Bruce, 1943); hence, the term *capacitance* in our description.

We desire a description that is based entirely on rates. To do this we use a linear productivity model as

$$q = J(\bar{p} - p_{wf}) \dots\dots\dots (2)$$

where p_{wf} and J are the flowing bottom hole pressure (BHP) and productivity index of the producer, respectively. Equation 2 holds only for stabilized flow, which is unlikely to be accurate in circumstances in which rates are constantly changing. Its appropriateness can only be established by numerical simulation and application. We note, however, that the productivity Eq. 2 (and its analogous alternative definitions) is almost universally applied in describing well performance in practice.

Eliminating the average pressure between Eqs. 1 and 2 gives

$$\tau \frac{dq}{dt} + q(t) = i(t) - \tau J \frac{dp_{wf}}{dt} \dots\dots\dots (3)$$

where τ is the "time constant" of the drainage volume, and is defined by:

$$\tau = \frac{c_t V_p}{J}$$

The solution to Eq. 3 is (Yousef, 2006):

$$q(t) = q(t_0)e^{\frac{-(t-t_0)}{\tau}} + \frac{e^{-t/\tau}}{\tau} \int_{\xi=t_0}^{\xi=t} e^{\xi/\tau} i(\xi) d\xi$$

$$+ J \left[p_{wf}(t_0)e^{\frac{-(t-t_0)}{\tau}} - p_{wf}(t) + \frac{e^{-t/\tau}}{\tau} \int_{\xi=t_0}^{\xi=t} e^{\xi/\tau} p_{wf}(\xi) d\xi \right] \dots\dots\dots (4)$$

where, t_0 is the initial time at which time $q = q(t_0)$ and ξ is a variable of integration.

Equation 4 is the basic capacitance model. It suggests that the output signal at producer $q(t)$ can be decomposed into three components. The first component, the first term on the right of Eq. 4, is the response of the initial (pre-injection) production rate, which accounts for primary production associated with the total production. The second component is the contribution from the injection input signal; it is the main subject of this work. The last component is the output signal caused by changing the BHP of the producer.

In the capacitance model (Eq. 4) all variables are known except for the time constant of the drainage volume, τ . The contribution or the shape of each component is solely determined by τ .

1.2.1.1 Discrete model

Fitting the capacitance model to injection and production data require discretizing the integrals in Eq. 4. n is a time-like variable, and Δn is the selected discretization interval. The

form of the discrete version of the capacitance model for one injector and one producer at constant BHP is given by:

$$q(n) = q(n_0)e^{-(n-n_0)/\tau} + \sum_{m=n_0}^{m=n} \alpha_m i(m) \dots\dots\dots (5)$$

where,

$$\alpha_m = \frac{\Delta n}{\tau} e^{-\frac{(m-n)}{\tau}}$$

are the built-in filter coefficients, which determine the form of the output signal caused by the injection. For fixed Δn , the α 's are primarily described by the time constant, τ . Therefore, the time constant τ accounts for attenuation and time lag between injector and producer pair. Since the second term on the right of Eq. 5 is of the form of the original MLR approach, the coefficients have an identical effect as the filtering procedure in AL.

The time constant τ is a direct measure of the dissipation of pressure between an injector and producer pair, identical to the relationship of voltage or current to the resistance-capacitance product which governs the propagation (delay and attenuation) of electromagnetic waves in a transmission line (Muskat, 1949, p. 568-574). For example, a large τ (a large total compressibility, a large pore volume, and/or a small productivity J or permeability) indicates large dissipation. If there were no dissipation between a well pair, τ would be small and a change in the injection rate would cause an equivalent and simultaneous change in the production rate, regardless of the distance between the pair. In fact, the unfiltered AL model assumes such instantaneous transmission. Our models revert to the AL model in the limit of zero compressibility.

Equation 5 states that the total production rate at step n is function of the primary production component, and the injection history between n and n_0 . The contribution of each step in the injection history is controlled by the time constant, τ . The parameter τ basically transforms, through the built-in filter coefficients, the injection input signal to take the form of the output signal at the producer in an incompressible medium. Therefore, the integration form, the second term in Eq. 4, or its discrete version, the second term in Eq. 5, represents a convolved form of the input injection signal, a phenomenon which is common to electrical and heat-flow systems (Bruce, 1943). The convolved injection is referred to as a filtered injection rate.

Figure 1 illustrates the effect of τ on defining the shape of the output signal caused by a step injection rate change. For three different values of τ , the convolved injection rates are depicted. For $\tau < 1.0$ time unit, the producer signal nearly coincides with the step injection, indicating that the injection change causes a nearly instantaneous and equal change at the producer. Because the attenuation and the time lag between the injector and the producer are negligible, the filter coefficient at step n , α_n , is the largest and equal to one while the remaining coefficients are zero. For moderate attenuation and time lag, the injection step will reach the producer in the form of the signal depicted for $\tau = 10$ time units (Fig. 1). In this case, the injection at every step n will not have its entire effect instantaneously acting on the producer. Injection from previous steps contributes to production at step n . The filter coefficient at step n , α_n , is less than one. The injection output signal at larger τ ($\tau = 50$ time units), results in larger attenuation and more time lag, as depicted in Fig. 1. The larger the τ the more attenuated and delayed is the production peak. This discussion leads to the conclusion that the filtering in the AL paper is equivalent to using time constants in the capacitance model. The time constants here, however, as the result of data fitting.

1.2.1.2 Extension to multiple producers and injectors

In a real waterflood, there are multiple producers and injectors acting simultaneously. The total production rate at one producer is usually supported by more than one injector. Thus, the capacitance model, derived above for one injector-producer pair, must be generalized to describe a system consisting of one producer and multiple injectors.

One way is to apply Eq. 1 for every injector-producer pair assuming the corresponding injector is the only injector acting in the medium and the rate at the producer corresponds only to that injector. We define coefficients or weights λ_{ij} to incorporate the fact that one injector is shared by more than one producer. Then, by making use superposition in space, the governed material balance equation for producer j and I injectors is (Yousef, 2006):

$$\sum_{i=1}^I c_{tij} V_{p_{ij}} \frac{d\bar{p}_{ij}}{dt} = \sum_{i=1}^I \lambda_{ij} i_i(t) - \sum_{i=1}^I q_{ij} \dots\dots\dots (6)$$

where c_{tij} , $V_{p_{ij}}$, and \bar{p}_{ij} are now all pertain to the volume drained by producer j when injector i is only active in the medium. q_{ij} is the production rate at producer j that corresponds only to injector i . The last term in Eq. 6 is the total production rate at producer j when all injectors are active. When $c_{tij} = 0$, hence, the weights (λ_{ij}) in Eq. 6 are analogous to the MLR weights in AL. Eliminating the average pressure (\bar{p}_{ij}) using an indexed version of Eq. 2, gives:

$$\sum_i \tau_{ij} \frac{dq_{ij}}{dt} + \sum_i q_{ij}(t) = \sum_{i=1}^I \lambda_{ij} i_i(t) - \frac{dp_{wf_j}}{dt} \sum_{i=1}^I \tau_{ij} J_{ij} \dots\dots\dots (7)$$

where,

$$\tau_{ij} = (c_{tij} V_{p_{ij}})/J_{ij}$$

Equation 7 provides one time constant (τ_{ij}) as well as one weight (λ_{ij}) for each (ij) injector-producer pair. Having different time constants will capture the possible different degrees of attenuation between well pairs. In addition, Eq. 7 allows for changes in the BHP of producer j .

The generalized capacitance model for producer j and I injectors in a discrete form is given by (Yousef, 2006):

$$q_j(n) = \lambda_p q(n_0) e^{-\frac{(n-n_0)}{\tau_p}} + \sum_{i=1}^I \lambda_{ij} i'_{ij}(n) + v_j \left[\begin{array}{c} p_{wf_j}(n_0) e^{-\frac{(n-n_0)}{\tau_j}} \\ - p_{wf_j}(n) + p'_{wf_j}(n) \end{array} \right] \dots\dots\dots (8)$$

where,

$$i'_{ij}(n) = \sum_{m=n_0}^{m=n} \frac{\Delta n}{\tau_{ij}} e^{-\frac{(m-n)}{\tau_{ij}}} i_{ij}(m)$$

$$p'_{wf_j}(n) = \sum_{m=n_0}^{m=n} \frac{\Delta n}{\tau_j} e^{-\frac{(m-n)}{\tau_j}} p_{wf_j}(m)$$

λ_p and τ_p are the weighting factor and time constant for the primary production contribution to the rate of producer j . λ_{ij} is the weight between injector i and producer j that indicates the

connectivity between the (ij) well pair; τ_{ij} is the time constant for the medium between injector i and producer j; $i_{ij}(n)$ is the convolved or filtered injection rate at step n and $p_{wfj}(n)$ is the convolved BHP at step n for producer j; v_j is a coefficient that determines the effect of changing the BHP of producer j. The entire last term disappears if the producer BHP is constant.

Competition for fluid among producers can also influence a production rate; this is referred to as producer-producer interactions. An intuitive way is to extend Eq. 8 to account for producer-producer interactions by incorporating the BHP's of other producers in the BHP term, or:

$$q_j(n) = \lambda_p q(n_0) e^{\frac{-(n-n_0)}{\tau_p}} + \sum_{i=1}^{i=I} \lambda_{ij} i'_{ij}(n) + \sum_{k=1}^{k=K} v_{kj} \left[\begin{array}{c} p_{wf_{kj}}(n_0) e^{\frac{-(n-n_0)}{\tau_{kj}}} \\ - p_{wf_{kj}}(n) + p'_{wf_{kj}}(n) \end{array} \right] \dots \dots \dots (9)$$

where v_{kj} is a coefficient that determines the effect of changing the BHP of producer k on the production rate of producer j; $p_{wf_{kj}}(n)$ is the convolved BHP at step n for producer k. The time constants in the BHP term (and the definitions for convolved BHP) have been changed from τ_j to τ_{kj} to account for additional interactions. The entire last term disappears if all K of the producer BHP's are constant.

Equation 9 is heuristic, though it can be partially justified by the superposition of pressures. The form is consistent with the use of linear regression as was done in AL and the entire equation reverts to the MLR in the unfiltered AL paper for incompressible flow with no producer-producer interactions. Thus, Eq. 9 is the capacitance model that incorporates the effects of primary production, multiple injectors, and BHP change for multiple producers. For each injector and producer pair, there are two parameters to be determined: the weight (λ), and the time constant (τ). λ describes the extent of connectivity and τ describes the dissipation between injector i and producer j.

1.2.1.3 Parameter Estimation

The weights λ_{ij} and other coefficients (λ_p , and v_{kj}) can be determined by minimizing the squared errors between measured production rates and those generated by Eq. 9. To insure balance, we enforce the average measured rate to be equal to the average predicted by Eq. 9 through Lagrange multipliers. See Yousef¹² for more details. For each producer, this minimization will generate a set of I+K+2 linear equations that can be solved for λ_p , λ_{ij} , and v_{kj} . The weights λ_{ij} and the time constant parameters τ_{ij} are the one targeted in this work. We will refer to this procedure as the balanced capacitance model (BCM).

To determine the optimum solution of λ_{ij} and τ_{ij} , an optimization procedure is required. In the optimization, τ 's are set to be the free parameters and the objective function is to minimize the squared errors between measured production rates and those generated by Eq. 9. For a given set of τ 's, MLR is used to determine λ 's, because Eq. 9 becomes linear in λ 's when the τ 's are known. After iterating in τ 's, the optimum set of λ 's is obtained. Therefore, the optimum λ_{ij} and τ_{ij} are obtained at the end of this procedure. This procedure, relying as it does on linear regression, allows up to use the error estimates of the weights based on MLR.

The weights λ_{ij} obtained from the optimization provide a quantitative expression of the connectivity between each (ij) pair; the larger the λ_{ij} , the greater the connectivity. The time

constants τ_{ij} are direct measures of the dissipation between each pair; the larger the τ_{ij} , the larger the dissipation.

1.2.2 Unbalanced Capacitance Model (UCM)

A waterflood is unbalanced when the field-wide injection rate is significantly different from field-wide total production rate. If this is the case, a constant rate q_{0j} should be added to the capacitance model (Eq. 9). The minimization proceeds as before with this additional parameter for each production well.

UCM should be used when the field is unbalanced, or if only a portion of the waterflood field is being analyzed, where there will be flow across the open boundaries of the selected portion. Therefore, UCM should be again used without any modification in the injection rates of the wells close to the boundaries.

1.3 Validation of the Model

Validation of the capacitance model comes from showing that the estimated time constant (τ) reflects the characteristics of the medium between injector and producer. In other words, is the estimated τ equivalent to $c_t V_p / J$. Once validated, the further issue will be how much better this model estimates interwell connectivity than the AL method.

For a waterflood consisting of one injector and one producer, the pore volume (V_p) component in the estimated τ should be equal to the static pore volume of the field. If we could demonstrate this, we conclude that τ captures its theoretical definition.

The capacitance model was applied to numerically simulated data (Eclipse) on a homogenous synthetic field consisting of one injector and one producer (1x1 Synfield). Then, different 1x1 Synfield cases were run by changing the total compressibility (c_t).

The Synfield dimension and the grid size are $31 \times 31 \times 5$, and $40 \times 40 \times 6$ ft, respectively. The oil and water compressibility are equal so that the total compressibility is independent of saturation, the rock compressibility is set to be zero, and the oil-water mobility ratio is equal to one. The injection rate is a step change where the injection rate drops from 830 to a zero rate at 35 months. The producer BHP is constant. The simulation extends for 100 months for a history of 100 data points of rate.

For each case, the parameter τ is estimated using BCM and the productivity index (J) is estimated from its basic definition Eq. 2.

From all cases, a plot of the estimated τ vs. the total compressibility gives a straight line, which is in agreement with the basic definition of τ (Fig. 2). However, there is a small shift in τ of about 0.37 time units. This shift is attributed to errors in the numerical approximation of the analytical solution of the capacitance model. For large τ , the correction becomes insignificant and the estimated pore volume is close to the static pore volume of the field (Yousef, 2006).

From the basic definition of τ and the values of c_t and J , the pore volume component (V_p) is calculated using the corrected τ . Figure 3 shows the trend of V_p normalized by the static pore volume of the field (V_{pf}) with the corrected τ . For $\tau > 1$ time unit, the estimated pore volume is equal to the static pore volume. This indicates that a τ in this range reflects the characteristics of the medium between the well pair. While, for $\tau < 1$ time unit, the pore volume is less than the static pore volume. In this range, the attenuation and time lag between the injector and the producer are negligible and the injection signal will propagate instantaneously to the producer so that there is not enough time delay for the injection signal to capture or feel the field pore volume. Since the injection and production data are sampled every 1 time unit, the minimum

time lag is 1 time unit. This observation indicates that τ must be greater than the sampling rate to meaningfully determine properties.

We repeated the 1x1 Synfield analysis for different permeabilities; all other parameters being the same as before. Following the same procedure and incorporating the correction in the estimated τ , we found τ is inversely proportional to J (Fig. 4), as expected. From these and further tests, described in Yousef (2006), we concluded that the model and evaluation procedure were functioning as required.

1.4 Results

The technique was tested through its application to two other synthetic fields and then to two real fields in Argentina and the North Sea. The results of these applications are presented and discussed in this section.

1.4.1 Application to synthetic fields

The two versions of the capacitance model, BCM and UCM, were applied to two numerically simulated synthetic fields (Synfields) with a five-spot injection pattern: one of 5 injectors and 4 producers (the 5x4 Synfield) and a second of 25 injectors and 16 producers (the 25x16 Synfield). They both are flowing undersaturated oil. The injector-producer distance is 800 ft for the 5x4 Synfield and 890 ft for the 25x16 Synfield. The oil, water, and rock compressibility are 5×10^{-6} , 1×10^{-6} , and 1×10^{-6} psi^{-1} , respectively. The oil-water mobility is equal to one. Both synfields have only vertical wells. Unless stated otherwise, all producers BHP's are equal. The characteristics of the synfields are similar to those of the real case to which the techniques will be applied later.

1.4.1.1 5x4 Synfield

Several cases were analyzed for this field. The emphasis will be on new aspects that the BCM has over the purely resistive model, MLR. We used the same injection data as did AL. These data were randomly selected from different wells in a real field and proportionally modified to be in agreement with the Synfield injectivity. The numerical simulation extends to $n = 100$ months, with $\Delta n = 1$ month. See Albertoni (2002) for these data.

1.4.1.1.1 Homogeneous reservoir. The first and simplest case is of a single-layered homogenous reservoir with an isotropic permeability of 40 md. Because the total production rate is equal to the total injection rate, the BCM approach is applied (Tables 1 and 2). In Fig. 5, the λ_{ij} are represented by arrows or cones that start from injector i and point to producer j . The larger the arrow, the larger the value of the weight and the greater connectivity between the two wells. Similarly, Fig. 6 shows the same representation for τ_{ij} which the larger the arrow, the larger the value of the time constant and the dissipation between the two wells.

Figures 5 and 6 reveal different characteristics of the medium between each injector and producer pair. The λ 's are larger for near well pairs (e.g. λ_{11} , λ_{12}) than for more distant well pairs (e.g. λ_{14} , λ_{15}) corresponding to greater connectivity between closer well pairs. Unlike λ 's, the τ 's are larger for distant well pairs (e.g. τ_{14} , τ_{15}) than for near well pairs (e.g. τ_{11} , τ_{12}) indicating a larger swept volume for the former. This also indicates that λ 's and τ 's manifest distinct characteristic of the medium.

Another important characteristic is the symmetry in λ 's and τ 's. AL pointed out the symmetry in λ 's and concluded that λ 's do not depend on injection rates. We further examined

this observation using the BCM and confirmed that the λ 's do not depend on injection rates; they only depend on the reservoir properties and the relative location of the wells (Yousef, 2006). Since both the τ 's and the λ 's are symmetric, this suggests that τ and the corresponding λ are not totally independent. A physical interpretation of λ 's will be addressed later.

Figure 7 shows a comparison between the predicted total production rate using BCM and the total production rate observed in the numerical simulation. Applying the AL purely resistive model (BMLR), the coefficient of determination (Jensen and others, 2003, p. 199) is $R^2 = 0.969$; the BCM improves the correlation to $R^2 = 1.000$ as shown in the figure. For the same case, AL reported $R^2 = 0.993$ using the BMLR with diffusivity filters. This indicates that the BCM captures the attenuation and time lag in the field as well as or better than the diffusivity filters.

All matches of production rates in the Synfields cases yielded $R^2 > 0.99$. As a consequence, we do not show additional plots like Fig. 7. See Yousef (2006) for others.

We applied the UCM to the same injection and production data with the aim that the model itself tells us the balance in the data without imposing the balance through using the BCM approach. UCM produced zero constant terms ($q_{oj} = 0$ for all j) and the same set of λ 's and τ 's that were obtained by BCM.

To give an insight about the nature of λ 's and τ 's estimated in this application, we repeated the homogenous 5x4 case (base case) so that only one injector and four producers are active at a time. We ran this case five times, once for each injector i.e., five 1x4 models. Then we estimated separately the λ 's and the corresponding τ 's. Figure 8 shows a cross plot of the λ 's estimated from these individual cases against the λ 's from the base case where all injectors are active. Figure 9 shows the same plot for the τ 's.

The λ 's from both sets are the same (Fig. 8). This is clear evidence that the weights λ 's do not by themselves account for the interaction between injectors. The set of λ 's between one injector and producers is the same as the one estimated when all injectors are active. Also, there are three groups of λ 's corresponding to different interwell distances and well placement: 1) short distance for corner injectors ($\lambda \approx 0.33$); 2) short distance for center injectors ($\lambda \approx 0.25$); and 3) long distance for corner injectors ($\lambda \approx 0.17$).

For τ 's, the small deviation between the τ 's from individual cases and the τ 's from the base case suggests that the τ 's also do not account for interaction between injectors¹². From all of the above, we conclude that neither the λ 's nor the τ 's account for the interaction between injectors. This is in agreement with the derivation of the capacitance model (Eq. 9) which is generalized from one injector-producer pair using superposition.

A similar conclusion holds when comparing the results to tracer tests analysis (Yousef, 2006).

1.4.1.1.2 Extended injector shut-in periods. The AL model gives unsatisfactory results for fields in which injectors have extended shut-in periods. If we shorten the time period involved in the analysis to only cover times when a particular injector is functioning, we lose information about the production during the shut-in times as well. The capacitance model has the ability to include shut-in periods.

We modified the injection rates used in the base case to impose a long shut-in period (Fig. 10); only injector I04 is active. The shut-in period started at 10 months and ended at 90 months. The total effective injection period is only 20 months. The BCM was applied and both sets of parameters showed an excellent match with the base case results (Figs. 11 and 12).

For the purpose of comparison, the AL model (BMLR) was also applied. The resulted λ 's are scattered compared to the base case (Fig. 13). The most affected group of weights is the one for the center injector (I03) and for injector I02. Since 80% of the injection rates are zero, the deviation from the base case results is attributed to large correlation between the rates of injectors. However, the capacitance model suppressed this effect.

1.4.1.1.3 Changing producer BHP. In this case, the bottom hole pressure of producer P01 decreases from 500 to 100 psi at 27 months and then returns to 500 psi at 60 months. The injection rates are decreased from the base case injection by 50% in I01 and I02, and by 30% in I03, I04, and I05. First, we applied the BCM approach without using the BHP data of producer P01, omitting the last term in Eq. 9. Figure 14 shows the estimated λ 's versus the base case values. The λ 's are very scattered, especially for the λ 's associated with producer P01, and there are several negative λ 's and large λ 's. Overall, the λ 's are different from the base case values and do not associate with the distance and well location. Also, the R^2 values of prediction the production rates for each producer are small especially for producer P01 ($R^2 \approx 0.532, 0.837, 0.701, 0.815$ for P01, P02, P03, and P04, respectively).

With the BHP data of producer P01, the BCM estimated λ 's and τ 's that are the same as the results of the base case (Figs. 15 and 16). Table 3 shows the numerical values of the weighting coefficients λ_{ij} , λ_p , and v_{kj} in which v_{kj} represents the effect of changing the BHP of producer P01 on the production rate of each producer. Incorporating the BHP data improves the R^2 of producer P01 from 0.532 to 0.999.

1.4.1.1.4 Large reservoir compressibility. In this case, the oil compressibility is 5×10^{-5} psi⁻¹, which is 10 times greater than that of the base case. All other parameters are similar to the base case. The attenuation and time lag are large as depicted by large τ 's (Fig. 17) but the estimated λ 's are the same as the base case (Fig. 18). With the AL model (BMLR), the predicted total production rate yields $R^2 = 0.666$; while applying the BCM approach gives $R^2 = 0.997$ (Fig. 19).

1.4.1.1.5 Other cases. We further studied the application of the BCM to the 5x4 Synfield introducing more complications to the reservoir properties: anisotropic reservoir, presence of sealing fault, presence of partially sealing fault, and multi-layered reservoirs. The estimated λ 's and τ 's are consistent with the existence of preferential flow trends and the presence of transmissibility barriers. However, when dissipation of the reservoir was significantly increased in the homogenous-isotropic synfield, the technique produced weights that are inconsistent with the base case results. This is expected because the perturbations caused by an injector will be fully dissipated before being seen in the production³. Therefore, the multiple linear regression will fail to inform the contribution of each injector in the production rate. However, the BCM will still indicate the dissipation in the reservoir through the estimated τ 's.

1.4.1.2 25x16 Synfield

The BCM technique was tested on a homogenous field with many more wells. The injection rates are actual data of one of the real fields presented in this paper. A history of 65 data points was initially used. This synthetic case is also used for comparison with an application of the technique to real cases.

Figure 20 shows the results for the BCM applied to the 25x16 homogenous Synfield. The results, in general, are as expected in which λ decreases with distance between the well pairs. Because the reservoir is homogenous, we expect the λ 's to be symmetric across planes of

symmetry. Overall, the symmetry reflected by λ 's (Fig. 20) is adequate but it is not as good as the one shown in the 5x4 Synfield. Also, a few (27 out of 400) negative weights occur (Fig. 21), but they are small, in the range of -0.04 to 0. The lack of symmetry is caused by lack of symmetry in the injection rates, but the negative weights, for which there is no physical explanation, is caused by the injection rates not being entirely independent of each other, or collinearity.

Correlation between the injection rates is a cause of negative weights, especially with short data sets. The effects of collinearity on linear estimation procedures have a long statistical history (Snee, 1983; Hocking, 1983; Belsley, 1991). Collinearity causes the estimated coefficients (the λ 's in our case) to be inflated and to have an incorrect sign. In multiple linear regression, the variance of the MLR weights consists of two main components: the mean squared error (MSE) and the variance inflation factor (VIF) defined as (Marquardt and Snee, 1975):

$$s^2(\lambda_{ij}) = \text{MSE} \times \text{VIF}_{ij} \dots\dots\dots (10)$$

where,

$$\text{MSE} = \frac{\text{Var}(q_j - \hat{q}_j)}{N - (I + 1)}$$

N is the total number of data points and I is the total number of injectors. The VIF for the i^{th} regression coefficient (weight) is the i^{th} diagonal element of the inverse of the injector-injector correlation matrix. The VIF is a direct measure of the collinearity between injectors. Therefore, the variance of the estimated λ 's is directly proportional to its VIF and inversely proportional to (N-I-1). In other words, the smaller VIF and the more data points, the more precise (smaller s^2) the determination of the λ 's. The λ 's will also be more precise with fewer injectors.

The maximum VIF value determined for the N = 65 history is about 100, which shows that the variance of the corresponding λ 's is poor. Since all estimated negative weights are very small, this suggests that collinearity is the cause behind negative weights.

The only remedy to collinearity is to collect more data; a longer injection history will be less likely to be collinear. According to Eq. 10, an increase in the number of the data points with small VIF values should give more precise weights. Figures 22 and 23 show the results obtained when using 415 randomly generated data points for which the maximum VIF = 2.5. The symmetry observed in Fig. 22 is excellent and there are no negative λ 's (Fig. 23). All the negative λ 's estimated from short data set (N = 65) become small positive numbers in the analysis of long data set (N = 415).

The estimated τ 's using the long data set show the symmetry expected with the homogenous reservoir (Fig. 24). However, the τ 's for the most distant well pairs do not show the attenuation and time lag associated with the large distance. This can be seen clearly in Fig. 25. We found that the τ 's for the most distance well pairs (distances greater than 4000 ft) often did not change from their original value. This suggests that distant injectors did not directly support the production, a conclusion consistent with Fig. 23 in which the λ 's for pairs greater than this distance are also small.

We further examined this observation by plotting the reduction in the error variance, $\text{Var}(q - \hat{q})$, for each producer when injector i is included in the BCM model. This was separately done for each injector in the 25x16 Synfield. The results of this analysis for only injectors I01 and I25 are in Fig. 26.

Several things can be noted in this figure. Because the reservoir is homogenous and injectors I01 and I25 are symmetrically located, the trends of reduction of the error variance are approximately the same. The reduction in the error variance, as anticipated, decreases with well pair distance. In other words, the larger the distance between an injector-producer pair, the less the influence of the injector. Therefore, varying the τ 's of the most distant well pairs will not significantly improve the prediction. This explains the insensitivity of the distant injectors to the τ 's.

1.4.2 Application to field data

The technique was applied to two different sets of field data. The results of these applications are presented and discussed in this section. Unlike the Synfield applications we have no concrete standards (e.g. symmetry or agreement with numerical simulation) against which to compare results. Our truth test will be comparison against known geological features, as much as possible, and against MLR results.

1.4.2.1 *The first real field application*

The technique was applied to a portion (25 injectors and 16 producers) of the Chihuido de la Sierra Negra (ChSN) Field in Argentina. The field is undergoing a waterflood on a five-spot pattern. The reservoir conditions are similar to those of the synthetic fields but, of course, the ChSN is not homogenous. Since only a portion of the field was analyzed and the boundaries are open, the UCM approach is applied.

The data selected for the analysis was determined by examining the production, and injection rates and the producing gas oil ratio (GOR). The GOR had a peak at approximately month 60 that sharply decreased after water injection started. By month 74, the GOR was at a minimum and approximately equal to the solution gas-oil ratio, all of which suggests that the hydrocarbon in the reservoir is single-phase. Also, injection and production rates are in acceptable balance. Therefore, the analysis is carried out using the data starting in month 74 which left 52 data points for the analysis. With this short injection and production data and 25 injectors, the maximum VIF = 25. We know in advance that we will obtain suboptimal results and the estimated λ 's will be imprecise. Moreover, the open boundaries introduce errors in the estimation of the λ 's and some of the assumptions used to derive Eq. 9 are not met. However, some general features can be inferred from the application of UCM model to the ChSN Field data. The four center wells were chosen to minimize the effects of the boundaries.

Figures 27 and 28 show representations of the positive λ 's and the τ 's, respectively, in which a structural map obtained from the operator is overlain in both figures. In general, injectors in the north-west of the field have smaller λ 's than those in the south. Five injectors (F14, F18, E14, E15 and E18), particularly, seem to have little influence on inner producers. The orientation of the λ 's in wells C14, C15, B14 and B15 are in agreement with the presence of a fault slightly south of C14 and C15. The orientation of the τ 's in the south wells, mainly B14 and B15, confirms the presence of the fault. However, some λ 's relate injectors B16 and B17 to inner producers, which is in disagreement with the presence of this fault. This error could be attributed to a boundary effect, the large collinearity between injectors, or the fault may not be completely sealing. The τ 's seem to be more consistent with known geological features of the field.

For the purpose of comparison, the purely resistive model (MLR) was also applied. Figure 29 shows a comparison between the two sets of λ 's estimated by UCM and MLR. In general, both sets are in agreement, which can be justified by small compressibility of the field as depicted by relatively small τ 's (Fig. 28). Because the capacitance model accounts for the

compressibility effects, we expect a deviation between the two sets of weights as shown in the figure.

Since there is moderate collinearity between the injection rates, and changing production conditions, we expect negative weights to occur. Figure 30 shows λ 's versus well pair distance. Reasonable λ 's are obtained for the near well pairs, but very large and even negative weights are obtained for more distant pairs. The negative weights are more than can be explained by collinearity. We conclude that the BHP of the producers must be changing, but we have no direct way of verifying this since we do not have pressure data for ChSN. The modeled total production rate for the four center wells is $R^2 = 0.977$.

1.4.2.2 The second field application

The UCM technique was also applied to a portion of the Magnus Field in the UK North Sea. The injection and production data is taken daily from permanent downhole measurements. The number of data points is over 6,000 for one injector-producer pair; hence, the MSE should be very small. The field is characterized by wells having frequent shut-in periods. The waterflood is essentially peripheral intended to provide pressure support for the crest area. For the first 12 years of production, the field produced in primary production; the waterflood is for general pressure support. In the early 90's, the field rate came off plateau production when water broke through in flank producers. When the complexity of the field became apparent, the strategy of the waterflood management was shifted to implement zonal water injection where producers and injectors were completed in specific layers to maintain production. Injection support for two key zones (the G and A sands) in the crest area of the field significantly improved the field production (Day and others, 1998).

The best period for UCM analysis is after the zonal water injection began, where inference about the connectivity between well pairs is feasible. Thus, the time period starting in early 1998 was selected for the analysis. The number of data points is $N = 230$ points, which is equivalent to 7 months. 7 injectors and 8 producers in the crest area is the target zone (Fig. 31). We will refer to this portion of the field as the MGCT field.

Figure 32 shows the injection rate and production rate of the MGCT field. The moving average curves represent a 10-day average of the corresponding rate. Since the waterflood is peripheral and the wells are far apart, we know that inferring interwell connectivity will be challenging. Also, the open boundaries introduce errors in the estimated λ 's and again many assumptions behind Eq. 9 are not met. However, some general features can be inferred from the application of UCM to the MGCT field.

Figure 33 shows a representation of the positive λ 's. The injection wells show small λ 's for producers in the north-west of the MGCT field. Producers M33C7, M27B2, and M24B2 appear to be unsupported. The orientation of the λ 's in all injectors indicates the direction of the connectivity is mainly south-west to west.

From Day and others (1998), we know that most of the production during the selected period came from two key zones (the G and A sands). In applying the UCM, we found that well pairs completed in the G sand have large τ 's. The primary production component is dominant in the G sand. Figure 34 shows an example of the rates of well pairs completed in the G sand. For $\tau = 39$ days, the injection rate of both injectors are significantly attenuated. In contrast, wells completed in the A sand have small time constants ($\tau < 1.0$ day); the primary production component is insignificant and the production appears to be well supported by the injection. Figure 35 shows an example of well pairs completed in the A sand. The difference in τ for both layers indicates that either the A sand has better flow characteristics (a larger permeability) than

the G sand, or their pore volumes differ significantly. To validate any of these observations would require other data.

The fits to the production data are not particularly good. Some of this is because of the importance of the primary production, but we also suspect that the production rates are noisy. This is discussed at the end of this paper.

1.5 Discussion

This section discusses the properties of the weights, the properties of the time constants, the possible sources of errors, and the use of the technique presented as a predictive tool.

1.5.1 A rational interpretation of weights

As discussed before, the estimated λ 's depend only on the relative location of the wells and the reservoir properties. Also, we have seen from the application to synthetic cases that the λ 's do not reflect the interaction between injectors because the set of λ 's between one injector and producers are the same as those estimated when all injectors are active in the field. In other work (Gentil, 2005), we found out that the λ of an injector-producer (ij) pair is:

$$\lambda_{ij} = \frac{T_{ij}}{\sum_j^K T_{ij}} \dots\dots\dots (11)$$

where T is the transmissibility and K is the total number of producers. This equation states that the ratio of the transmissibility between injector i and producer j to the sum of the transmissibility between the same injector and all producers is equal to the estimated weight between the (ij) well pair. This equation indicates that the sum of weights initiated from one injector should add to one, which is in agreement with all our applications of the capacitance model to synthetic fields.

For the purpose of comparison, we applied Eq. 11 to estimate the λ 's of 5x4 homogenous Synfield in which T_{ij} is defined as

$$T_{ij} = \frac{\bar{k}_{ij} A_{ij}}{\mu L_{ij}}$$

where \bar{k}_{ij} is the average permeability between injector i and producer j; A_{ij} is the cross section area, μ is the reservoir fluid viscosity and L_{ij} is the distance between the (ij) well pair. Incorporating the given definition of T_{ij} , Eq. 11 could be approximated by:

$$\lambda_{ij} = \frac{1/L_{ij}}{\sum_j^K 1/L_{ij}}$$

Figure 36 shows an excellent match between the two sets of λ 's estimated by BCM and Eq. 11. This indicates that the presented physical definition of λ (Eq. 11) is in agreement with the results of 5x4 homogenous cases obtained by the BCM. From all above discussion, we conclude that the estimated λ 's in this work do quantify the connectivity between injector and producer pairs.

1.5.2 Properties of the time constants

As discussed earlier, the τ 's are functions of the total reservoir compressibility, the pore volume, and the productivity index. Like the weights, the τ 's do not account for interaction

between injectors so that the set of τ 's estimated between a single injector and many producers are the same as the set of τ 's estimated when all injectors are active. Also, for an injector-producer pair the λ and the corresponding τ are not totally independent in which they carry some similar components. Equation 11 indicates that the λ_{ij} is directly proportional to the transmissibility or the productivity index between injector i and producer j whereas the corresponding τ_{ij} (Eq. 3) is inversely proportional to the same productivity index. Thus, the λ and the corresponding τ are inversely related. The log-log plot of λ 's against τ 's estimated from the 5x4 homogenous Synfield gives an approximate straight line of slope -1 indicating that the λ is inversely proportional to the τ , which is in agreement with their basic definition (Fig. 37). However, the τ 's explicitly indicate the attenuation and time lag between well pairs while λ 's quantify the connectivity.

1.5.3 Assumptions

The assumptions can be listed as the following:

Linear well productivity. All producers should exhibit linear productivity so that changes in an injection rate will cause changes in pressure in the surroundings of a producer. Also this restriction imposes that the BHP's of all producers must be constant during assessment intervals. However, if BHP data is available, the capacitance model has the ability to integrate these data to enhance the investigation about interwell connectivity. Thus, the inferring about weights from well-rate fluctuations is feasible.

No producer extended shut-in periods. Since the set of weights initiated from one injector is function of the number of active producers, shutting any producer during the assessment interval will impose a new set of weights. Therefore, time intervals dominated by production wells having extended shut-in periods (highly transient flow) must be avoided.

No new production wells. The number of production wells must remain constant within the assessment interval. The drilling of new production wells will impose a new set of weights.

No new completions. No new layers should be completed during the analyzed period.

Slightly compressible fluids. Reservoir fluids should have a small compressibility. Existing free gas will impose large dissipation in the reservoir in which perturbations in injection rate will be dissipated before being seen in the production rate. Changes in reservoir gas saturation can be determined by the GOR; therefore, the GOR should be constant and equal to the dissolved gas-oil ratio in the assessment interval.

1.5.4 Sources of error

Under the stated assumptions, the estimated λ 's should not be negative or exceed one (i.e., $0 \leq \lambda \leq 1$). $\lambda < 0$ and $\lambda > 1$ are considered errors in estimation of the interwell connectivity. The possible sources of error can be summarized as follows:

Deviation from the above assumptions. Deviation from stated assumptions will introduce errors. As we have seen in the application to synthetic fields, changing the BHP causes negative weights to appear.

Collinearity and short data. Collinearity between injection wells rates is one source of negative weights, especially with short data. As we have seen in the application to 25x16 Synfield, using longer injection-production history reduces the effect of collinearity. However, in real waterflood field, using longer data is not an option and we are restricted to deal with data as it exists. Ridge regression (e.g., Hoerl and Kennard, 1970a,b) has a long statistical history for reducing errors introduced by collinearity. It enabled the MLR technique to determine more stable weights (Yousef, 2006).

Data quality. The technique is relatively sensitive to the quality of injection and production rate measurements. We performed different error sensitivity analyses by introducing white noise (uncorrelated, zero mean and normally distributed) to the observed injection and production data before using the capacitance model. In general, introducing white noise errors shrinks the weights towards the zero and decreases the R^2 (Yousef, 2006). Figure 38 shows how the estimated weights shrink with introducing white noise errors in error-free well rates for 5x4 homogenous Synfield. The system consists of producer P01 and injectors I01, I02, I03, I04, and I05. The C parameter represents the ratio of introduced white noise error variance to the variance of the corresponding error-free well rates. In this analysis, the fractional error variances of all well rates are equal. Figure 39 depicts the reduction in R^2 with introduced errors. For example, if the fractional error variance is only 0.6, the R^2 is expected to drop from 1.000 (error-free) to 0.804. Since we observed small R^2 (= 0.682) for the MGCT data, we are tempted to conclude that the daily rate data contained substantial white noise.

1.5.5 Selection of assessment interval

The selection of the appropriate period of time to apply the technique is essential. Special attention should be paid to minimize the deviation from the assumptions when selecting the data. As commented before, periods that are highly dominated by transient flow should be avoided.

1.5.6 Use as a predictive tool

This technique can be used to predict the total production rate in each producer using the injection rates as input. Figure 40 shows the comparison between the BCM model and the production rate observed in the 5x4 Synfield homogenous reservoir using the first 20 data points to estimated λ 's and the last 80 data points to test the prediction. The maximum VIF for the 20 training data points is 9.0, which indicates that the collinearity is relatively insignificant in the data. Thus, the excellent results ($R^2 = 0.999$) obtained in the prediction were expected. Also, this further supports that the λ 's are time-independent, which confirms that the λ 's are unique measure of interwell connectivity. Testing the predictive capability of this technique in the other cases also showed very good results (Yousef, 2006). Predicting the total rate from injection rate fluctuations is not the same as predicting the oil rate. However, other work (Gentil, 2005) has shown that an oil rate can be inferred from the total rate using petrophysical data.

1.6 Conclusions

We report on an improved technique to quantify communication between vertical wells in a reservoir using mainly injection and production rate data. The technique combines a nonlinear signal processing model (the capacitance model) and multiple linear regression analysis to provide information about preferential transmissibility trends and the presence of flow barriers. The connectivity between wells is described by coefficients (weights) that depend only on medium properties and relative location of the wells; they are independent of injection/production rates and do not reflect interaction between injectors. A rational interpretation of estimated weights was provided that is consistent with the results of synthetic field applications. Also, the technique provides parameters (time constants) that explicitly indicate the attenuation and time lag between injector and producer pairs without subjective judgment. The capacitance model was validated by showing that time constants are consistent with their basic definition.

The technique has been also validated by applications to synthetic fields, which showed that the capacitance model captures the true attenuation and time lag between injector and producer pairs and also the connectivity between well pairs.

The quality of expected results depends on data quality and deviation from assumptions. Collinearity, small data sets, and changing bottom-hole pressures are all sources of nonphysical weights.

The technique was first applied to a field in Argentina. Even with a small assessment interval, some features could be inferred. The validation of these results is very difficult; however, our results do seem to agree with the presence of known geological features. Also, the technique was applied to data from the Magnus Field in the North Sea. Since the noise in the production rates is large and the primary production is significant, the estimated weights should be interpreted in a qualitative manner. However, the time constants indicate different flow characteristics of two key zones in the crest area of the field. These results agree with observations from reported studies related to this field.

The new procedure resolves many limitations of existing methods and extends the range of applications. It can be applied to fields in which wells are shut-in frequently or for long periods of time, it allows for application to fields where the rates have a remnant of primary production, and it has the capability to use bottom hole pressure data (if available) to enhance the investigation about wells connectivity.

1.7 Tables and Figures

Table 1: The weight λ_{ij} for 5x4 homogenous Synfield plotted in Figure 5.

	P01	P02	P03	P04
I01	0.33	0.33	0.17	0.17
I02	0.33	0.17	0.33	0.17
I03	0.25	0.25	0.25	0.25
I04	0.17	0.33	0.17	0.33
I05	0.17	0.17	0.33	0.33
λ_p	1.00	1.00	1.00	1.00

Table 2: The time constant τ_{ij} (month) for 5x4 homogenous Synfield plotted in Figure 6.

	P01	P02	P03	P04
I01	0.60	0.59	0.81	0.80
I02	0.65	0.86	0.61	0.84
I03	0.66	0.62	0.63	0.62
I04	0.79	0.62	0.81	0.61
I05	0.81	0.81	0.62	0.62
τ_p	0.00	0.00	0.00	0.00

Table 3: The weighting factors λ_{ij} , λ_p and v_{kj} for 5x4 homogenous Synfield, change producer P01 BHP. The λ_{ij} are plotted in Figure 15.

	P01	P02	P03	P04
I01	0.33	0.33	0.17	0.17
I02	0.33	0.17	0.33	0.17
I03	0.25	0.25	0.25	0.25
I04	0.18	0.33	0.17	0.33
I05	0.17	0.16	0.33	0.32
λ_p	1.00	1.00	1.00	1.00
P01 BHP	0.66	-0.23	-0.24	-0.17

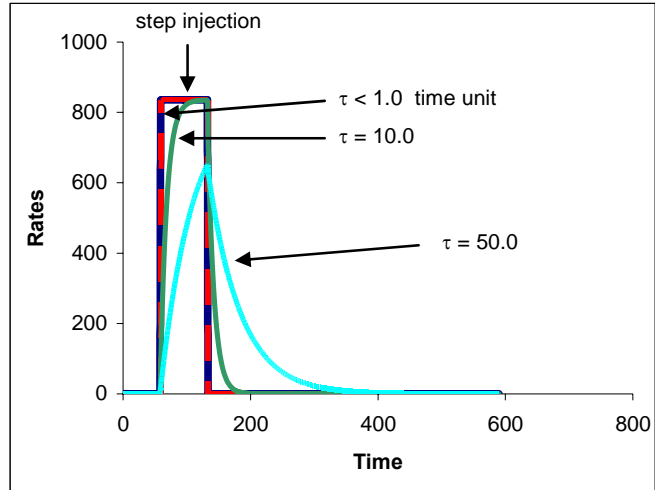


Figure 1: Injection unit-step and convolved or filtered injection rates at different values of the time constant (τ).

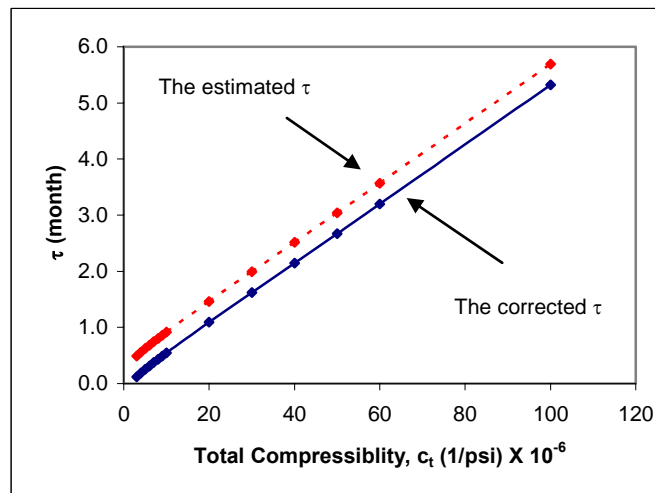


Figure 2: The estimated τ versus the total compressibility, 1x1 Synfield. The dashed line represents the estimated τ and the solid line represents the corrected τ .

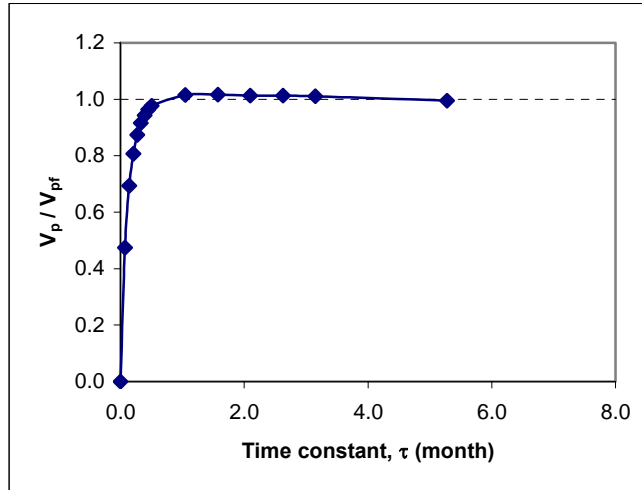


Figure 3: The estimated pore volume (V_p) normalized by the static pore volume (V_{pf}) versus the corrected τ , 1x1 Synfield.

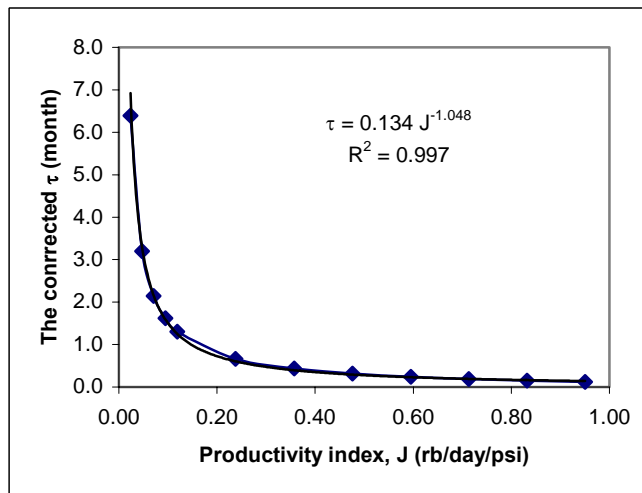


Figure 4: The corrected τ versus the productivity index (J), 1x1 Synfield (changing the field permeability).

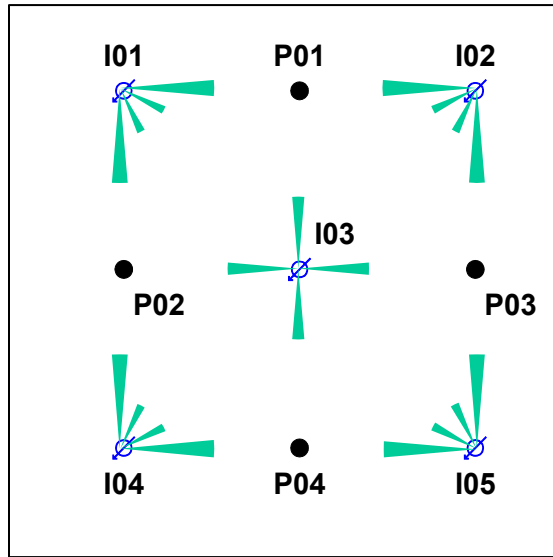


Figure 5: Representation of the weights λ_{ij} , shown in Table 1. The length of the arrow is proportional to the value of the weight. 5x4 Synfield, homogenous reservoir.

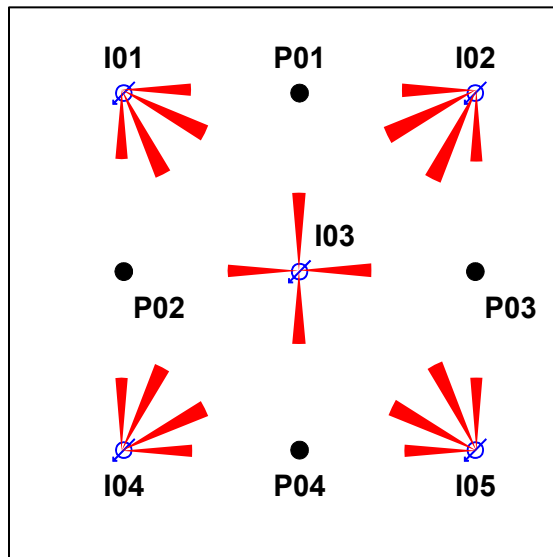


Figure 6: Representation of the time constants τ_{ij} , shown in Table 2. The length of the arrow is proportional to the value of τ . 5x4 Synfield, homogenous reservoir.

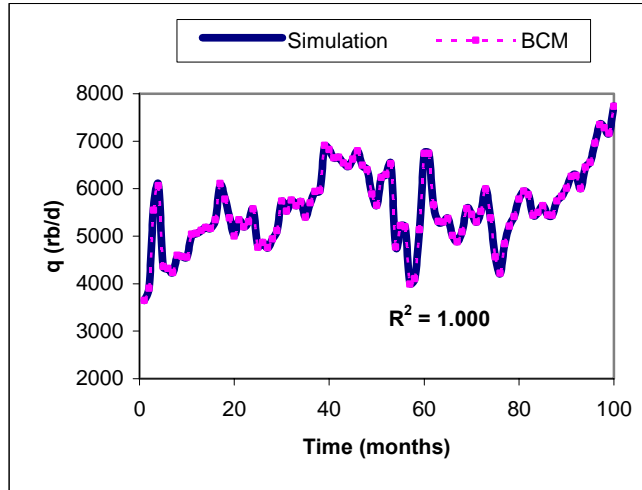


Figure 7: Comparison between modeled total production rate using the balanced capacitance model (BCM) and the total production rate observed in the simulation. 5x4 homogenous Synfield.

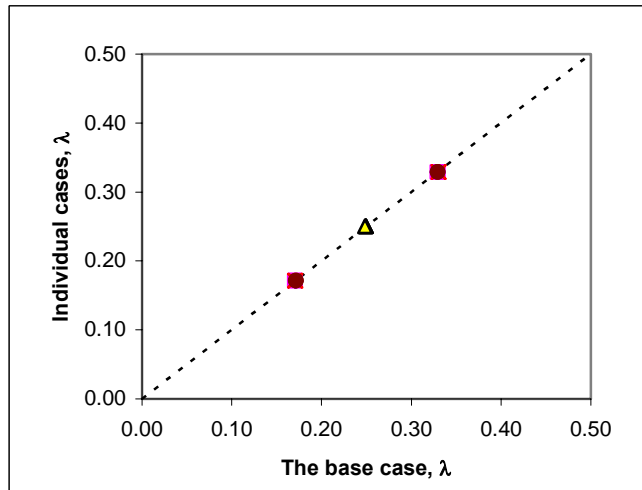


Figure 8: A crossplot of the λ 's estimated from individual cases (one injector is only active) against the λ 's estimated from the base case (all injectors are active). The dashed line represents the 45° line. 5x4 homogenous Synfield.

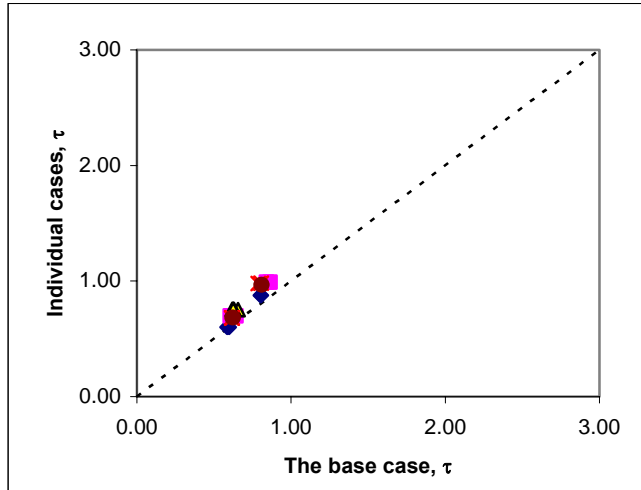


Figure 9: A crossplot of τ 's estimated from individual cases (one injector is only active) against the τ 's estimated from the base case (all injectors are active). The dashed line is the 45° line. 5x4 homogenous Synfield.

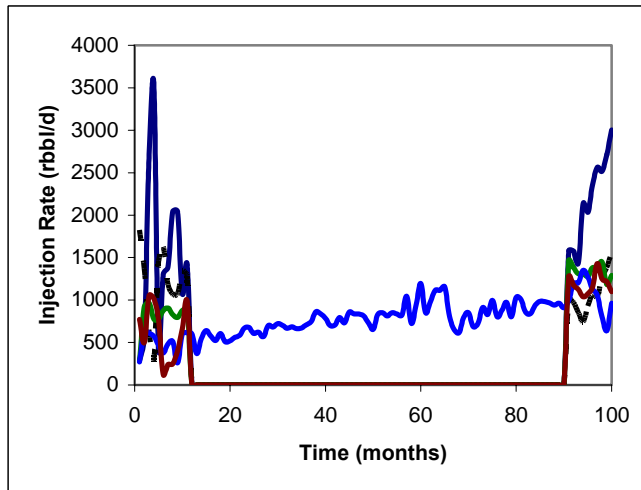


Figure 10: Rates for five injectors. 5X4 homogenous Synfield with extended shut-in period.

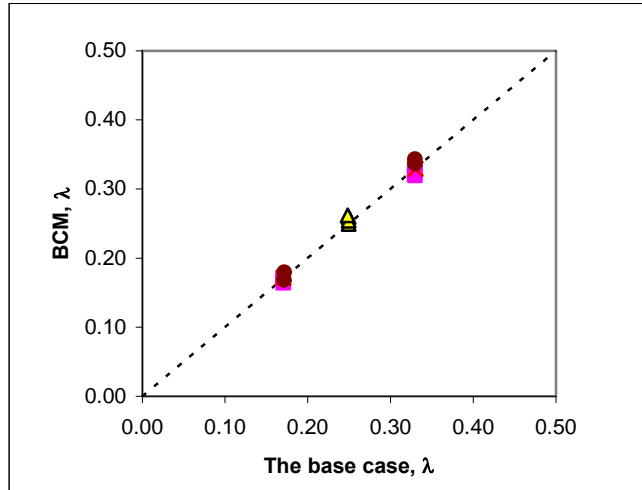


Figure 11: A crossplot of the λ 's estimated from the extended shut-in period against the λ 's estimated from the base case. The dashed line represents the 45° line. 5x4 homogenous Synfield, the extended shut-in period.

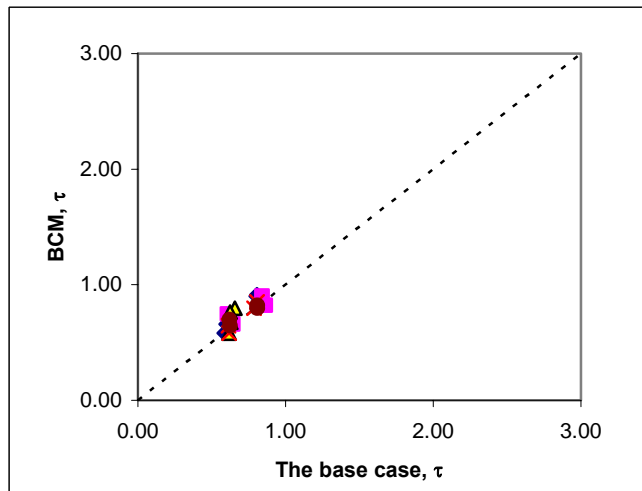


Figure 12: A crossplot of the τ 's estimated from the extended shut-in period against the τ 's estimated from the base case. The dashed line represents the 45° line. 5x4 homogenous Synfield, the extended shut-in period case.

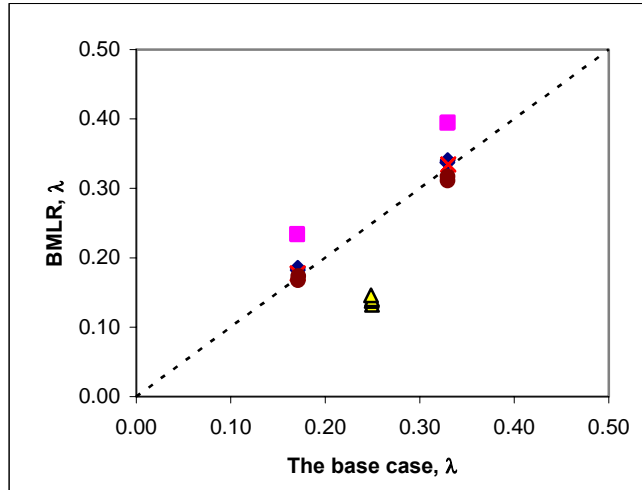


Figure 13: A crossplot of the λ 's estimated from the extended shut-in period using the purely resistive model (BMLR) against the λ 's estimated from the base case. The dashed line represents the 45° line. 5x4 homogenous Synfield, the extended shut-in period case.

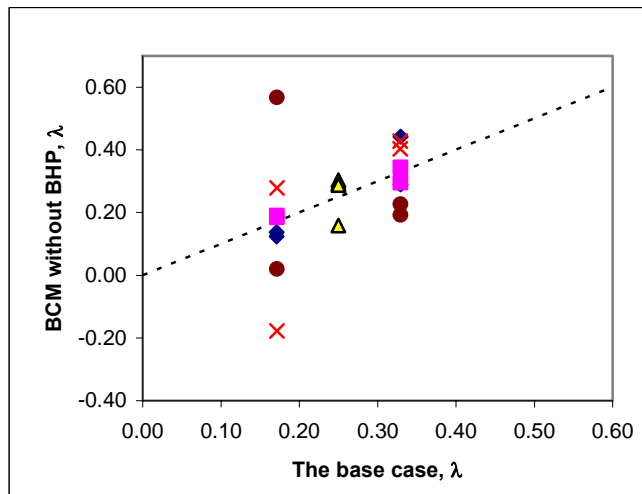


Figure 14: A crossplot of estimated λ 's from BCM without BHP data against the base case results. 5x4 homogenous Synfield, changing producer BHP case.

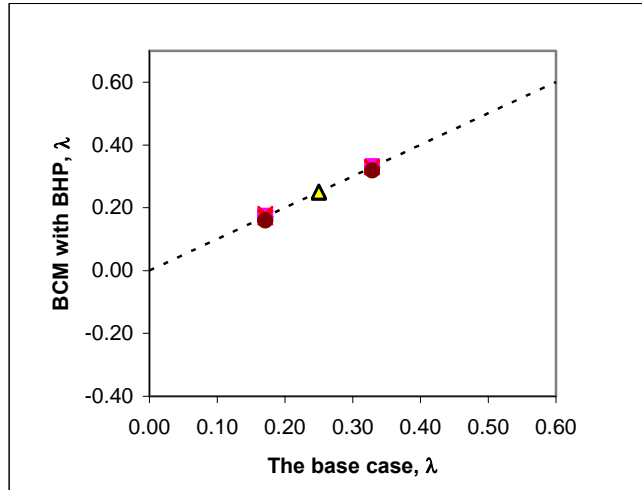


Figure 15: A crossplot of estimated λ 's from BCM with BHP data against the base case results. 5x4 homogenous Synfield, changing producer BHP case.

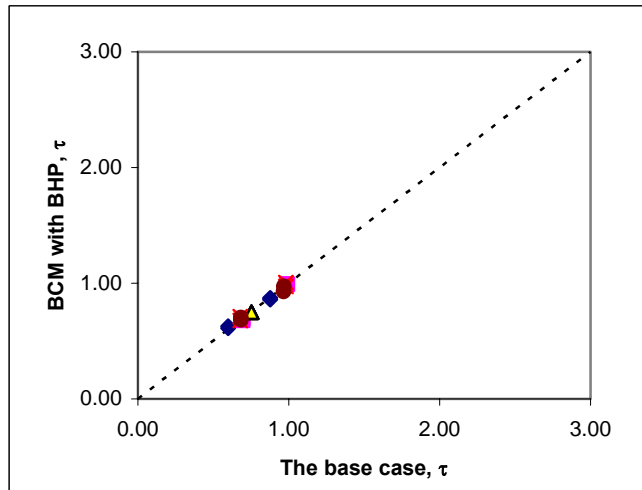


Figure 16: A crossplot of estimated τ 's from BCM with BHP data against the base case results. 5x4 homogenous Synfield, changing producer BHP case.

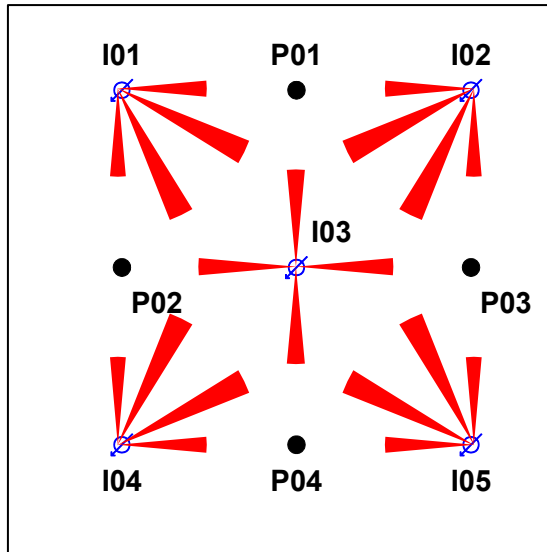


Figure 17: Representation of the time constants τ_{ij} . The length of the arrow is proportional to the value of τ . 5x4 homogenous Synfield, large compressibility case.

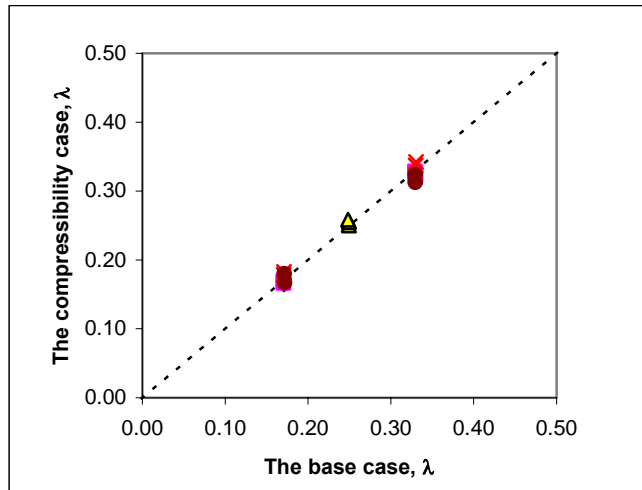


Figure 18: A crossplot of estimated λ 's using the BCM model against the base case results. 5x4 homogenous Synfield, large compressibility case.

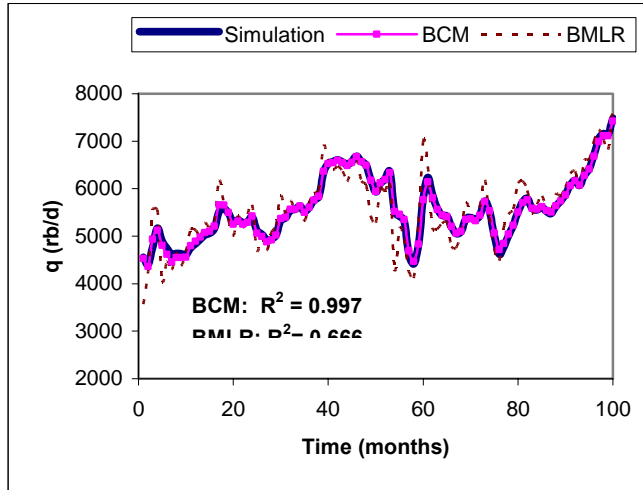


Figure 19: Comparison between modeled total production rate using BCM and BMLR (purely resistive model) and the production rate observed in the simulation. 5x4 homogenous Synfield, large compressibility case.

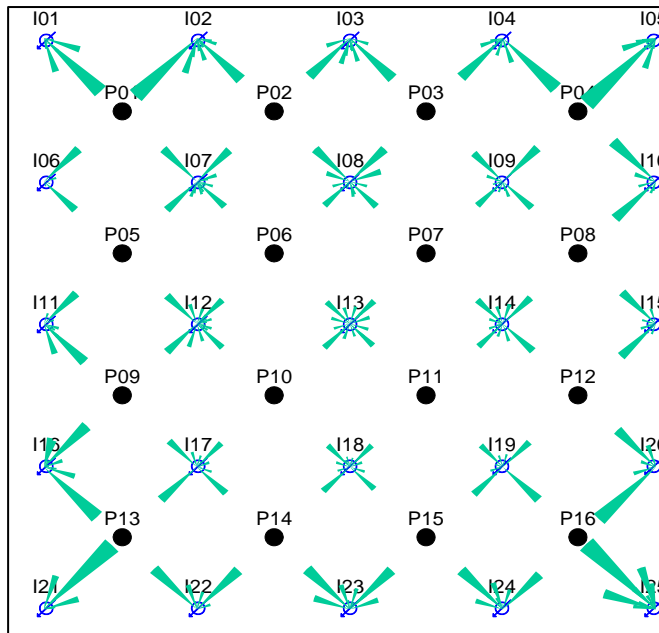


Figure 20: Representation of the weights, λ 's, using 65 data points with maximum VIF = 100. 25x16 homogenous Synfield.

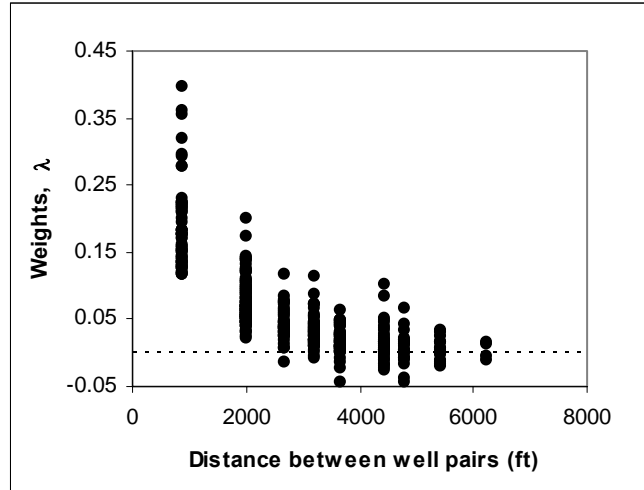


Figure 21: The weight, λ , versus distance, using 65 data points with maximum VIF = 100. 25x16 homogenous Synfield.

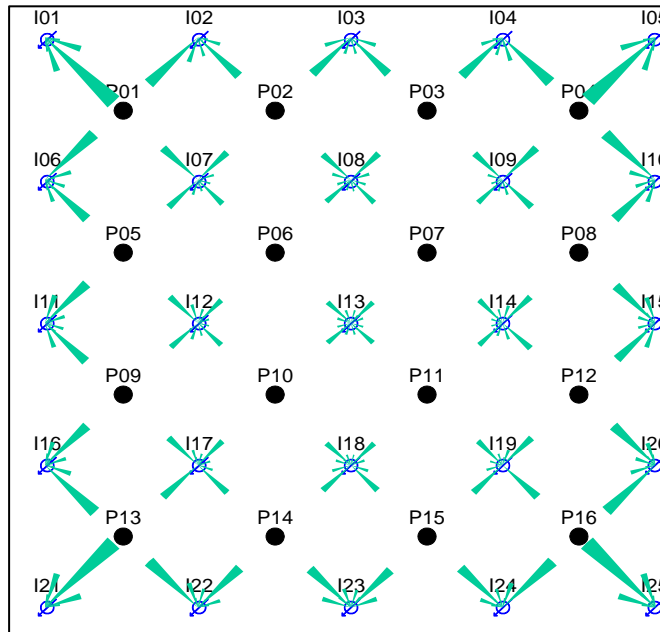


Figure 22: Representation of the weights, λ 's, using a long data set randomly generated with maximum VIF = 2.5. 25x16 homogenous Synfield.

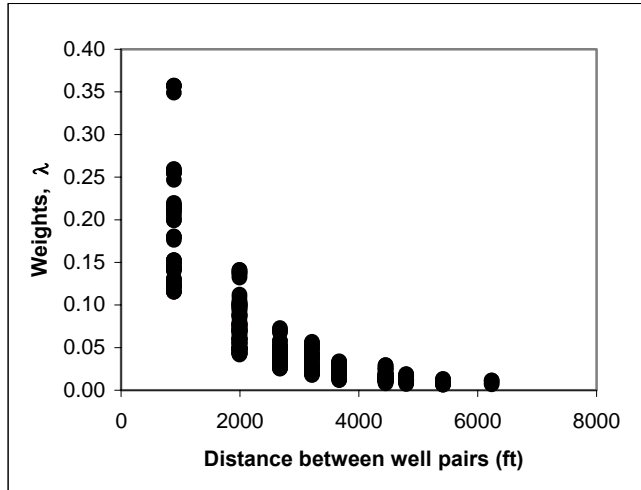


Figure 23: The weight, λ , versus distance, using a long data set randomly generated with VIF = 2.5. 25x16 homogenous Synfield.

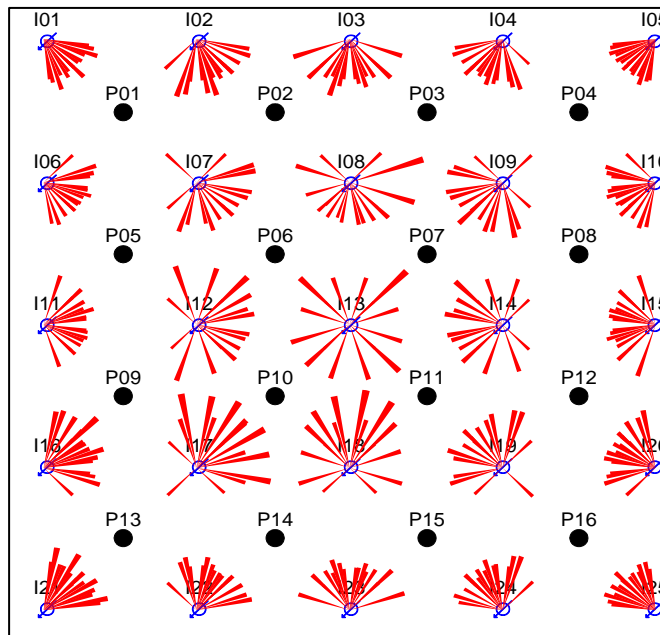


Figure 24: Representation of the time constants, τ 's, using a long data set randomly generated with VIF = 2.5. 25x16 homogenous Synfield.

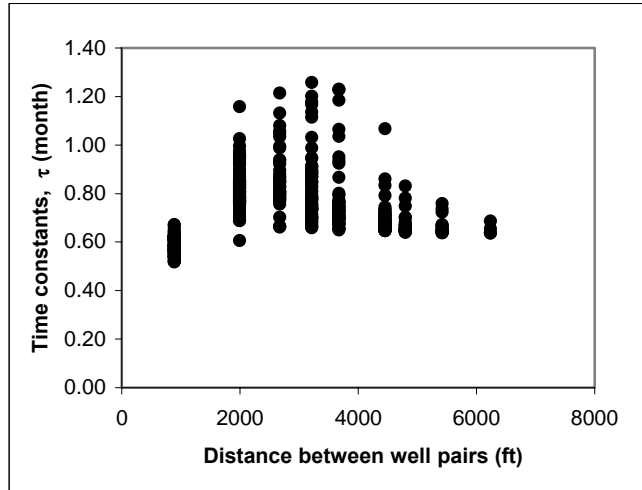


Figure 25: The time constant, τ , versus distance, using a long data set randomly generated with VIF = 2.5. 25x16 homogenous Synfield.

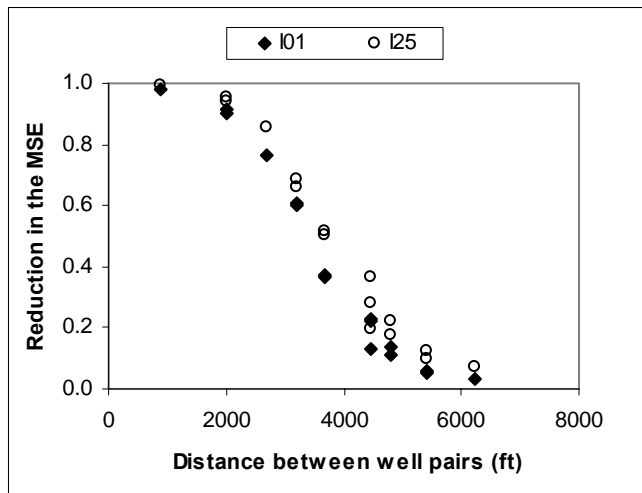


Figure 26: A reduction in the MSE, $\text{Var}(q - \hat{q})$, for each producer when injector I01 and injector I25 separately excluded from BCM model versus the distance from these injectors to each producer. The long data set randomly generated with maximum VIF = 2.5. 25x16 homogenous Synfield.

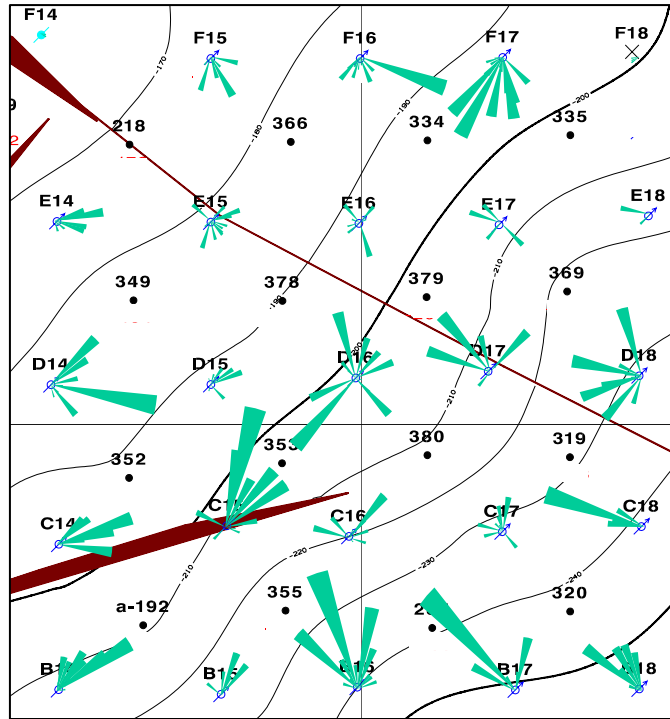


Figure 27: Representation of the positive weights, λ 's, in the ChSN field and comparison with known geological features. A structural map is overlain. Weights are in green, faults are in dark red.

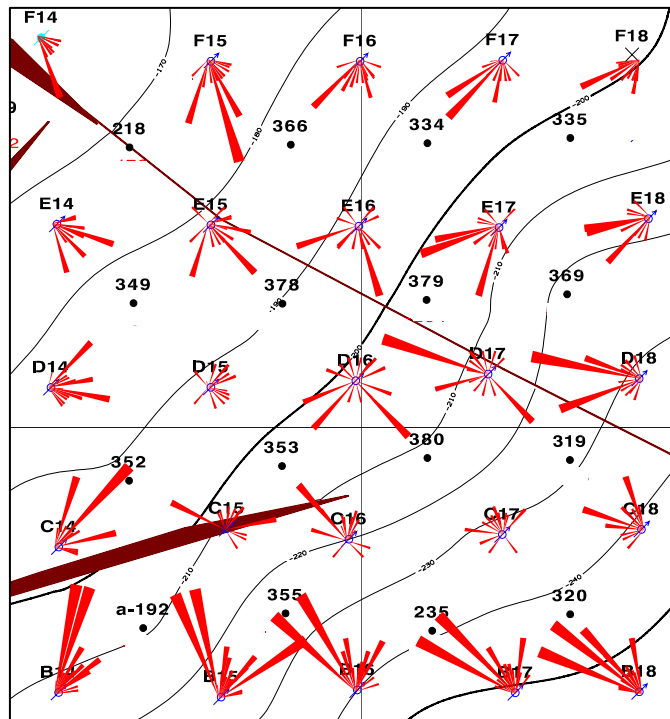


Figure 28: Representation of the time constants, τ 's, in the ChSN field and comparison with known geological features. A structural map is overlain. Time constants are in red, faults are in dark red.

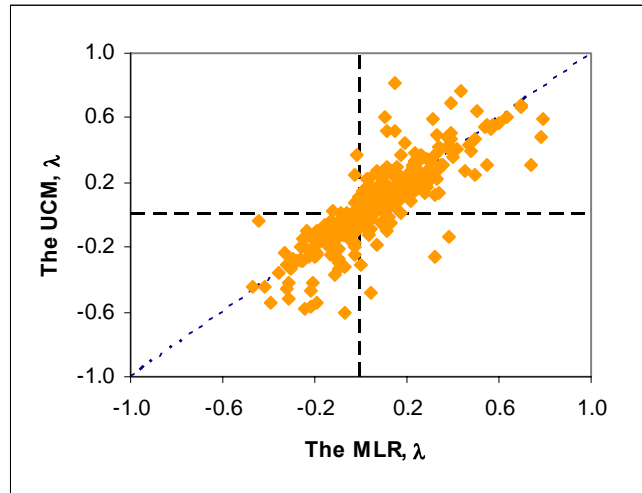


Figure 29: A crossplot of estimated λ 's from UCM against the λ 's from MLR. The ChSN field.

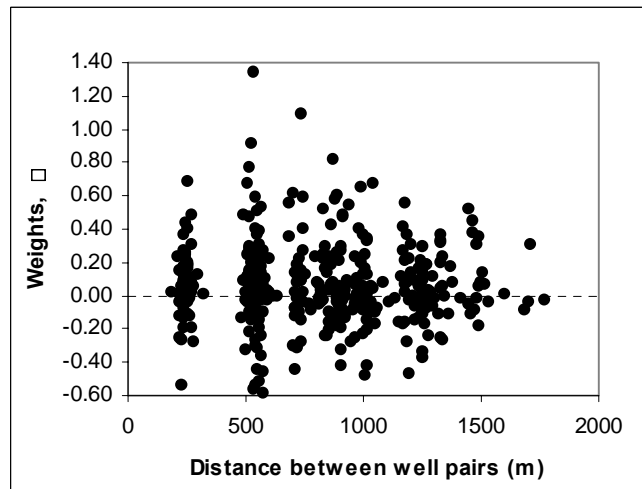


Figure 30: Application of UCM to the ChSN field with maximum VIF = 25. Weights λ versus distance.

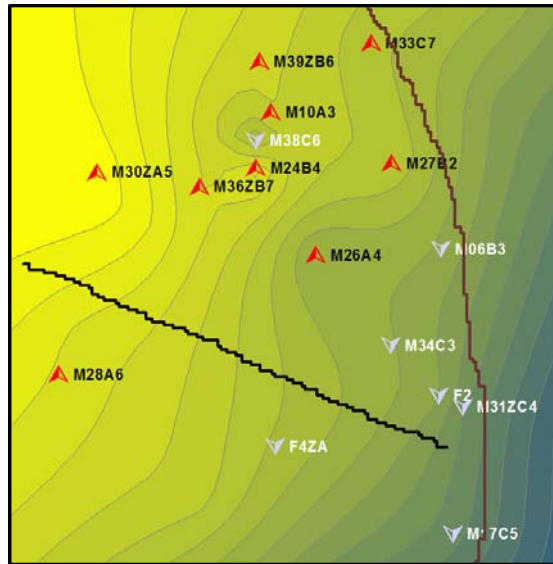


Figure 31: Magnus Field, the crest area. Lines represent known faults in the field.

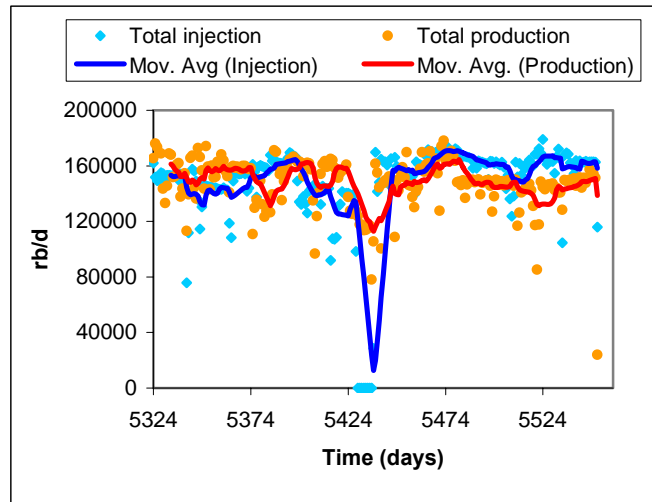


Figure 32: Magnus Field, injection rate, production rate and the moving average curves of the selected portion of the field.

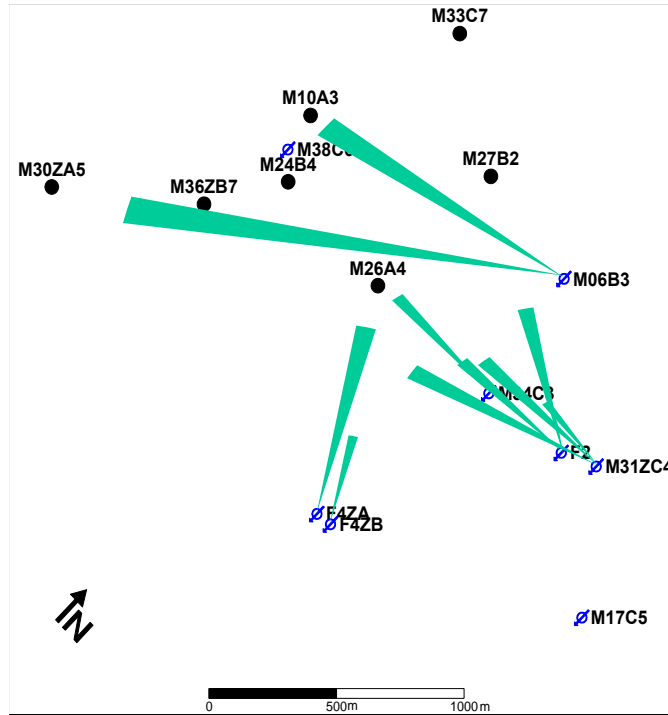


Figure 33: Application of UCM to the MGCT field. Representation of the positive weights, λ .

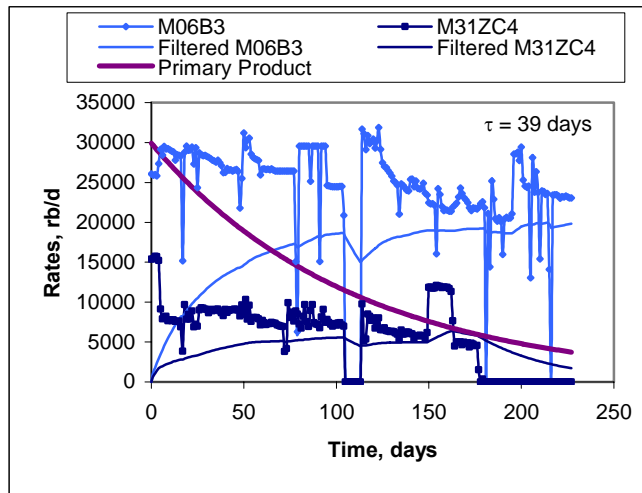


Figure 34: Application of UCM to the MGCT field. The system consists of producer M30ZA5 and two injectors (M06B3, M31ZC4). Primary production, injection rate and the filtered injection rate for two injectors in the G sand.

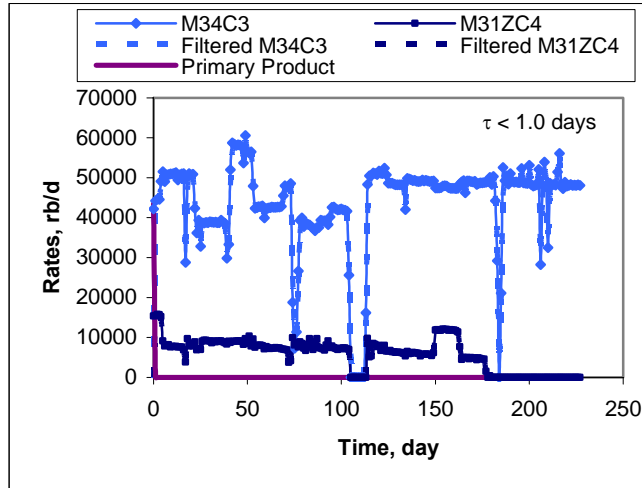


Figure 35: Application of UCM to the MGCT field. The system consists of producer M26A4 and two injectors (M34C3, M31ZC4). Primary production, injection rate and the filtered injection rate for two injectors in the A sand. The filtered injection rate for both injectors coincides with the raw injection rates.

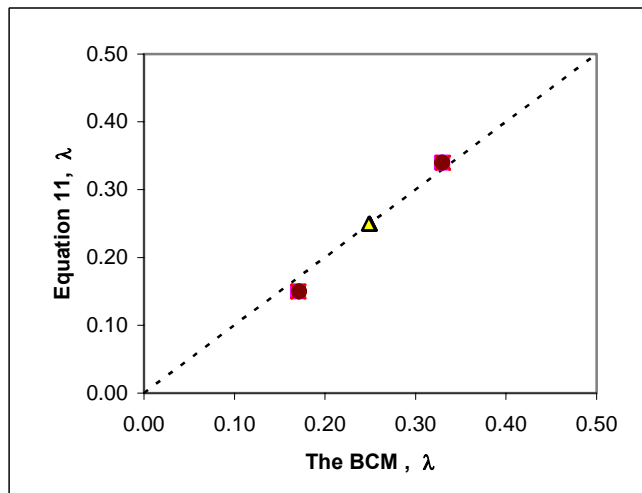


Figure 36: A crossplot of the λ 's estimated by Equation 11 against the λ 's estimated by the BCM. 5x4 homogenous Synfield.

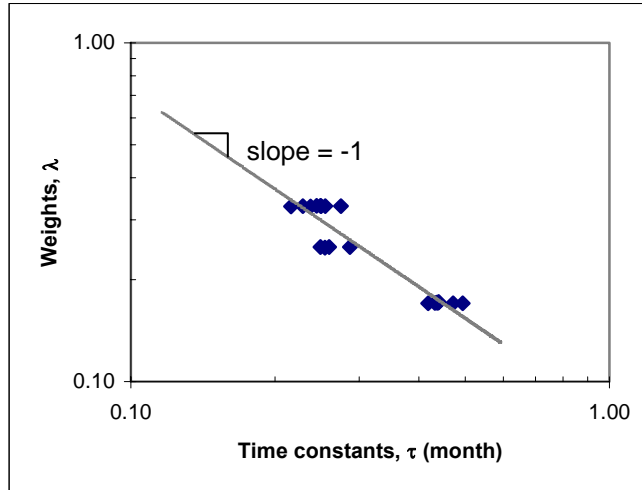


Figure 37: Log-log plot of λ 's vs. τ 's with a slope of approximately -1. 5x4 homogenous Synfield.

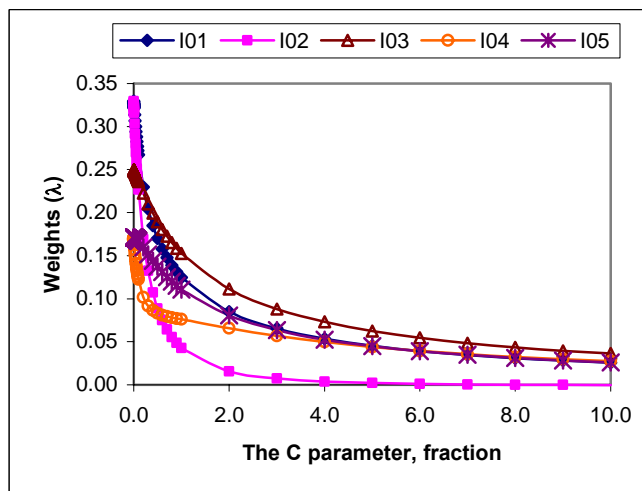


Figure 38: Effect of data quality on the estimated weights, λ . System consists of producer P01 and injectors I01, I02, I03, I04, and I05. The C parameter represents the ratio of introduced white error variance to the variance of the corresponding error-free well rates. In this analysis, the fractional error variances of all well rates are equal. 5X4 homogenous Synfield.

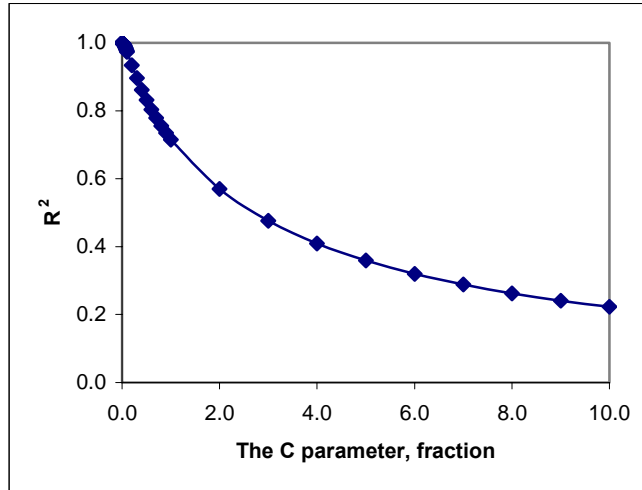


Figure 39: Effect of data quality on the coefficient of determination. System consists of producer P01 and injectors I01, I02, I03, I04, and I05. The C parameter represents the ratio of introduced white error variance to the variance of the corresponding error-free well rates. In this analysis, the fractional error variances of all well rates are equal. 5X4 homogenous Synfield.

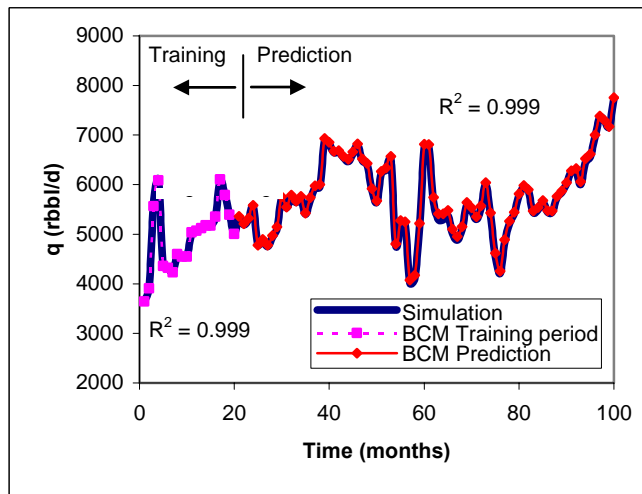


Figure 40: Comparison between modeled total production rate using BCM and the total production rate observed in the simulation. The weights were obtained using a training period of 20 data points and the rest is predicted. 5x4 homogenous Synfield.

RESULTS AND DISCUSSION

PART 2. RESERVOIR DIAGNOSIS USING CAPACITANCE MODEL PARAMETERS

In the capacitance model, two coefficients are determined for each injector-producer pair; one parameter, λ , quantifies the connectivity and another, τ , quantifies the fluid storage in the vicinity of the pairs. This section describes the development of this method into a diagnostic tool to enhance inference about preferential transmissibility trends and the presence of flow barriers.

2.1 Introduction

Most real reservoirs, if not all, undergoing a waterflood are heterogeneous where different geological conditions usually exist in the vicinity of injector-producer pairs. Different methods have been used to quantitatively determine the interwell connectivity and map reservoir heterogeneity from comparing the rate performance of a producing well with that of the surrounding injectors. Albertoni and Lake (2003) estimated interwell connectivity based on a linear model with coefficients estimated by multiple linear regression. The linear model coefficients quantitatively indicate the communication between a producer and the injectors in a waterflood. Yousef and others (2006b) used a more complete model that includes capacitance (compressibility) as well as resistive (transmissibility) effects. For each injector-producer pair, two coefficients are determined; one parameter (the weight) quantifies the connectivity, and another (the time constant) quantifies the degree of fluid storage between the wells. All the synthetic field applications exhibited in Yousef and others (2006b) were homogeneous; the emphasis was on validation of the new aspects that the capacitance model has over the method proposed by Albertoni and Lake (2003).

The capacitance model (CM) incorporates the effects of primary production, multiple injectors, and bottom hole pressure (BHP) change for multiple producers, or (Yousef and others, 2006b):

$$\hat{q}_j(n) = \lambda_p q(n_0) e^{-\frac{(n-n_0)}{\tau_p}} + \sum_{i=1}^{i=I} \lambda_{ij} i'_{ij}(n) + \sum_{k=1}^{k=K} v_{kj} \left[\begin{array}{c} p_{wf_{kj}}(n_0) e^{-\frac{(n-n_0)}{\tau_{kj}}} \\ - p_{wf_{kj}}(n) + p'_{wf_{kj}}(n) \end{array} \right] \dots \dots \dots (1)$$

where,

$$i'_{ij}(n) = \sum_{m=n_0}^{m=n} \frac{\Delta n}{\tau_{ij}} e^{-\frac{(m-n)}{\tau_{ij}}} i_{ij}(m)$$

$$p'_{wf_{kj}}(n) = \sum_{m=n_0}^{m=n} \frac{\Delta n}{\tau_{kj}} e^{-\frac{(m-n)}{\tau_{kj}}} p_{wf_{kj}}(m)$$

λ_p and τ_p are the weighting factor and time constant for the primary production contribution to the estimated rate \hat{q}_j of producer j . λ_{ij} is the weight between injector i and producer j that indicates the connectivity between the (ij) well pair; τ_{ij} is the time constant for the medium between

injector i and producer j ; $i'_{ij}(n)$ is the convolved or filtered injection rate at step n and $p'_{wfkj}(n)$ is the convolved BHP at step n for producer k ; v_{kj} is a coefficient that determines the effect of changing the BHP of producer k on the production rate of producer j . The entire last term disappears if all K of the producer BHP's are constant (Yousef and others, 2006b).

In our previous work, two versions of the capacitance model were introduced: the balanced capacitance model (BCM), and the unbalanced capacitance model (UCM). A waterflood is balanced when the field-wide injection rate is approximately equal to field-wide production rate. If this is the case, the BCM (Eq. 1) should be used. However, if the waterflood is unbalanced, a constant term (q_{oj}) should be added to Eq. 1, which forms the UCM.

In both versions, the model parameters (λ_{ij} , and τ_{ij}) are the ones targeted in this work where they are determined by using the injection and production data through an optimization procedure (Yousef, 2006).

This paper exhibits new applications of the CM to synthetic fields with complex geological features. Since a producer usually communicates with multiple injectors, the complex geological conditions are often not easily identified using the λ and τ values individually. However, combining both sets of parameters in certain representations enhances the inference about the geological features. Two different representations are used: one representation is a log-log plot of the λ 's against the τ 's for a producer and nearby injectors, and another representation is the flow capacity plot where the λ 's and the τ 's are combined using the idea of Lorenz plots. Both of representations enhance the inference about specific geological features in the vicinity of a producer.

The synthetic field and real field applications show that the relation between λ 's and corresponding τ 's are consistent with the known heterogeneity, the distance between wells, and their relative positions. The flow capacity plots and the log-log plots are capable of identifying whether the connectivity of an injector-producer well pair is through fractures, a high-permeability layer, multiple-layers or through partially completed wells.

2.2 Procedure

Two different representations are proposed to enhance the inference about reservoir heterogeneity using the estimated parameters from the CM: the flow capacity plot, and the log-log plot of λ 's against the τ 's. The mathematical developments of both representations are addressed in this section.

2.2.1 The flow capacity plot

The idea of flow versus storage was developed initially in the petroleum literature to estimate injection sweep efficiency in layered reservoir. This method relates the relative flow of a given layer to its associated pore volume, usually in a flow-storage diagram (Lorenz plots or flow capacity plots). These plots can be used quantitatively to describe reservoir geology. For example, 50 % of flow comes from only 10 % of the pore volume of a reservoir or a layer, which indicates fast flow paths.

The flow capacity plots estimated from the model parameters are different from the conventional Lorenz plots (Schmalz and Rahme, 1950). The Lorenz plots are based on permeability and sometimes porosity data obtained from measured samples (usually core plugs) taken from the reservoir where the spatial relationships of the samples are ignored, while the flow capacity plots are based on inferred parameters (λ 's and τ 's) from dynamic data (injection and production) in which these parameters account for all variations in reservoir properties in the

vicinity of a producer. Shook (2003) also developed such plots (flow-storage diagram) based on estimated results from tracer tests. Therefore, the flow capacity plots, based on dynamic data, are likely to honor the flow paths and geological features in a reservoir.

The Lorenz plot, suggested by Schmalz and Rahme (1950), is used together with the estimated sets of λ 's and τ 's between a producer and multiple injectors, to form the flow capacity plot. The Lorenz curve (Fig. 1) is a plot of cumulative flow capacity, F_m , versus cumulative thickness, H_m , where

$$F_m = \frac{\sum_{i=1}^{i=m} k_i h_i}{\sum_{i=1}^{i=n} k_i h_i} \dots\dots\dots (2)$$

$$H_m = \frac{\sum_{i=1}^{i=m} h_i}{\sum_{i=1}^{i=n} h_i} \dots\dots\dots (3)$$

for a reservoir of n layers. The layers are arranged in order of decreasing permeability so that $m = 1$ is the layer with thickness h_1 and the largest permeability k_1 whereas $m = n$ is the layer with thickness h_n and the smallest permeability k_n . By definition, $0 \leq F_m \leq 1$ and $0 \leq H_m \leq 1$ for $1 \leq m \leq n$. Because of the layer ordering, the Lorenz plot monotonically increases from $m = 1$ to $m = n$ with a monotonically decreasing slope. If the medium is homogeneous, all the permeability values are identical and the Lorenz plot is a straight line. Increasing levels of heterogeneity are indicated by movement of the Lorenz plot away from the straight line.

The Lorenz procedure can be modified by including porosity in the calculation (Craig, 1971; Lake, 1989). In place of the cumulative thickness, H_m , the cumulative storage capacity, C_m , is used, or:

$$C_m = \frac{\sum_{i=1}^{i=m} \phi_i h_i}{\sum_{i=1}^{i=n} \phi_i h_i} \dots\dots\dots (4)$$

In this plot, a fraction of F_m is provided by a fraction of C_m of the reservoir. If porosity is constant, the Lorenz plot remains unchanged. The data must be arranged according to the ratio k/ϕ .

By analogy to the Lorenz plot, the flow capacity plot is formed using sets of λ 's and τ 's for a producer and nearby injectors. This requires revisiting the physical definitions of the λ and the τ , introduced by Yousef and others (2006b), to re-define the cumulative flow capacity (F_m) and cumulative storage capacity (C_m) in terms of model parameters.

The physical interpretation of the λ of an injector-producer (ij) pair is given by:

$$\lambda_{ij} = \frac{J_{ij}}{\sum_j J_{ij}} \dots\dots\dots (5)$$

where J is the partial productivity index and K is the total number of producers. This equation states that the ratio of the productivity between injector i and producer j to the sum of the productivity between the same injector and all producers is equal to the estimated weight between the (ij) well pair. Letting the dominator of Eq. 5 be constant, the λ is equivalent to $k_{ij}h_{ij}$ between the (ij) well pair. In other words, the λ quantifies the flow capacity between the (ij) well pair.

On another hand, the basic definition of the corresponding time constant is given by:

$$\tau_{ij} = \frac{c_{t_{ij}} V_{p_{ij}}}{J_{ij}} \dots\dots\dots (6)$$

where c_t , V_p , and J are the total compressibility, the pore volume and the partial productivity between the (ij) well pair, respectively. Based on their definitions, the λ and its corresponding τ are not totally independent because the λ is directly proportional to J and the τ is inversely proportional to the same J.

Because we desire another parameter that reflects only the storage capacity between the injector-producer pair, the λ multiplied by the corresponding τ provides this parameter, or:

$$\lambda_{ij} \tau_{ij} = \frac{c_{t_{ij}} V_{p_{ij}}}{\sum_j J_{ij}} \dots\dots\dots (7)$$

Similar to Eq. 5 by letting the dominator of Eq. 7 be constant, the $\lambda \times \tau$ quantifies the storage capacity between the well pair. Thus, the λ and its corresponding $\lambda \times \tau$ are independent where the λ quantifies the flow capacity and the $\lambda \times \tau$ quantifies the storage capacity for the medium between the same well pair.

Similar to Eqs. 2 and 4, the flow capacity curve is a plot of cumulative flow capacity (F_m) against cumulative storage capacity (C_m) where,

$$F_m = \frac{\sum_{i=1}^{i=m} \lambda_{ij}}{\sum_{i=1} \lambda_{ij}} \dots\dots\dots (8)$$

and

$$C_m = \frac{\sum_{i=1}^{i=m} \lambda_{ij} \tau_{ij}}{\sum_{i=1} \lambda_{ij} \tau_{ij}} \dots\dots\dots (9)$$

for producer j with I injectors. The data are arranged in order of decreasing $1/\tau_{ij}$ so that $i = 1$ is the injector-producer well pair with the smallest τ while $i = I$ is the injector-producer well pair with the largest τ . Because of the data ordering, the flow capacity curve monotonically increases from $i=1$ to $i = I$ with a monotonically decreasing slope.

The flow capacity plots can also be used to indicate specific geological features in the vicinity of an injector. In this case, sets of λ 's and τ 's for one injector and all producers are used to form the flow capacity plot.

The procedure, based on Lorenz plots, can make use of the extensive literature already available on the interpretation of such plots (Albertoni and Lake, 2003; Gunter and others, 1997; Cortez and Corbett, 2003).

2.2.2 The log-log plot

As discussed earlier, the λ and the corresponding τ are inversely related through the productivity index J . For homogeneous reservoirs where each producer communicates with all injectors, a log-log plot of λ 's against τ 's for each producer with all injectors should give a straight line of slope -1. As described in our previous work, the log-log plot of λ 's against τ 's estimated from a homogenous synthetic field gives an approximate straight line of slope -1. Compared to homogeneous reservoirs, the deviation of the λ 's and the τ 's estimated from non-homogeneous reservoirs will indicate specific geological conditions in these reservoirs.

2.3 Results

The technique was tested through its application to two synthetic fields and then to three real fields. The results of these applications are presented and discussed in this section.

2.3.1 Application to synthetic fields

This section provides new applications of the CM to synthetic fields with different geological features. The emphasis will be on the consistency of the estimated model parameters (λ 's and τ 's) with the imposed geology, and the capability of the flow capacity plots to indicate the geological conditions imposed in each case.

The BCM approach was applied to the same numerically simulated synthetic fields (Synfields) exhibited in Yousef and others (2006b): one of 5 injectors and 4 producers (the 5x4 Synfield) and a second of 25 injectors and 16 producers (the 25x16 Synfield). The 5x4 Synfield consists of five layers while the 25x16 Synfield consists of three layers. They both are flowing undersaturated oil. The injector-producer distance is 800 ft for the 5x4 Synfield and 890 ft for the 25x16 Synfield. The oil, water, and rock compressibility are 5×10^{-6} , 1×10^{-6} , and 1×10^{-6} psi⁻¹, respectively. The oil-water mobility is equal to one. Both synfields have only vertical wells. All producers BHP's are equal. The characteristics of the synfields are similar to those of the real case to which the techniques will be applied later.

2.3.1.1 5x4 Synfield. Several cases with different geological conditions were analyzed for this field. We used the same injection data provided in our previous work. These data were randomly selected from different wells in a real field and proportionally modified to be in agreement with the Synfield injectivity. The numerical simulation extends to $n = 100$ months, with $\Delta n = 1$ month.

2.3.1.1.1 Homogeneous reservoir. The first and simplest case is a homogenous reservoir with an isotropic permeability of 40 md. Because the total production rate is equal to the total injection

rate, the BCM approach is applied. This case was demonstrated and extensively discussed in Yousef and others (2006b) where the λ 's and the τ 's are estimated and represented. Tables 1 and 2 list the numerical values of the λ 's and the τ 's, respectively.

As mentioned earlier, the λ and the corresponding τ are inversely related through the productivity index component (J). The log-log plot of λ 's against τ 's estimated from the 5x4 homogenous Synfield gives an approximate straight line of slope -1 (Fig. 2). All the data lump in one single group, which indicates that all injectors communicate with producers through layers having the same properties.

The flow capacity plots are developed using sets of λ 's and τ 's for each producer and all injectors (Fig. 3). All flow capacity plots are near straight lines, which indicate that the Synfield is homogeneous. The straight line suggests that the fraction of the total flow capacity observed in a producer is equal to the fraction of the total storage capacity swept by injectors. This is a typical behavior of homogeneous, isotropic field. Similar to the flow capacity plot, the conventional Lorenz plot is a straight line when the reservoir is homogeneous where all the permeability values are identical.

2.3.1.1.2 High permeability layer. As commented earlier, the 5x4 Synfield consists of five layers. In this case, a set of injectors is completed in large permeability layers, and another set is completed in small permeability layers. The permeability of layer 5 (L5) is large and equal to 500 md; the permeabilities of other layers (L1-L4) are relatively small and equal to 10 md. The vertical permeability is 0.1 md. Injectors I01, I02, and I03 are completed in L1-L4, while injectors I04 and I05 are only completed in the L5. All producers are completed in all layers. Figure 4 shows the layers, the permeability, and the completions of all wells. All other parameters are similar to the 5x4 homogeneous Synfield (the base case).

The BCM was applied and the λ 's and τ 's were estimated. The match to the total production rate yields $R^2 = 0.997$. In Fig. 5, the λ_{ij} are represented by arrows or cones that start from injector i and point to producer j . The larger the arrow, the larger the value of the weight and the greater connectivity between the two wells. Similarly, Fig. 6 shows the same representation for τ_{ij} which the larger the arrow, the larger the value of the time constant and dissipation between the two wells.

The estimated λ 's are the same as the base case results (Fig. 7) in which the λ 's do not carry information about the high permeability layer (L5) or about the well completions. Because each reservoir layer is homogeneous and all producers are completed in all layers, the λ 's estimated in this case, based on their basic definition (Eq. 5) are independent from reservoir permeability and they are only function of distance between wells and their relative locations. This explains that the estimated λ 's in this application are the same as the base case results. However, the estimated τ 's of I04 and I05 are much smaller than that of I01, I02, and I03 (Fig. 6). This is consistent with the completions of injection wells where I04 and I05 are completed in the high permeability layer (L5), and other injectors are completed in the low permeability layers (L1-L4). Therefore, the τ 's give more insight about the geological conditions and completions imposed in this case than the λ 's.

The inconsistency between the both sets of parameters in describing the geological conditions imposed in this case makes the inference about geological conditions from the λ and τ values separately not easy. Thus, combining both sets of parameters in certain representations (e.g. the log-log plots, the flow capacity plots) could enhance the inference about the geological features.

Unlike the base case, the log-log plot of λ 's against τ 's estimated in this case naturally separate into two different groups where each group gives an approximate straight line of slope -1 (Fig. 8).

One group consists of parameters estimated with I04 and I05, and a second group includes parameters estimated with I01, I02, and I03. Since the estimated λ 's are the same as the base case results and the group of parameters associated with I04 and I05 is characterized by smaller τ 's than the group with other injectors, we conclude that I04 and I05 communicate with all producers through large permeability layers, while other injectors communicate through small permeability layers. This is consistent with the geological conditions imposed in this case. Therefore, the log-log plot of λ 's against τ 's enhance the inference about certain geological conditions than can not be easily identified using the λ and τ values separately.

Another representation to combine both sets of parameters is the flow capacity plot. The flow capacity plots are developed using sets of λ 's and τ 's for each producer and all injectors (Fig. 9). All flow capacity curves (dynamic F-C curves) are not straight lines, which indicate that the Synfield is not homogeneous. For each producer, the flow capacity plot indicates two distinct geological layers, as depicted by the two straight lines (Fig. 9). The first straight line with a large slope consists of I04 and I05, while the small slope straight line consists of I01, I02, and I03. Because the estimated λ 's are the same as the base case results, we conclude that I04 and I05 communicate with all producers through a high permeability layer while other injectors communicate with all producers through a small permeability layer. This is consistent with the geological conditions imposed in this case. Therefore, the flow capacity plots constructed from the λ 's as well as τ 's reveal certain geological features that can not be easily identified using the λ and τ values separately.

The static flow capacity curve estimated using permeability and porosity values of each grid block is depicted in Fig. 9. Similar to the dynamic F-C curves, the static F-C curve indicates two distinct geological conditions; however, the deviation shown by the static F-C curve from the homogeneous behavior is larger than that depicted by the dynamic F-C. The Lorenz coefficient (Schmalz and Rahme, 1950) (L_c) is a measure of movement or deviation of the F-C curve from the 45° line. If the medium is homogeneous, the flow capacity plot is the 45° line and consequently $L_c = 0$. Increasing the level of heterogeneity are indicated by movement of the flow capacity plot away from the 45° line with L_c increasing but always less than unity. For this case, the L_c for the static F-C curve is 0.7 while the L_c 's for the dynamic F-C curves of P01, P02, P03, and P04 are 0.2, 0.3, 0.3, and 0.5 respectively.

2.3.1.1.3 Fractures. Two fractures both with one grid-size thickness are introduced in this case: one fracture between I01 and P01 with permeability of 1000 md, and a second between I03 and P04 with smaller permeability (500 md). The rest of the Synfield is only 5 md. The two fractures extend to all layers and injectors and producers are completed in all encountered layers. All other parameters are similar to the base case.

The BCM was applied and the λ 's and τ 's were estimated. The match to the total production rate yields $R^2 = 0.997$. Figures 10 and 11 show the representations of the λ 's and the τ 's.

The λ 's between I01-P01 and I03-P04 are large, while the corresponding τ 's are very small. I01 and I03 mainly support P01 and P04, respectively (Fig. 10). This is consistent with the two fractures existing in this case. Also, the near injectors (I04 and I05) to P04 and I02 to P01 exhibit large λ 's, while the corresponding τ 's are relatively large (Fig. 11). Therefore, both sets of parameters reflect the heterogeneity of the field.

The log-log plot of λ 's against τ 's indicates three different groups (Fig. 12). Group 1, which includes the data for I01-P01 and I03-P04, reflects the two fractures existing in the field. Group 2 represents near well pairs with large λ 's and large τ 's, and Group 3 shows distant well pairs

with small λ 's and large τ 's. The data are very scattered, which indicates a large deviation from homogenous reservoir. All of these observations are consistent with the imposed geology.

The flow capacity plots of P01 and P04 show a large deviation from the 45° line (homogeneous reservoir) while the flow capacity plots of P02 and P03 do not reflect the heterogeneity of the field (Fig. 13). Because all injectors mainly support P01 and P04, the flow capacity plots of these producers will carry more insight about the imposed geology than that of other producers. This explains the small deviation of the flow capacity curves of P02 and P03 from the 45° line (homogeneous reservoir).

The flow capacity plots of P01 and P04 indicate two distinct geological conditions in the vicinity of these producers. In both plots, two straight lines can be fitted to the flow capacity curves; the first is steeper than the second one. For each plot, the steep straight line suggests that a large fraction of the total flow capacity is provided by a very small fraction of the total pore volume swept by the injectors, which is usually an indication of existing fractures in the vicinity of the corresponding producer. Because P01 and P04 are supported by I01 and I03 through fractures, their flow capacity plots decisively indicate these fractures by the steep straight line. Also, the first straight line in the flow capacity of P01 is much steeper than that of P04, which is consistent with the difference in permeabilities of the fractures. The second straight line in both plots suggests that a small fraction of total flow capacity is provided by a large fraction of the total volume of the field; this usually contributes from injectors communicating through the matrix of the reservoir.

The static flow capacity curve estimated using permeability and porosity values of each grid block is depicted in Fig. 13. Similar to the dynamic F-C curves of P01 and P04, the static F-C curve indicates two distinct geological conditions; however, the deviation shown by the static F-C curve from the homogeneous behavior is larger than that depicted by the dynamic F-C of the two producers. Thus, the L_c for the static F-C curve is 0.9 while the L_c 's for the dynamic F-C curves of P01 and P04 are 0.68, and 0.52, respectively.

Compared to the high permeability layer case, the first straight lines in both plots of P01 and P04 are much steeper than that observed in the high permeability layer case (Fig. 9). This indicates that the flow capacity plots are capable of identifying whether the connectivity of an injector-producer well pair is through a fracture or a high-permeability layer.

2.3.1.1.4 Producer with partial completion. In this case, P04 is only completed in layer 5 (L5), while the other producers and injectors are completed in all layers (L1-L5). All reservoir layers are homogeneous and have the same permeability (40 md). The vertical permeability is 0.4 md. All other parameters are similar to the base case.

The BCM was applied and the λ 's and the τ 's were estimated. The partial completion of P04 can be easily inferred from the λ 's representation (Fig. 14). The λ 's of all injectors with P04 are very small, which are consistent with small productivity observed in P04 because of its completion. However, the estimated τ 's are the same as the base case results where the τ 's do not carry information about the partial completion of P04 (Fig. 15). Because the pore volume (V_p) and the productivity (J) in the basic definition of the τ (Eq. 6) are both function of the pay thickness of the corresponding producer, the τ does not depend on the pay thickness (Raghavan, 1991; Ibragimov and others, 2005). Therefore, the estimated τ 's in this case are expected not to reflect the partial completion of P04.

The log-log plot of λ 's versus τ 's clearly indicates the partial completion of P04, represented by Group 2 (Fig. 16). Group 1 represents the parameters associated with other producers. However, all flow capacity plots do not indicate the partial completion of P04 (Fig. 17). This is

attributed to the definitions of the cumulative flow capacity (Eq. 8) and the cumulative storage capacity (Eq. 9). Because the λ 's are used in both equations and the geological conditions in this case are not reflected by the corresponding τ 's, the flow capacity plot for each producer usually shows a homogeneous reservoir flow capacity. Therefore, the flow capacity plot defined in this chapter is not able to indicate problems associated with completion of production wells.

2.3.1.2 25x16 Synfield. Two cases are studied for this field: a homogeneous reservoir and reservoir with different sealing faults. We used a randomly generated injection data. The numerical simulation extends to $n = 415$ months, with $\Delta n = 1$ month (Yousef and others, 2006b; Yousef, 2006).

2.3.1.2.1 Homogeneous reservoir. This case was extensively discussed in our previous work where the λ 's and the τ 's are estimated and represented. The applications of the log-log plot and the flow capacity plot give the same results as that of the 4x5 homogeneous Synfield (Yousef, 2006).

2.3.1.2.2 Presence of sealing faults. In this case, four different sealing faults divide the entire reservoir into five isolated compartments. All layers are homogeneous and have the same permeability (40 md). Wells are completed in all encountered layers. Other parameters are similar to the 25x16 homogeneous Synfield.

Figures 18 and 19 show the results for the BCM applied for this case. Results are just as expected. The presence of sealing faults can be easily inferred from the λ 's and the τ 's representations. The values of λ corresponding for well pairs located in different compartments are close to zero, while the corresponding values of τ for the same well pairs are very large. This shows no communication between these wells, which is consistent with the presence of the sealing faults.

The log-log plot of λ 's versus τ 's indicates two different groups (Fig. 20). Group 1 reflects the values of λ and τ for well pairs located in the same compartment. This group is characterized by relatively large λ 's and small τ 's. Group 2, characterized by very small λ 's ($\lambda < 0.03$) and very large τ 's, includes the values of λ and τ for well pairs located in different compartments. All of these observations are consistent with the presence of the sealing faults.

All flow capacity plots indicate two distinct geological conditions. The flow capacity plots for the four center producers (P06, P07, P10, P11) and the outer producers (P01, P04, P13, P16) are only shown in Figs. 21 and 22, respectively. The first straight line, parallel to the 45° line, represents a homogeneous reservoir flow capacity. Because each compartment is homogeneous and the first straight line in each plot includes the model parameters for well pairs located in the same compartment, this straight line represents the fraction of total flow capacity provided by well pairs located in the same compartment. However, the straight line with flat behavior indicates that a fraction of the total storage capacity provides a negligible fraction of the total flow capacity. This is a typical aspect of presence of a reservoir seal. Therefore, all flat straight lines decisively indicate presence of the sealing faults in the vicinity of producers.

2.3.2 Application to field data

The technique was applied to three different sets of field data. The results of these applications are presented and discussed in this section. Unlike the Synfield applications we have no concrete standards (e.g., agreement with imposed geology) against which to compare results. Our truth test will be comparison against known geological features as much as possible.

2.3.2.1 The first real field application. The technique was applied to a portion (18 injectors and 13 producers) of the South Wason Clearfork (SWCF) Field in West Texas. The reservoir is primarily dolomite and the average porosity and permeability are 6 % and 4 md, respectively. Waterflooding began in 1980 where the initial waterflood pattern was inverted nine-spot, and then was converted to five-spot pattern in 1987. Fractures were observed in the SWCF injectors, which typically exist in carbonate reservoirs (Burbank, 1992). Since only a portion of the field was analyzed and the boundaries are open, the UCM approach is applied.

The data selected for the analysis was determined by examining the production, and injection rates and the producing gas oil ratio (GOR) of the SWCF field. The GOR was large when the waterflood started. By month 70, the GOR was at a minimum and approximately equal to the solution gas-oil ratio, which indicates that the hydrocarbon in the reservoir is single-phase. Also, injection and production rates are in acceptable balance. However, the GOR fluctuated after month 137. Therefore, the analysis is carried out using the data starting in month 70 until month 137 which left 68 data points for the analysis. With this short injection and production data and 18 injectors, we know in advance that we will obtain suboptimal results and the estimated λ 's will be imprecise. Moreover, the open boundaries introduce errors in the estimation of the λ 's and some of the assumptions of the technique are not completely met. However, some general features can be inferred from the application of UCM model to the SWCF field data.

Figures 23 and 24 show representations of the positive λ 's and the τ 's, respectively. The injection wells in the north and the west of the field have smaller λ 's than those in the south-east. The interwell connectivity improves from the north-west to the south-east. Three injectors (7501, 7502, and 7505) mainly seem to have little influence on inner producers. Also, producers 7518, 7528, 7526, 7520 and 7540 appear to be unsupported. Injectors 7532, 7507, and 7506 predominantly exhibit much larger connectivity with producers in the south-east of the field than that of other injectors. With knowing that the field is very heterogeneous and also has very small average permeability (4 md), the estimated τ 's initiated from these injectors (Fig. 24) are relatively smaller than the ones observed in the synthetic field applications with permeability less than 5 md (Yousef, 2006). All of these observations suggest that these injectors communicate with producers through high permeability layers, or most likely through fractures.

We investigated this issue by use the log-log plot of λ 's versus τ 's. The log-log plot of λ 's versus τ 's for all wells shows that the λ and the corresponding τ are not inversely related, which is expected since the reservoir is not homogeneous (Fig. 25). Two groups can be determined according to the spread in τ . Group 1, characterized by very small τ , indicates that certain injectors communicate with producers through high permeability layers or through fractures while Group 2, described by large τ , indicates that well pairs communicate through the matrix of the reservoir.

Figure 26 shows the flow capacity plots for producers supported by the three injectors (7532, 7507, and 7506). By comparing these flow capacity plots, especially for produces 7516 and 7519, with the ones observed in synthetic case where one or more injector-producer pairs communicate through a fracture (see 5x4 Synfield with fractures), we are tempted to conclude that fractures exist in the vicinity of these two producers, or the key injectors (7506, 7507, and 7532) communicate to producers 7516 and 7519 through fractures. However, the flow capacity plots of producers 7524, 7521, and 7513 do not reflect heterogeneity. This is attributed to the open boundaries effect. To validate any of these observations would require other data.

The fits to the production data are relatively good. For example, the R^2 for producers 7516 and 7519 are 0.923 and 0.937, respectively.

2.3.2.2 The second real field application. The UCM was applied as well to a portion (8 injectors and 12 producers) of the North Buck Draw (NBD) Field in Wyoming. The reservoir average porosity is 9.5 %, and the average permeability is 10.7 md. The reservoir fluid is near-volatile oil; fluid properties fall between those of black and volatile oils. The fluid meets the majority of volatile-oil criteria, including large oil formation volume factors and solution gas-oil ratios. The bubblepoint pressure is 4680 psia, and the reservoir fluid is a single-phase, low-viscosity fluid above this pressure (Sellars and Hawkins, 1992).

The field commercial production began in June 1983. In 1988 a pressure maintenance project was initiated by injecting gas. Since the field is undergoing gas injection, the reservoir total compressibility is very large and is not constant, which violates one of the main assumptions of the technique, slightly compressible fluids. However, if the product of $c_i \Delta p$ is much smaller the one, the assumption of the slightly compressible fluids will be attained. In this situation, the technique will provide reasonable λ 's while the estimated τ 's will indicate the dissipation associated with large compressibility.

The data selected for the analysis was determined by the same procedure used in the application of the UCM to SWCF field. However, the GOR increases with gas injection, as expected. The analysis is carried out using the data starting in month 35, which left 56 data points for the analysis. Because the reservoir total compressibility is large, the inference procedure most likely will not be able to indicate the connectivity between distant injector-producer pairs. Therefore, the UCM approach is applied to producers and only their adjacent injectors.

Figure 27 shows the representation of the positive λ 's. The injection wells in the west of the field have larger λ 's than those in the east. Producers 33-6, 31-7, and 33-7 appear to be unsupported. The orientation of the λ 's in wells 13-18, 11-18, and 12-7 indicate that the connectivity north-south direction is better than that of other directions.

Radioactive tracers were injected into the reservoir, and their occurrence was monitored at the producing wells from February 1989 until March 1993. Refunjol and Lake (1997) applied Spearman analysis to determine preferential flow trends in the NBD field and compared the results with injected tracer response. They related injection wells with their adjacent producers and used time lags to find an extreme coefficient (r_s).

Because the Spearman correlation coefficient (r_s) is another measure of the connectivity between injector-producer pair, a comparison between the r_s 's and the λ 's should provide a relation that is consistent with interwell connectivity between well pairs. When the two parameters are positive, the r_s tends to be larger than the corresponding λ . Similarly, the r_s is larger when both parameters are negative. Thus, the estimated λ 's are more sensible than the r_s 's in describing the connectivity between well pairs.

Figure 28 shows representations of the estimated τ 's, the Spearman time lags, and the tracer response breakthrough times. The orientation of the τ 's in wells 13-18, 11-18, and 12-7 suggest that the dissipation in the north-south direction is relatively smaller than that of other directions, which is in agreement with the orientation of the corresponding λ 's in these wells (Fig. 27).

Because the tracer response breakthrough times are considered real field measurements, we use them as a base for validating the τ 's and the Spearman time lags. For injector 23-8, the estimated τ 's are in agreement with the tracer response breakthrough times observed in the surrounding producers. For injector 11-18 and producer 33-7, Refunjol and Lake (1997) reported maximum r_s of 0.8 with 13 months time lag while the UCM estimates λ of 0.1 and τ of 0.1 month for the same well pair. Because the tracer response was not observed in producer 33-7, we are

tempted to conclude that the capacitance model results are more accurate than that of the Spearman analysis. Similar situation can be noticed for injector 31-7 and producer 23-8.

Figure 29 shows the flow capacity plots for some producers in the NBD field. The flow capacity plots for producers 33-18, 33-7, and 31-18 indicate certain geological features in the surrounding area of each producer. These plots indicate two different geological features in which certain injectors communicate with the corresponding producer through fast flow paths or high permeability layers and the other injectors communicate through slow flow paths or low permeability layers. The flow capacity plots for the other producers (33-6, 33-13, and 13-7) do not carry information about the medium between these producers and the corresponding injectors. To validate any of these observations would require other data.

The fit to the production data are relatively good. For example, the R^2 for producers 13-7 and 33-12 are 0.942 and 0.974, respectively.

2.4 Discussion

From applications of the CM exhibited in this work and others described in Yousef (2006), we can identify specific trends of the flow capacity curve according to the corresponding geological feature present in the surrounding area of a producer. To illustrate this point, Fig. 30 shows three curves of the flow capacity plot estimated from sets of λ 's and τ 's. The first curve indicates a presence of fractures in the drainage volume of a producer represented by the steeper segment of the curve; the second indicates that certain injectors communicate with producer through high permeability layers and the other injectors communicate through low permeability layers. For the last curve, the flat behavior shows that a fraction of the total storage capacity or the total pore volume swept by injectors provides a negligible fraction of the total flow capacity. This is a typical aspect of nonpay zone or a reservoir seal.

However, there are cases where the flow capacity plots are not able to reflect the geological conditions present in the vicinity of the producer. As discussed earlier, the flow capacity plot can not identify the partial completion of a producer even though this can be easily inferred from the model parameters (λ 's and τ 's). As commented before, this is attributed to the definitions of the cumulative flow capacity (Eq. 8) and the cumulative storage capacity (Eq. 9) where both of them are function of the connectivity parameters (λ). In this case, the flow capacity plot will indicate a homogeneous flow capacity.

On another hand, the log-log plot of λ 's versus τ 's shows consistency with imposed geology in the application to synthetic fields where distinct groups corresponding to different geological conditions can be easily identified. In the application to real field data, the scattered in the data is large where distinct groups of data are not easily determined. The large scattered in the data is attributed to the typical heterogeneity of real fields.

Because the flow capacity plots are based on inferred parameters (λ 's and τ 's) from dynamic data (injection and production), different sources of error can render the inference about geological conditions. The possible sources of error are deviation from the assumptions on which the CM is based, correlation between injection rates and using short assessment interval, and the quality of injection and production rate measurements (Yousef and others, 2006b; Yousef, 2006).

2.5 Conclusions

The capacitance model τ 's and λ 's can be combined to enhance inference about preferential transmissibility trends and the presence of flow barriers. Complex geological conditions are often not easily identified using the λ and τ values individually. However, combining both sets of

parameters in certain representations enhances the inference about the geological features. Two different representations are used: one representation is the log-log plot of the λ 's against the τ 's for a producer and nearby injectors; another representation is the flow capacity plot where the λ 's and the τ 's are combined using the idea of Lorenz plots. Both of representations enhance the inference about specific geological features in the vicinity of a producer.

The synthetic field applications show that the relation between the λ 's and the corresponding τ 's are consistent with known heterogeneity, the distance between wells, and their relative positions. The flow capacity plots and the log-log plots are capable of identifying whether the connectivity of an injector-producer well pair is through fractures, a high-permeability layer, or through partially completed wells.

The technique was first applied to data from the South Wasson Clear Fork Field in West Texas. Knowing that the field is very heterogeneous and also has very small permeability, the estimated time constants between the key injectors and certain producers indicate that these injectors communicate with producers through high permeability layers, or most likely through fractures. The flow capacity plots and the log-log plot of λ 's versus τ 's confirm the existing of fractures in the vicinity of some producers. The verification of these results would require other data; however, fractures typically exist in carbonate reservoirs.

Finally, the technique was applied to the North Buck Draw Field. Even though the field is undergoing gas injection, the estimated time constants indicate the dissipation associated with large compressibility. Compared to the tracer results, the capacitance model results are more accurate than that of the Spearman analysis. The flow capacity plots indicate that certain nearby injectors communicate with some producers through fast flow paths and other injectors communicate through low permeability layers. Verification of such results would require other data.

2.6 Tables and Figures

Table 1: The weights λ_{ij} for 5x4 homogenous Synfield.

	P01	P02	P03	P04
I01	0.33	0.33	0.17	0.17
I02	0.33	0.17	0.33	0.17
I03	0.25	0.25	0.25	0.25
I04	0.17	0.33	0.17	0.33
I05	0.17	0.17	0.33	0.33
λ_p	1.00	1.00	1.00	1.00

Table 2: The time constants τ_{ij} (month) for 5x4 homogenous Synfield.

	P01	P02	P03	P04
I01	0.60	0.59	0.81	0.80
I02	0.65	0.86	0.61	0.84
I03	0.66	0.62	0.63	0.62
I04	0.79	0.62	0.81	0.61
I05	0.81	0.81	0.62	0.62
τ_p	0.00	0.00	0.00	0.00

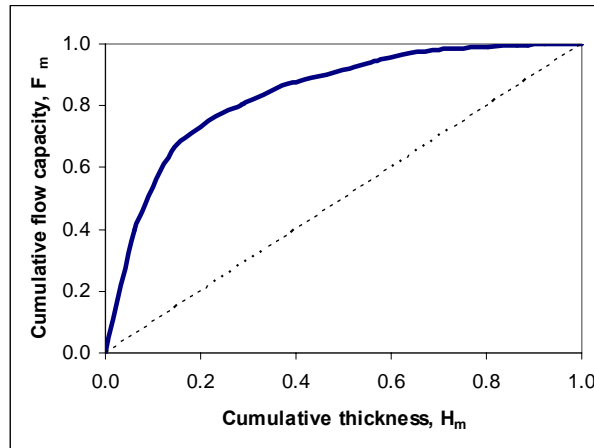


Figure 1: Cumulative flow capacity versus cumulative thickness. A schematic of the conventional Lorenz plot. The dashed line represents the 45° line.

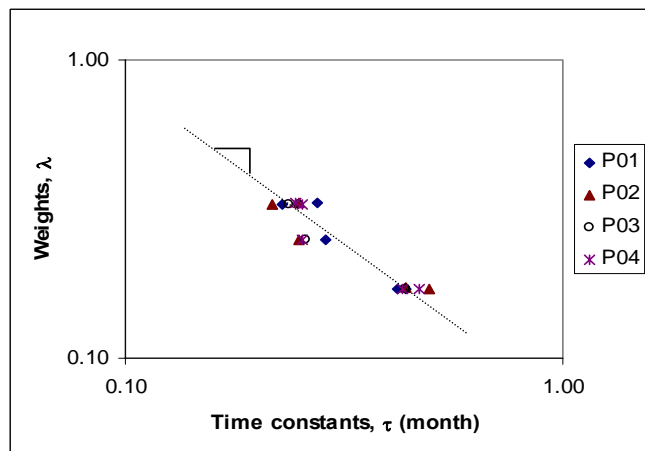


Figure 2: Log-log plot of λ 's versus τ 's with a slope of approximately -1. 5x4 homogeneous Synfield.

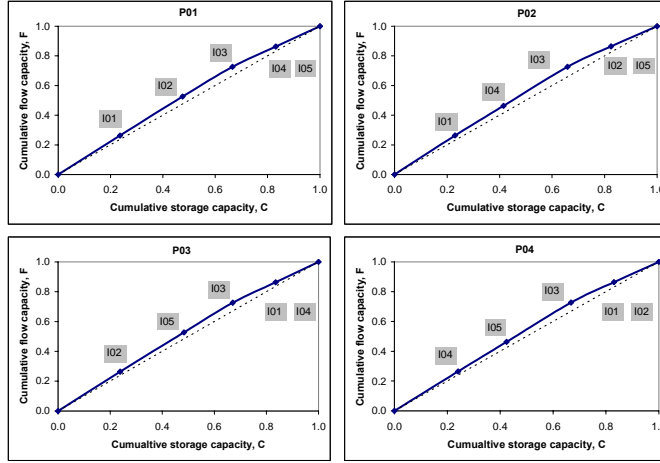


Figure 3: The flow capacity plots for all producers. The dashed line presents the 45° line. 5x4 Synfield, homogeneous reservoir.

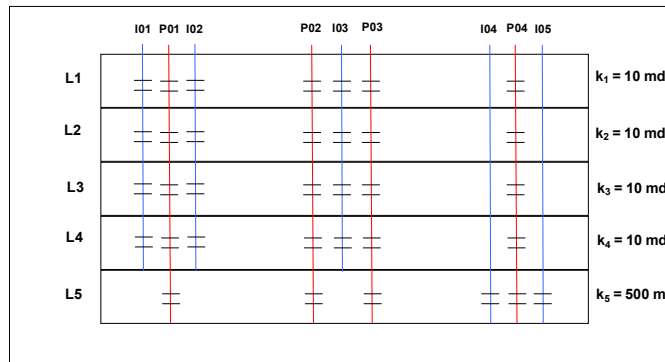


Figure 4: The layers, the permeabilities, and the well completions. 5x4 Synfield, high permeability layer.

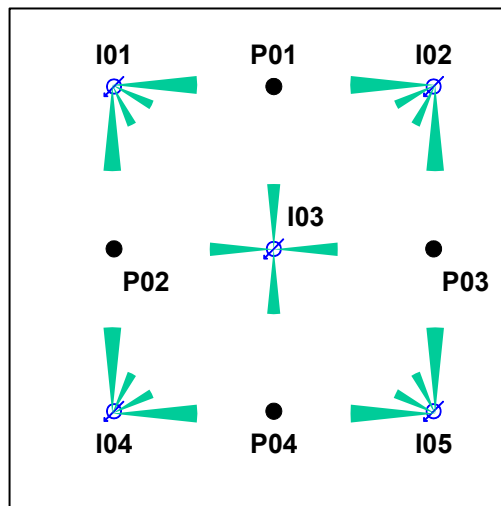


Figure 5: Representation of the weights λ_{ij} . The length of the arrow is proportional to the value of the weight. 5x4 Synfield, high permeability layer.

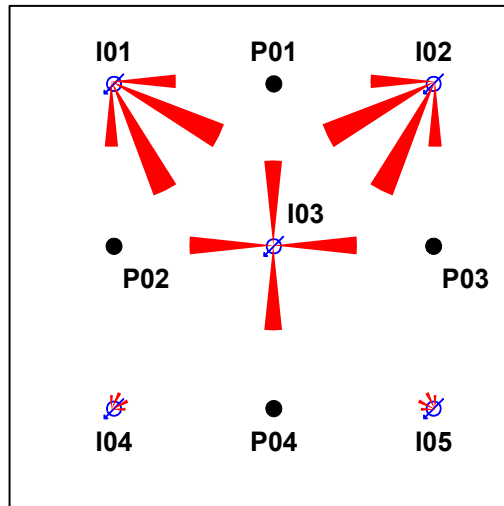


Figure 6: Representation of the time constants τ_{ij} (month). The length of the arrow is proportional to the value of τ . 5x4 Synfield, high permeability layer.

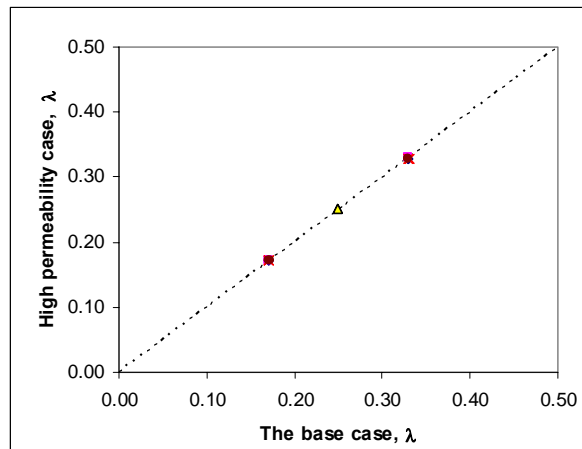


Figure 7: A crossplot of the λ 's estimated from the high permeability layer case against the λ 's estimated from the 5x4 homogeneous Synfield (the base case). The dashed line represents the 45° line. 5x4 Synfield, high permeability layer.

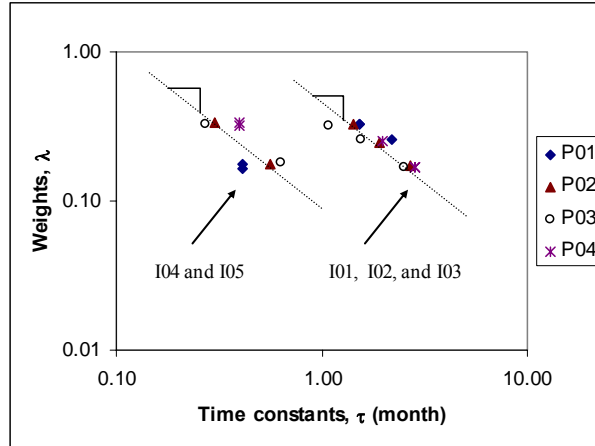


Figure 8 Log-log plot of λ 's versus τ 's. The data separate into two groups where each group gives an approximate straight line of slope -1. 5x4 Synfield, high permeability layer.

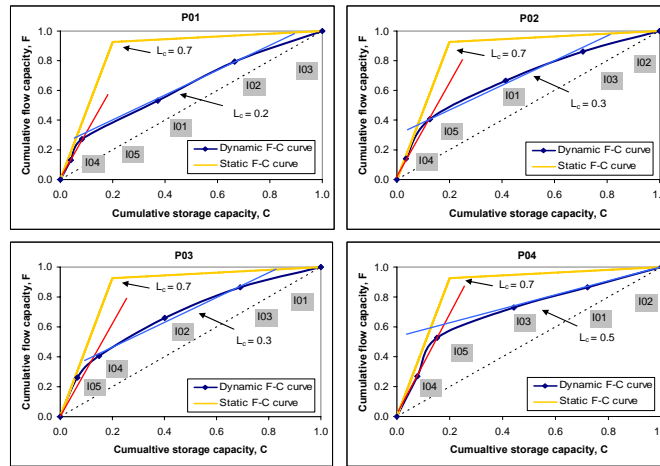


Figure 9: The flow capacity plots for all producers. Each plot shows two different geological layers represented by two straight lines. The dashed line presents the 45° line. The static flow capacity curve of the field is also depicted in each plot. The L_c is the Lorenz coefficient. 5x4 Synfield, high permeability layer.

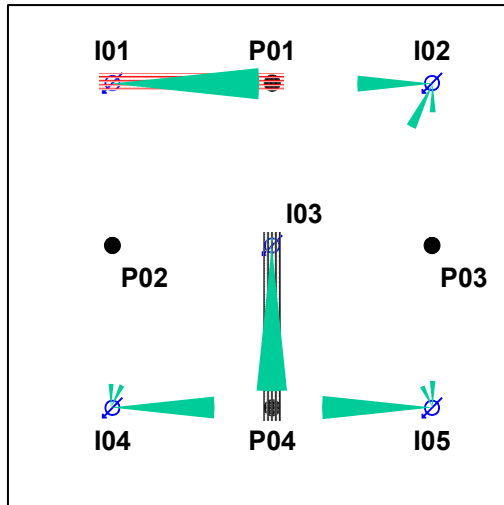


Figure 10: Representation of the weights λ_{ij} . The length of the arrow is proportional to the value of λ . The shaded areas represent the fractures. 5x4 Synfield, fractures.

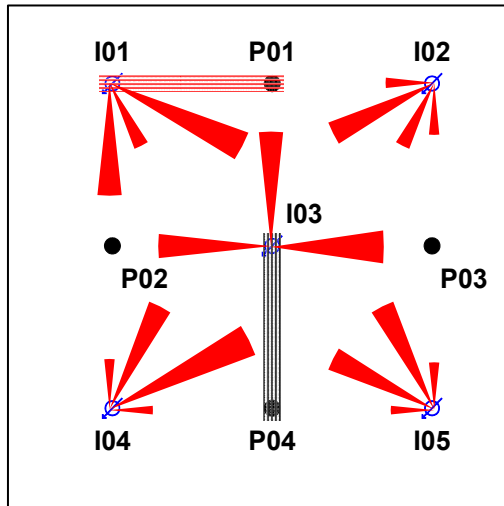


Figure 11: Representation of the time constants τ_{ij} (month). The length of the arrow is proportional to the value of τ . The shaded areas represent the fractures. 5x4 Synfield, fractures.

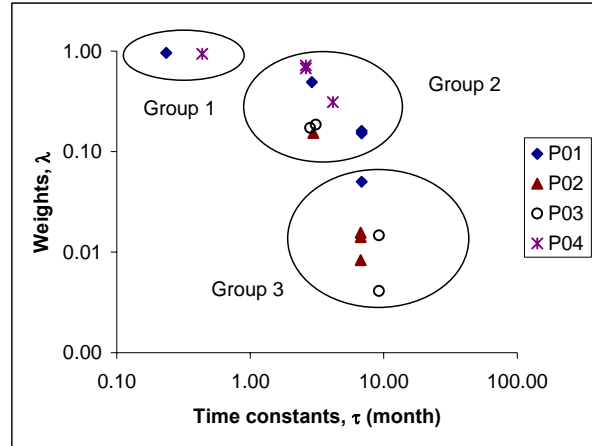


Figure 12: Log-log plot of λ 's versus τ 's. The data indicate three groups. 5x4 Synfield, fractures.

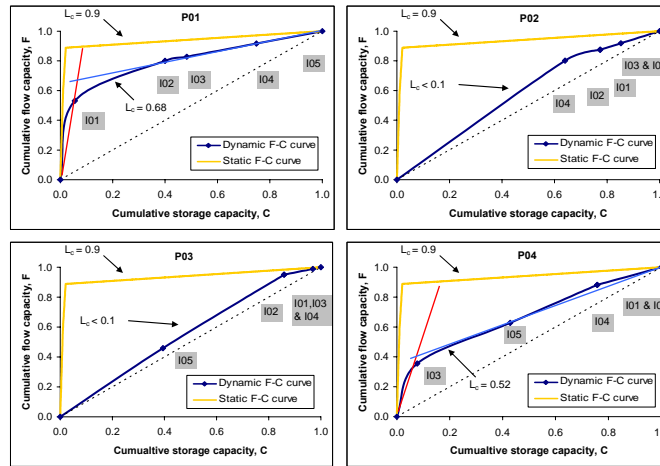


Figure 13: The flow capacity plots for all producers. The plots of P01 and P04 show two distinct geological conditions represented by the two straight lines. The dashed line presents the 45° line. The static flow capacity curve of the field is also depicted in each plot. The L_c is the Lorenz coefficient. 5x4 Synfield, fractures.

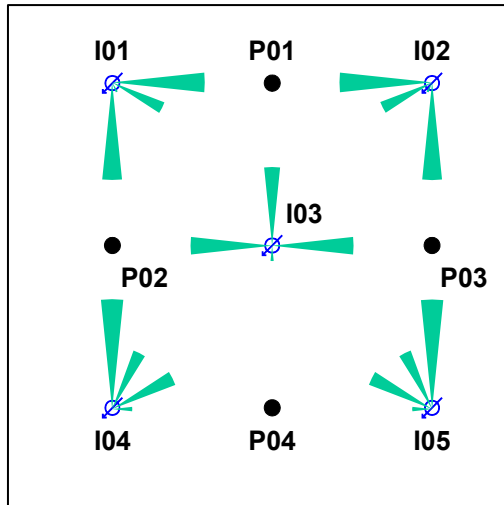


Figure 14: Representation of the weights λ_{ij} . The length of the arrow is proportional to the value of λ . 5x4 Synfield, producer with partial completion.

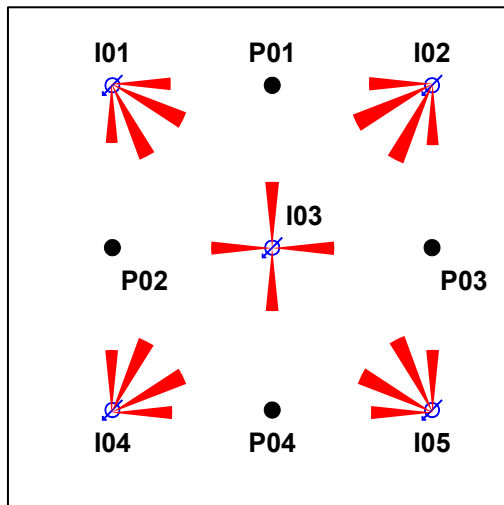


Figure 15: Representation of the time constants τ_{ij} . The length of the arrow is proportional to the value of τ . 5x4 Synfield, producer with partial completion.

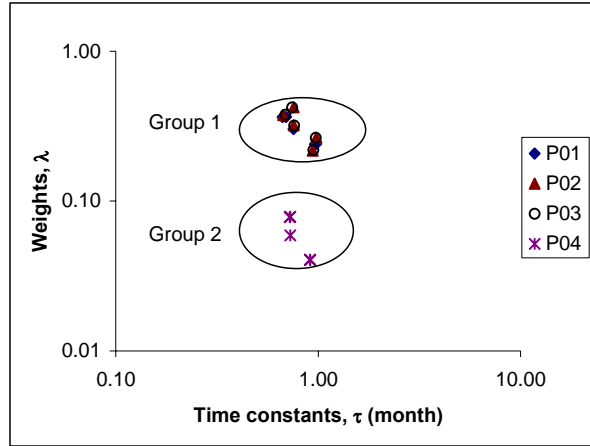


Figure 16: Log-log plot of λ 's versus τ 's. The data indicate two distinct groups. 5x4 Synfield, producer with partial completion.

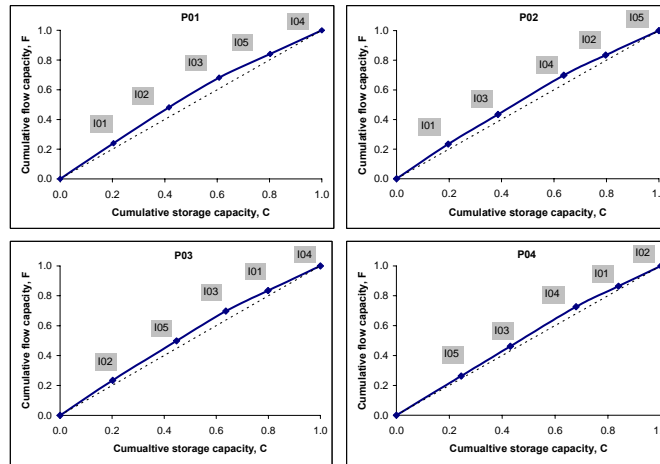


Figure 17: The flow capacity plots for all producers. All plots show a homogeneous reservoir flow capacity. The dashed line presents the 45° line. 5x4 Synfield, producer with partial completion.

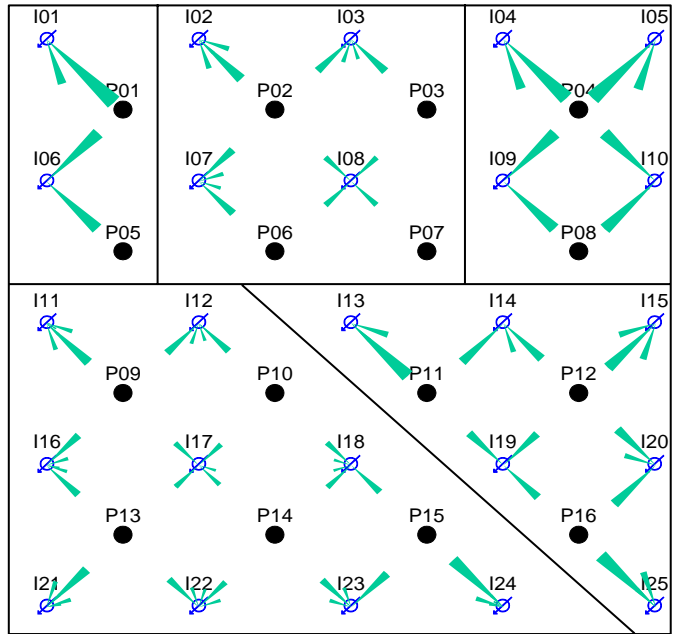


Figure 18: Representation of the weights λ_{ij} . The length of the arrow is proportional to the value of λ . The solid black lines represent the imposed faults. 25x16 Synfield, reservoir with sealing faults.

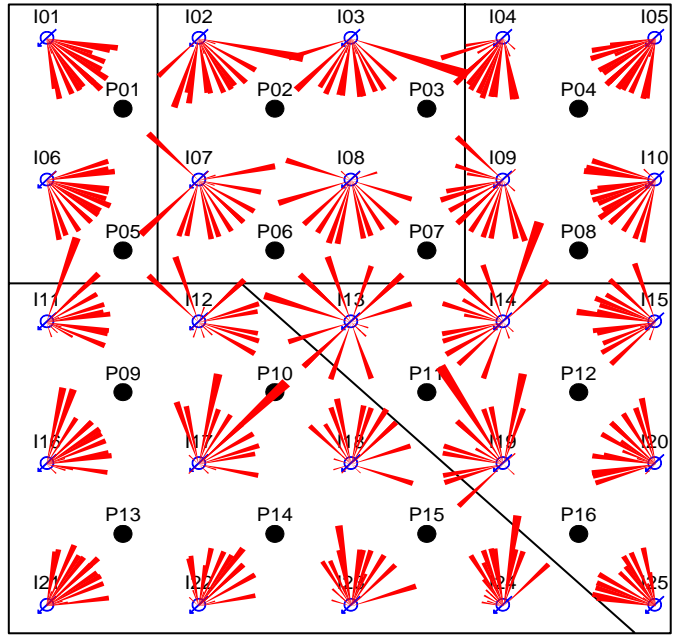


Figure 19: Representation of the time constants τ_{ij} . The length of the arrow is proportional to the value of τ . The solid black lines represent the imposed faults. 25x16 Synfield, reservoir with sealing faults.

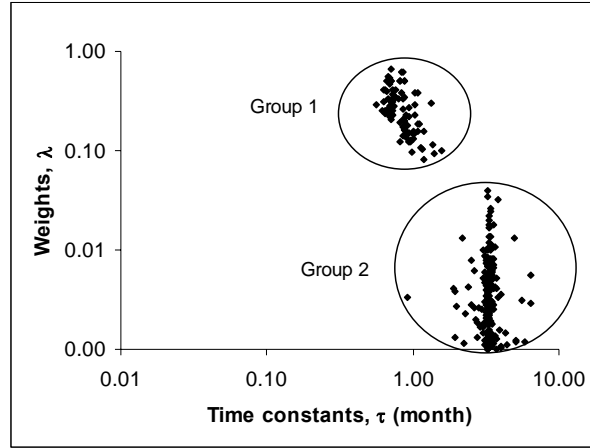


Figure 20: Log-log plot of λ 's versus τ 's for all producers. The data indicate two distinct groups. 25x16 Synfield, reservoir with sealing faults.

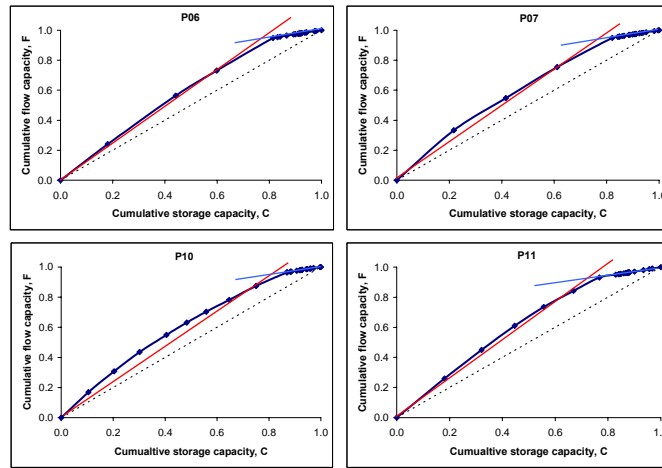


Figure 21: The flow capacity plots for the four center producers. All plots show two distinct geological conditions represented by the two straight lines. The dashed line presents the 45° line. 25x16 Synfield, reservoir with sealing faults.

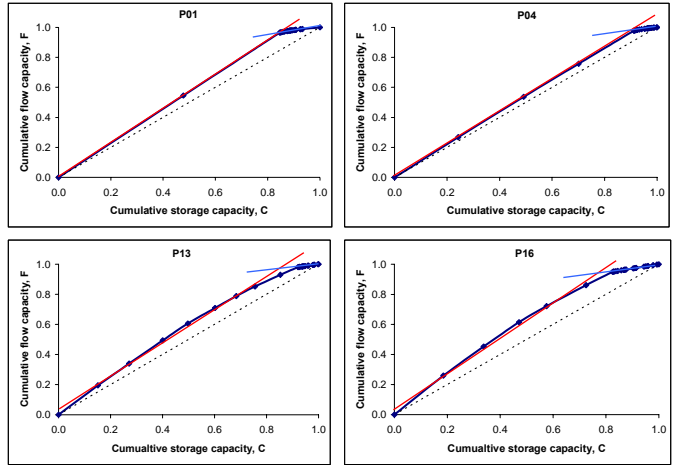


Figure 22: The flow capacity plots for the outer producers. All plots show two distinct geological conditions represented by the two straight lines. The dashed line presents the 45° line. 25x16 Synfield, reservoir with sealing faults.

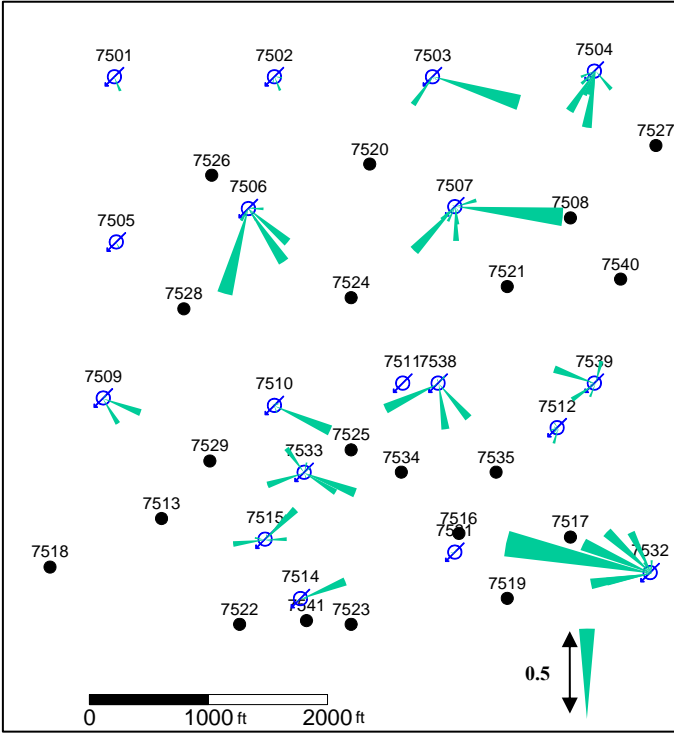


Figure 23: Application of UCM to the SWCF field. Representation of the positive λ 's.

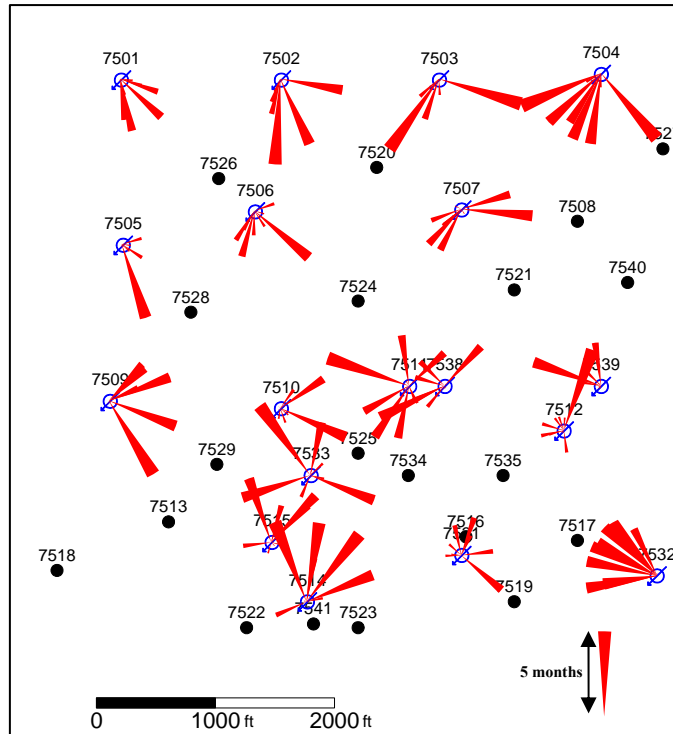


Figure 24: Application of UCM to the SWCF field. Representation of the τ 's (month).

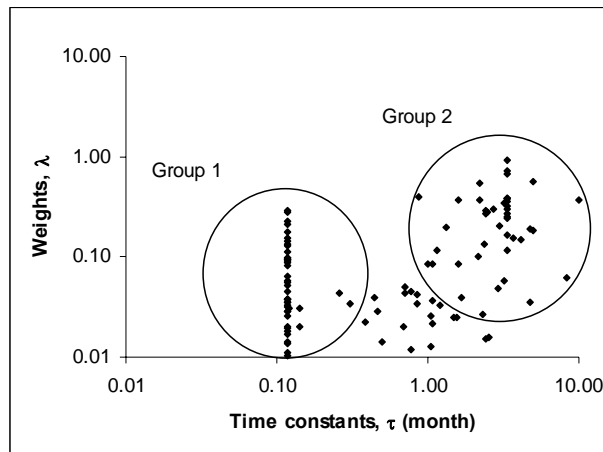


Figure 25: Log-log plot of positive λ 's versus τ 's for all producers in the SWCF field. The data indicate two groups.

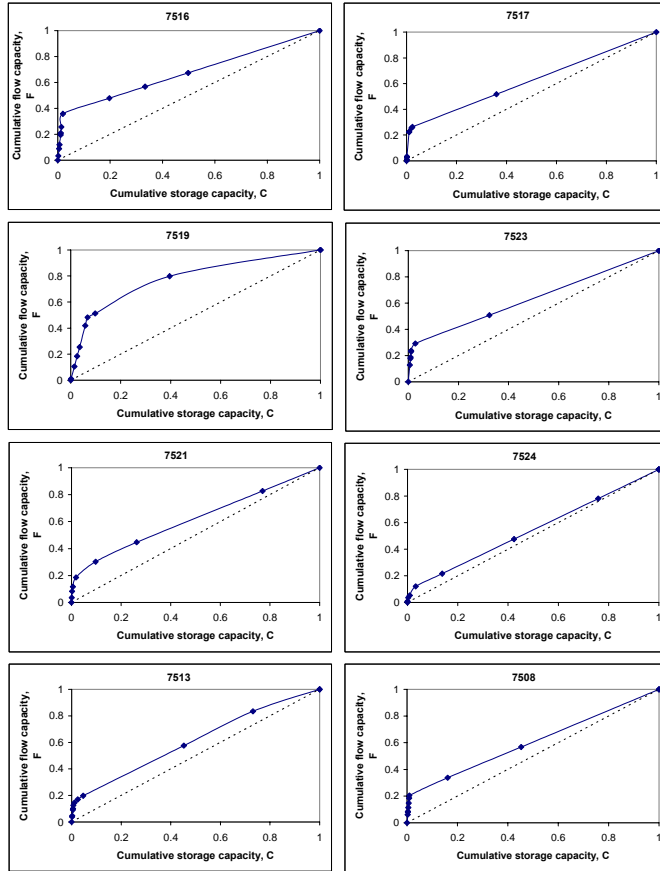


Figure 26: The flow capacity plots for producers well supported by injectors 7506, 7507, and 7532. The SWCF field.

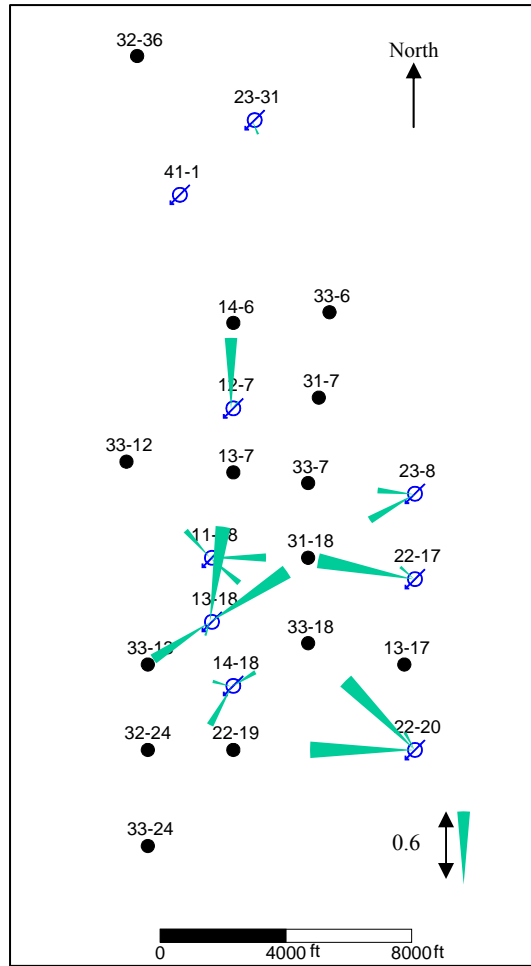


Figure 27: Application of UCM to the NBD field. Representation of the positive λ 's.

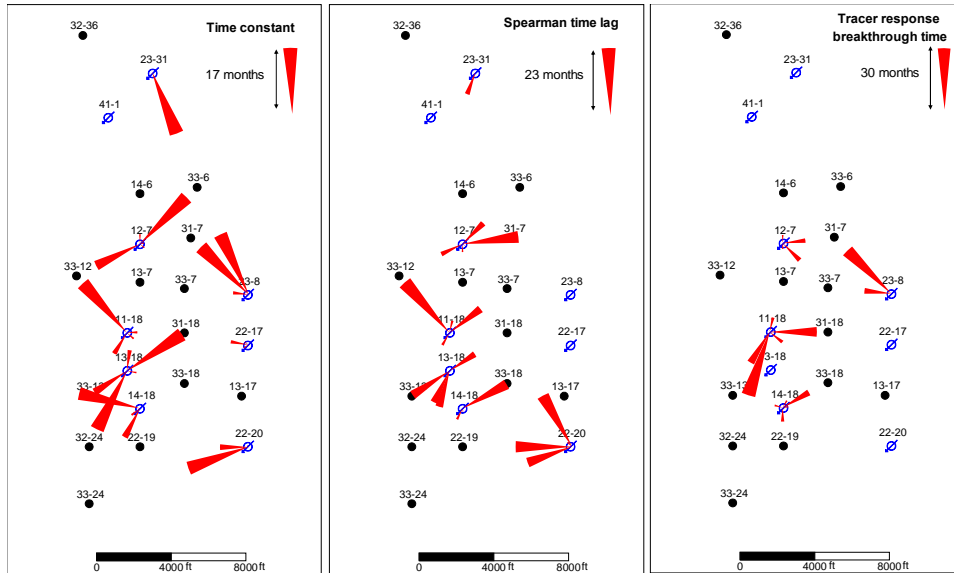


Figure 28: The time constants (τ 's), the Spearman time lags, and the tracer response breakthrough times for the NBD field. The first plot is for the τ 's, the second plot is for the Spearman time lags reported by Refunjol and Lake (1997), and the third plot is for the tracer response breakthrough times reported by Refunjol and Lake (1997).

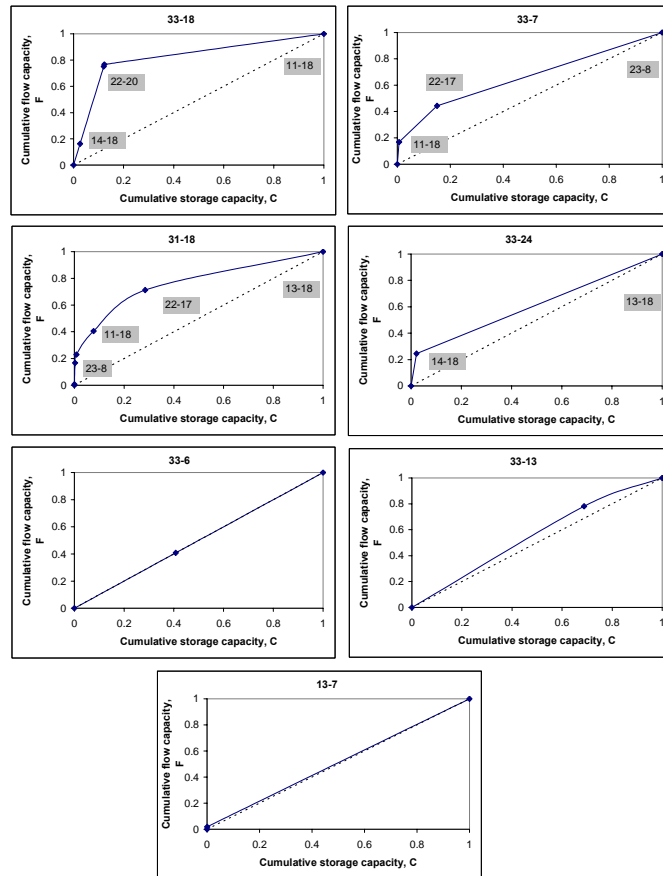


Figure 29: The flow capacity plots using the CM results for some producers in the NBD field.

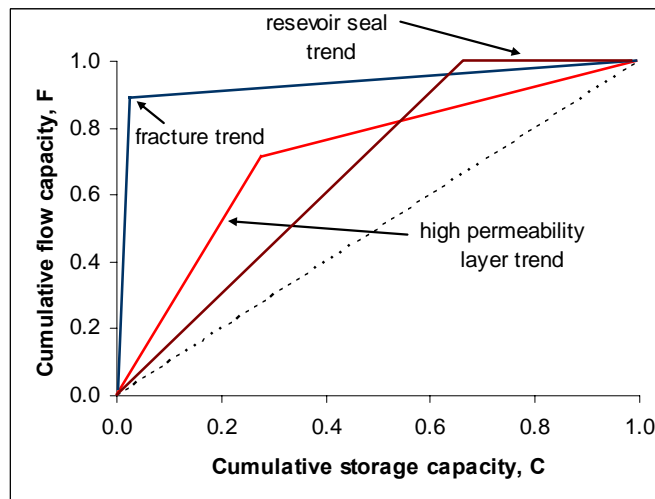


Figure 30: Different trends of the flow capacity curve estimated from the CM parameters according to the corresponding geological feature present in the vicinity of a producer.

RESULTS AND DISCUSSION

PART 3. WATERFLOOD OPTIMIZATION USING THE CAPACITANCE MODEL

3.1. Introduction

Managing production of an oil reservoir to maximize the future economic return of the asset is very important. The techniques to analyze past performance and then to predict the future vary from an educated guess to complex numerical approximations. Most models rely on fitting or matching of historical data.

In petroleum reservoirs, oil production is often constrained by the reservoir conditions, flow characteristics of the pipeline network, fluid-handling capacity of surface facilities, safety and economic considerations, or a combination of these considerations (Kosmidis and others, 2004; Wang and others, 2002a). While adjusting well production rates and allocating water-injected rates can control production, implementation of these controls in an optimal manner is difficult. Determination of the optimal operating conditions at a given time, subject to all constraints, is the objective of dynamic oil production optimization. This requires simultaneous consideration of the interactions between the reservoir, the wells, and the surface facilities. Typically, one maximizes the oil production rates or minimizes production costs.

Various aspects of oil production optimization have been addressed (Kosmidis and others, 2004; Wang and others, 2002a; Kosmidis and others, 2005) and can be classified into three categories: (1) sensitivity analysis using simulation, (2) heuristic methods, and (3) mathematical programming methods. Using heuristic rules and single well analysis, Barnes and others (1990) and Stoisits and others (1992) have studied the allocation of a limited amount of available gas lift wells. Martinez and others (1994) and Buitrago and others (1996) applied various mathematical programming techniques such as quasi-Newton and genetic algorithms. Fang and Lo (1996) proposed a linear programming model based on separable programming techniques to allocate gas lift and well rates subject to multiple flow rate constraints. Dutta-Roy and Kattapuram (1997) analyzed a gas lift optimization problem with two wells sharing a common flow line. They pointed out that when flow interactions among wells are significant, nonlinear optimization tools are required. Litvak and others (1997) developed an integrated reservoir and pipeline network model and employed heuristic rules to allocate well connections to manifolds. Wang and others (2002b) proposed a linear programming model for a well scheduling problem. To consider the allocation of wells to manifolds, they developed a partial enumeration procedure where only a subset of wells was allowed to switch to different manifolds.

Production and injection rates are the most abundant data available in any injection project. One can analyze these data to obtain information about interwell connectivity. The resulting information may be used to optimize subsequent oil recovery by changing injection patterns, assigning priorities in operations, recompletion of wells, and in-fill drilling.

Several methods have been used to compare the performance of a producing well with that of surrounding injectors. Albertoni and Lake (2003) used a linear model to estimate interwell connectivity in a reservoir using only total production and injection rate data. The coefficients estimated by multiple linear regressions quantitatively indicate the communication between producer and injectors in a waterflood. Filters were adopted to account for time lags between producer and injector.

Gentil (2005) explored the physical meaning of the weights and proposed a new way to interpret them. These insights are used to better understand the underlying assumptions of the model used by Albertoni and Lake and to construct a procedure for incorporating production data into geostatistical permeability distribution models.

Yousef and others (2006b) used a more complicated model than those in Albertoni and Lake (2003) and Gentil (2005) that includes capacitance (compressibility) as well as resistive (transmissibility) effects. Two coefficients are determined for each injector-producer pair: one parameter (a weight) quantifies the connectivity and the other (a time constant) quantifies the degree of fluid storage between the wells.

None of the previous papers provide an optimization procedure that optimizes the value of oil produced and the cost of the water injected or the water disposal cost. As a result, to optimize performance, oil production rates and water injection rates must be optimized simultaneously with well interconnections. The corresponding optimization problem is considered in this work.

As in Albertoni and Lake (2003), Gentil (2005) and Yousef and others (2006b), the reservoir is considered as a system that converts inputs (monthly injection rates) into outputs (monthly oil and water production rates). Compared with Yousef and others (2006b), a simpler capacitance model is considered first, where weights are calculated to indicate the connectivity between each injector-producer pair and time constants are determined to indicate the degree of fluid storage around each producer. Based on a power law relationship between the instantaneous water-oil ratio and the cumulative water injected, an oil production model with parameter pair a and b for each producer is then proposed. Our models and optimization formulation have been applied to numerically simulated data (Eclipse model) on a heterogeneous synthetic field with five injectors and four producers.

In Section 3.2, we present the capacitance model to indicate the connectivity and dissipation between wells. Section 3.3 contains an oil production model showing the relationship between the instantaneous water-oil ratio and the cumulative water injected. In Section 3.4, various optimization problems for oil production are formulated to maximize the future economic return of the reservoir asset. All models and formulation are tested on a heterogeneous synthetic field with five injectors and four producers and the results are shown in Section 3.5. Conclusions are drawn in Section 3.6.

3.2 Review of Capacitance Model

The capacitance model is a total mass balance with compressibility (Yousef and others, 2006b). In a real waterflood, there are multiple producers and injectors acting simultaneously and more than one injector usually influences the total production rate at a producer (Yousef and others, 2006b). In this work, we consider a drainage volume with m injectors and n producers.

The governing material balance at reservoir conditions can be described by the following differential equations:

$$q_j = \sum_{k=1}^m \lambda_{kj} i_k - c_t V_p \frac{d\bar{p}_j}{dt} \quad j = 1, 2, \dots, n \quad (1)$$

where c_t is the total compressibility; V_p is the original pore volume of the drainage; \bar{p}_j is the average pressure drained by producer j ; i_k is the injection rate in injector k and q_j is the total production rate in producer j . To obtain a description that is based entirely on rates, as Yousef and others (2006b) did, we use the same linear productivity model

$$q_j = J_j (\bar{p}_j - p_{wff}) \quad j = 1, 2, \dots, n \quad (2)$$

where p_{wff} and J_j are the flowing bottomhole pressure and productivity index of the producer j , respectively. Eliminating \bar{p}_j in Equations (1) and (2), we obtain

$$q_j = \sum_{k=1}^m \lambda_{kj} i_k - \frac{c_t V_p}{J_j} \cdot \frac{dq_j}{dt} - c_t V_p \frac{dp_{wff}}{dt} \quad j = 1, 2, \dots, n \quad (3)$$

In this work, we assume a constant flowing bottomhole pressure for simplicity. By defining $\tau_j = c_i V_p / J_j$, we obtain the following capacitance model

$$q_j = \sum_{k=1}^m \lambda_{kj} i_k - \tau_j \frac{dq_j}{dt} \quad j = 1, 2, \dots, n \quad (4)$$

This model provides one time constant τ_j for each producer j and one weight λ_{kj} for each injector-producer (k, j) pair, which is simpler than that in Yousef and others (2006b). The $m \times n$ weights provide a quantitative expression of the connectivity between each injector-producer pair; the larger the weight, the greater the connectivity. The n time constants are direct measures of the rate of dissipation around each producer; the larger the time constant, the larger the dissipation rate.

3.3 Oil Production Model

The oil production model is based on a power law relationship between the instantaneous water-oil ratio (WOR) and the cumulative water injected (Wi). The predicted water-oil ratio is assumed to have the following power law form:

$$\text{WOR} = a \text{Wi}^b \quad (5)$$

Once injection and production rates are in balance, total fluids produced approximate Wi and Wi is the approximate sum of the cumulative oil and water produced. Under this circumstance, equation (5) can be applied for each producer. Hence, any multivariate linear regression method can be used to obtain a total liquid prediction rate without explicit information regarding the origin of the water injected.

Assuming that the capacitance models provide information on how the water is being allocated from the injectors to the producers, a WOR-WI power law can be applied to each individual volume drained by each producer after solving for the capacitance model weights. The total oil rate produced by producer j is the total production rate multiplied by the oil fraction f_i at that time level:

$$q_{oj} = f_j q_j \quad j = 1, 2, \dots, n \quad (6)$$

The producing oil fraction is calculated from the estimated water-oil ratio as:

$$f_j = \frac{1}{1 + \text{WOR}_j} \quad j = 1, 2, \dots, n \quad (7)$$

A power law is used to model the water-oil ratio as a function of the total cumulative water injected for each producer j :

$$\text{WOR}_j = a_j \text{Wi}_j^{b_j} \quad j = 1, 2, \dots, n \quad (8)$$

The total cumulative water injected into the drainage area of producer j is:

$$\text{Wi}_j = \int_{s=t_0}^{s=t} \left[\sum_{k=1}^m \lambda_{kj} i_k(s) \right] ds = \sum_{k=1}^m \lambda_{kj} \int_{s=t_0}^{s=t} i_k(s) ds \quad (9)$$

Thus, we can express the oil production from region j as follows.

$$q_{oj} = \frac{q_j}{1 + a_j \left(\sum_{k=1}^m \lambda_{kj} \int_{s=t_0}^{s=t} i_k(s) ds \right)^{b_j}}, \quad j = 1, 2, \dots, n \quad (10)$$

After estimating the weights in the capacitance model, we can use Eq.(10) model to determine the parameter pair a_j and b_j for each producer by minimizing the squared errors between measured historical oil production rates and those generated by the discrete form of Equation (10). However, direct use of the above power-law model form makes it difficult to obtain accurate value of a_j and b_j . So, taking logarithms to linearize Equation (8):

$$\log(\text{WOR}_j) = \log(a_j) + b_j \log(\text{Wi}_j) \quad (11)$$

Using linear regression, $\log(a_j)$ and b_j are found by minimizing the relative sum of squared errors (note the errors are now in terms of logarithms). Naturally, linearization of Equation (8) comes at a price and some care must be taken when using it. It is recommended that only late time data be used for fitting, particularly if it shows a clear trend on a WOR-Wi cross plot.

3.4 Optimization Method

Formulation of the problem is very important in the practical use of optimization techniques. Possible objectives can be to maximize the total oil flow from the field or minimize the profitability of the reservoir. For maximizing the total oil production over the period $[t_0, t_f]$, we can use the following objective function.

$$Q_o = \sum_{j=1}^n \int_{s=t_0}^{s=t_f} q_{oj}(s) ds \quad (12)$$

To maximize the non-discounted revenue over the period $[t_0, t_f]$, we use the objective function

$$R = p_o \sum_{j=1}^n \int_{s=t_0}^{s=t_f} q_{oj}(s) ds - p_w \sum_{k=1}^m \int_{s=t_0}^{s=t_f} i_k(s) ds \quad (13)$$

where the coefficients p_o and p_w are the prices of oil and water injected, respectively. We can also consider the following objective function as the non- discounted revenue over the period $[t_0, t_f]$

$$R = p_o \sum_{j=1}^n \int_{s=t_0}^{s=t_f} q_{oj}(s) ds - \bar{p}_w \sum_{j=1}^n \int_{s=t_0}^{s=t_f} q_{wj}(s) ds \quad (14)$$

where p_o is the price of oil and \bar{p}_w is the cost of water disposed. Another objective function can be based on net present value; weighting is applied to cash flows in each time period to account for net present values.

The decision variables include the well production rates $q_j(t)$, $j=1, 2, \dots, n$, and the well injection rates $i_k(t)$, $k=1, 2, \dots, m$. The constraints include the capacitance model (4), oil production model (10) and some upper (u_k) and lower (l_k) bounds imposed on the injection rates for the m injectors.

$$l_k \leq i_k(t) \leq u_k, \quad k=1, 2, \dots, m \quad (15)$$

The minimum l_k usually is zero, which occurs when injector k is shut in. The maximum value is user specified. Now we can choose the optimal injection rates and production rates by solving one of the following optimization problems over the period $[t_0, t_f]$:

Maximize Q_o in (12) or R in (13) or (14)

$$\text{Subject to } q_j = \sum_{k=1}^m \lambda_{kj} i_k - \tau_j \frac{dq_j}{dt}$$

$$q_{oj} = \frac{q_j}{1 + a_j \left(\sum_{k=1}^m \lambda_{ki} \int_{s=t_0}^{s=t} i_k(s) ds \right)^{b_j}}, \quad j=1, 2, \dots, n$$

$$l_k \leq i_k(t) \leq u_k, \quad k=1, 2, \dots, m$$

This optimization problem formulation will be converted into a standard nonlinear constrained programming problem via discretization (Edgar and others, 2001), which can be

solved by an efficient algorithm such as sequential quadratic programming (SQP). However, the size of the discretized problem depends on the number of wells, the length of the period $[t_0, t_f]$ and the step size of discretization. It may have a large number of variables. Therefore, large-scale optimization techniques may be necessary to solve the problem.

3.5 Results

To show the utility of the capacitance model, oil production model and optimization formulation for oil production, we applied them to numerically simulated data (Eclipse) on a heterogeneous synthetic field (a Synfield, see Yousef, 2006, for the details). The results of these applications are presented and discussed below.

The Synfield consists of 5 injectors and 4 producers as shown in Figure 1. The field has only vertical wells. The Synfield is a multi-layered anisotropic reservoir with a homogenous permeability of 5 md except for two streaks: one between I01 and P01 (1000 md), the other between I03 and P04 (500 md). The Synfield dimensions and the grid size are $31 \times 31 \times 5$ and $40 \times 40 \times 6$ ft, respectively. The distance between nearest injector and producer is 800 ft. The oil-water mobility ratio is equal to one and the oil, water and rock compressibilities are 5×10^{-6} , 1×10^{-6} and 1×10^{-6} psi^{-1} , respectively. The flowing bottomhole pressures of the producer are constant. We used the same injection data as Yousef (2006). These data, as shown in Figures 2a-e, were randomly selected from different wells in a real field and proportionally modified to be in agreement with the Synfield injectivity. The numerical simulation extends for 100 months (approximately 3000 days), which represent a history of 100 data points of production. The corresponding total production rate, oil production rate and water production rate for the four producers are shown in Figures 3a-d.

The numerical values of the weights and time constants are obtained from the capacitance model by a standard constrained optimization solver in Matlab 7.1. These are shown in Tables 1 and 2. In Figure 4, the weights λ_{kj} are represented by arrows or cones that start from injector k and point to producer j . The larger the arrow, the larger the value of the weight and the greater the connectivity between the two wells.

Figure 4 reveals different characteristics of the medium between each injector and producer pair. As expected from a heterogeneous reservoir, the weights are not symmetric. The capacitance model describes the injection-production behavior and the weights quantify the connectivity between wells appropriately. The presence of two streaks, between I01 and P01 and between I03 and P04 as shown in Figure 1, is obvious from the weights. The water injected in injector I01 (I03) almost exclusively flows along the streak to producer P01 (P04). Producer P04 seems to be located within a high permeability area and for injectors I02, I03, I04 and I05, the weighting coefficient affecting P04 is larger than any of the coefficients affecting the other producers.

Figure 5 shows comparisons between the modeled total production rate using the capacitance model and the total production rate observed in the numerical simulation for producer P01. The coefficient of determination is $R^2=0.9989$. The agreement of the model prediction for other producers P02, P03 and P04 are not shown; their corresponding coefficients of determination are $R^2=0.9992$, $R^2=0.9999$ and $R^2=0.9986$. All matches of total production rate in the Synfield yielded $R^2>0.99$. As a consequence, we conclude the capacitance model successfully captures the attenuation and time lag in the field studied.

After obtaining the weights and time constants, we then used the oil production model to estimate the parameters a_j and b_j for each producer. To obtain accurate parameters, we use Equation 11. We eliminated the data in previous 60 months, that is, we only used the latest 40 months of data. A standard unconstrained optimization solver in Matlab 7.1 is used to estimate the parameters a_j and b_j for each producer; the results obtained are shown in Table 3.

Figures 6a-d show comparisons between the oil production rate modeled and the oil production rate observed in the numerical simulation for each producer. The matches of oil production rates in the whole region are not as good as desired, except for producer P02. But for the most recent 40 months, the R^2 's for producers P01-P04 are, respectively, 0.9776, 0.9998, 0.9952 and 0.9928. Therefore, the matches are quite good and the model yields accurate predictions on oil production.

Before the oil optimization, the lower (l_k) and upper (u_k) bounds imposed on the injection rates for the 5 injectors need to be specified first. For each injector, we take its lower bound as zero and its upper bound as the maximum value of its historical data. That is, we specify the lower and upper values for each injector as the following values (in RB/day):

$$l_k = 0, \quad k = 1, 2, \dots, 5$$

$$u_1 = 3531.916, \quad u_2 = 1963.172, \quad u_3 = 1456.326, \quad u_4 = 1346.799, \quad u_5 = 2209.986$$

If we take (12) as the objective function, that is, if we only maximize the total oil production, then the optimal injection rates in all five injectors take their upper extreme values. If we take (13) as the objective of revenue optimization with different prices of oil and water injected, then we can consider different scenarios of injection rates for each injector. In some cases, the oil prices are admittedly exorbitant to see where an injection policy might be changed. Using a fixed water price of \$2/RB (related to water disposed costs) and increasing the oil price in increments of \$1 from \$2/RB to \$600/RB resulted in the following series of revenue optimization results.

- When the oil price is between \$2-14/RB, all injectors are shut in;
- When the oil price is between \$15-34/RB, all injectors except injector I01 are shut in; injector I01 changes its rate between its lower and upper bounds. See Figure 7a-b as an example where oil price is \$20/RB.
- When the oil price is between \$35-82/RB, injectors I03, I04 and I05 are shut in; injector I01 takes its upper extreme value for all time, and, injector I02 changes its rate between its lower and upper bounds. A case with oil price \$60/RB is shown in Figure 8a-b.
- When the oil price is between \$83-292/RB, injector I03 is shut in, injector I01 and injector I02 take their upper extreme values, injectors I04 and I05 change their rates between their lower and upper bounds, respectively. Figure 9a-b shows the optimal injection rates for each injector under oil price \$180/RB.
- When the oil price is between \$293-599/RB, all injectors except injector I03 take their upper bounds; injector I03 changes its rate between its lower and upper extreme value. An example with oil price \$400/RB is shown in Figure 10a-b.
- When the oil price is equal to or larger than \$600/RB, all injectors take their upper extreme values.

If we take (14) as the objective of revenue optimization with different prices of oil and costs of water disposed, then we can obtain the following optimal injection policy with a fixed \$1/RB price of water disposed and increasing the oil price in increments of \$1 from \$1/RB to \$450/RB.

- When the oil price is between \$1-12/RB, all injectors are shut in;
- When oil price is equal to or larger than \$430/RB, all injectors take their upper extreme values;
- For oil price between \$13-429/RB, it is hard to classify the optimal injection patterns. Four examples with oil price \$20/RB, \$60/RB, \$120/RB and \$240/RB are shown in Figures 11-14.

3.6 Conclusions

We have shown an optimization procedure that systematically accounts for the interactions of an integrated oil and water production system and simultaneously optimizes the oil produced using injected water. A simpler capacitance model is sufficient to predict the dynamic behavior for injection and production wells in a reservoir, which represent a significant reduction in computational effort compared to that in Yousef and others (2006b). Using historical data, the estimated oil production matches that from a numerical simulation at long time.

Using the simplified reservoir model, we formulated various objective functions for future oil production, where production rates and water injection rates are optimized simultaneously. Solving the proposed optimization problem for different oil prices led to different scenarios of optimal injection.

The models and formulation were applied to numerically simulated data (Eclipse) on a heterogeneous synthetic field with 5 injectors and 4 producers. The results show that the proposed capacitance model can successfully capture the true attenuation and time lag behavior between injectors and producers. The formulation of optimal oil production can be used to maximize the future economic return of the asset and is appropriate for simultaneous optimization of well rates in the field where wells are shut-in frequently. The proposed optimization method can be used for real-time production control because all of the variables required for the model can be measured and the discrete data can be directly incorporated in the formulation.

3.7 Tables and Figures

Table 1. Interwell weights obtained

	P01	P02	P03	P04
I01	0.9374	0.0145	0.0084	0.0397
I02	0.2920	0.0135	0.2632	0.4313
I03	0.0316	0.0057	0.0044	0.9584
I04	0.1024	0.1607	0.0074	0.7295
I05	0.0395	0.0107	0.2168	0.7330

Table 2. Time constants (in months) obtained

	P01	P02	P03	P04
τ	0.2372	1.4813	2.4180	1.0438

Table 3. Parameters a [1/rb] and b obtained

	P01	P02	P03	P04
a	4.416e-07	3.551e-16	6.462e-13	6.486e-20
b	1.4098	3.9002	2.7559	3.8003

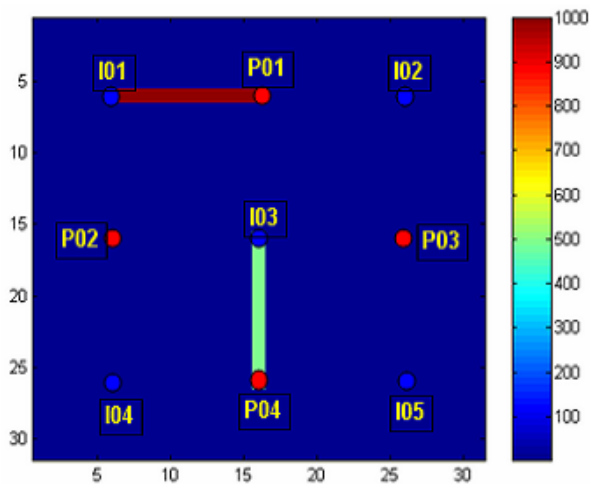


Figure 1. Locations of the vertical wells and permeability (in md) in the reservoir (Yousef, 2006).

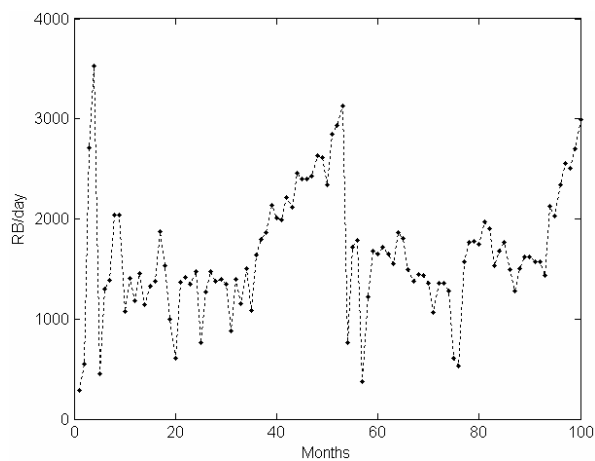


Figure 2a. Rate for injector I01

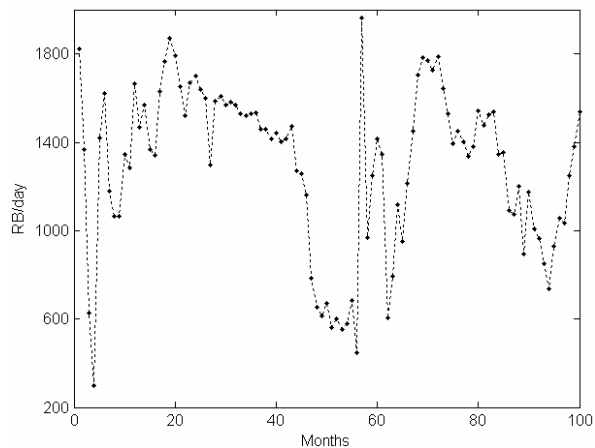


Figure 2b. Rate for injector I02

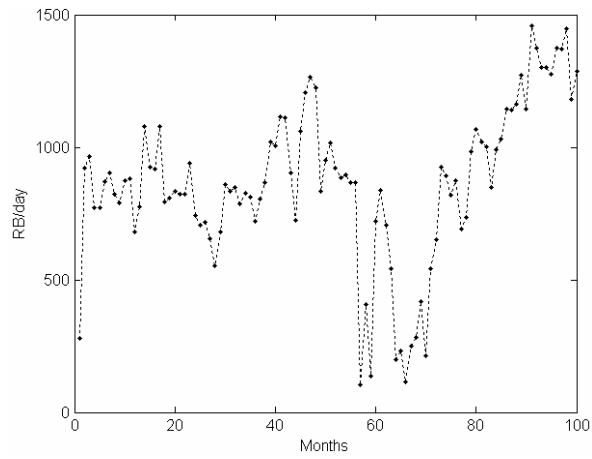


Figure 2c. Rate for injector I03

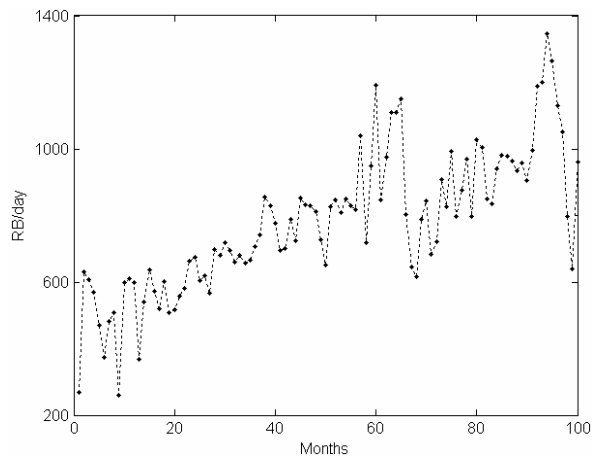


Figure 2d. Rate for injector I04

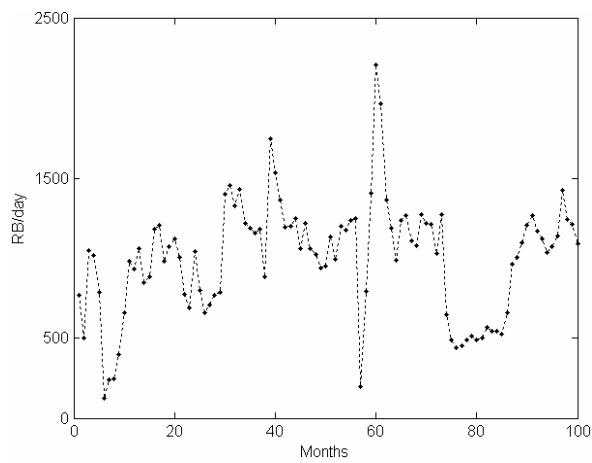


Figure 2e. Rate for injector I05

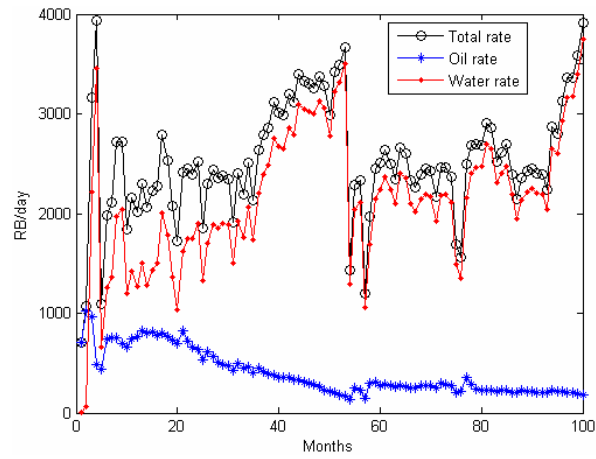


Figure 3a. Rates for producer P01

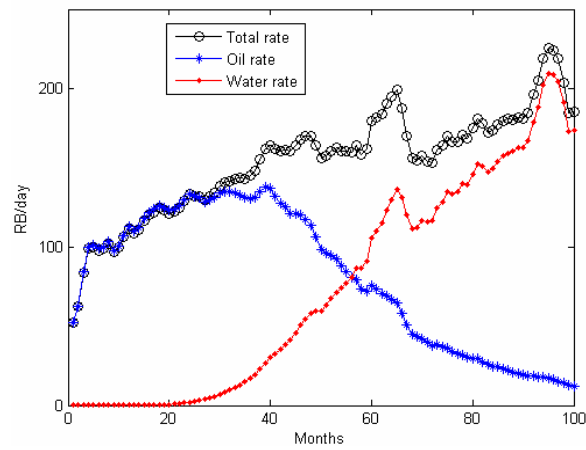


Figure 3b. Rates for producer P02

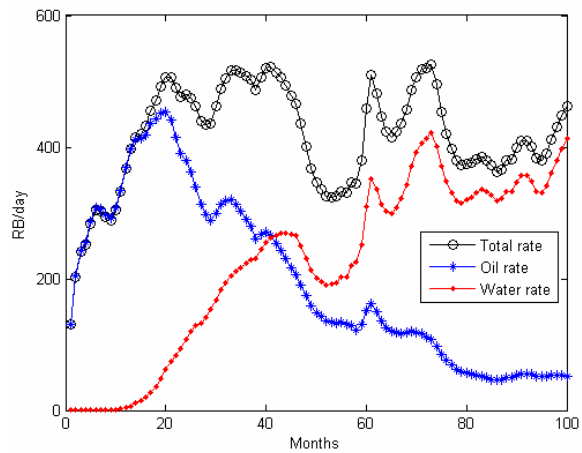


Figure 3c. Rates for producer P03

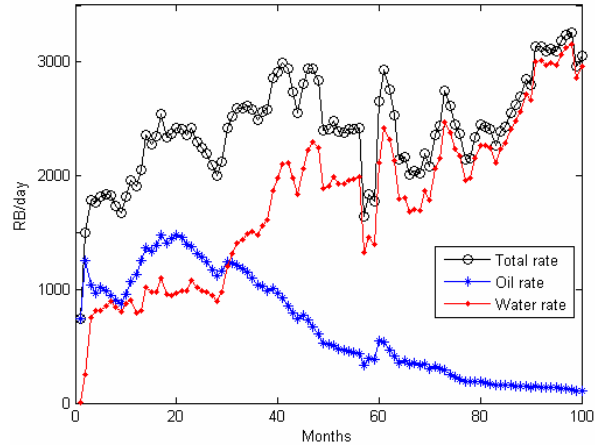


Figure 3d. Rates for producer P04

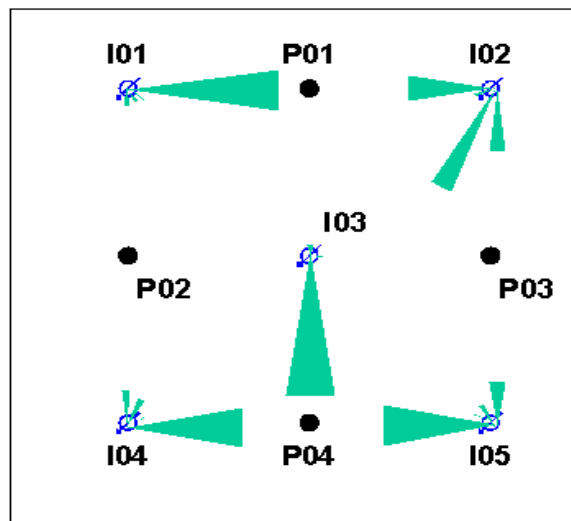


Figure 4. Representation of the Weights

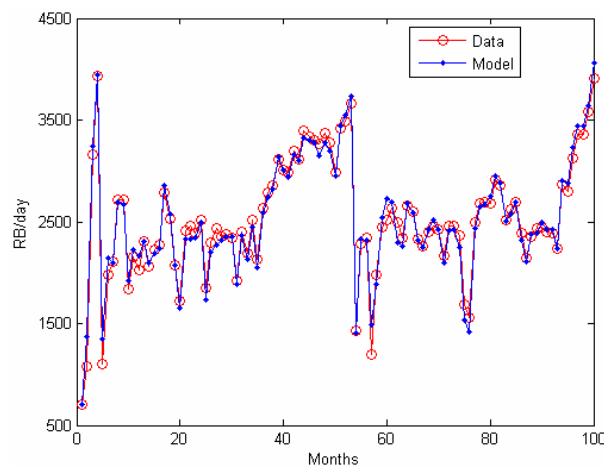


Figure 5. Capacitance model match for producer P01

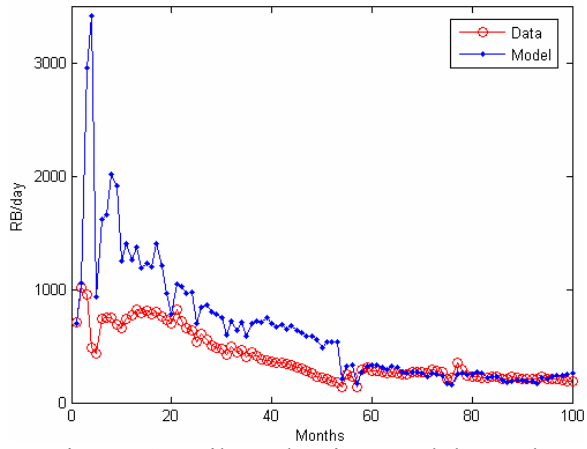


Figure 6a. Oil production model match for producer P01

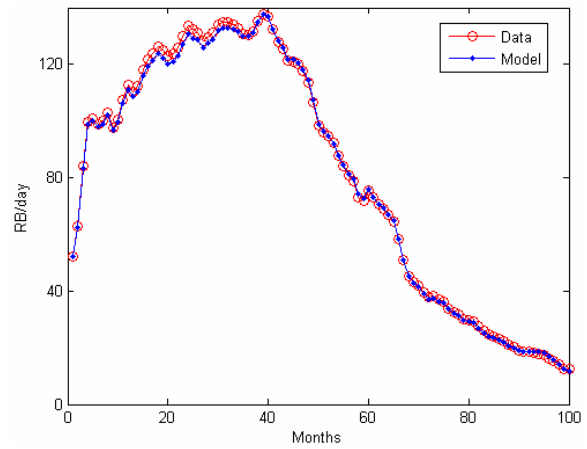


Figure 6b. Oil production model match for producer P02

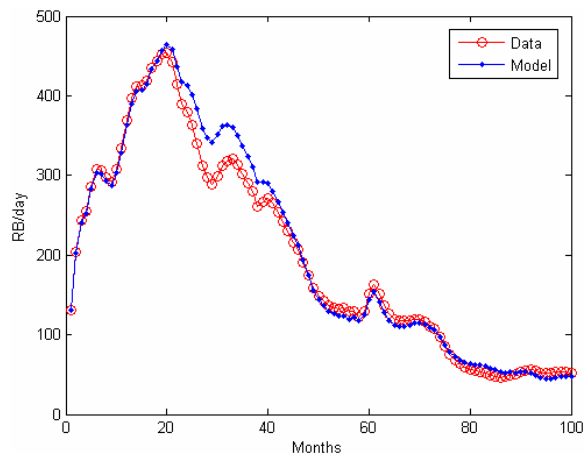


Figure 6c. Oil production model match for producer P03

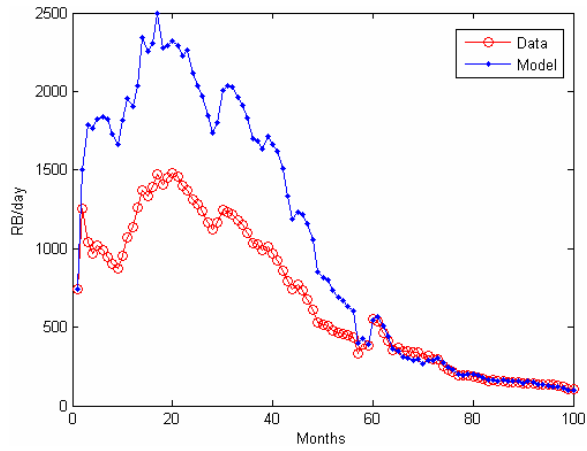


Figure 6d. Oil production model match for producer P04

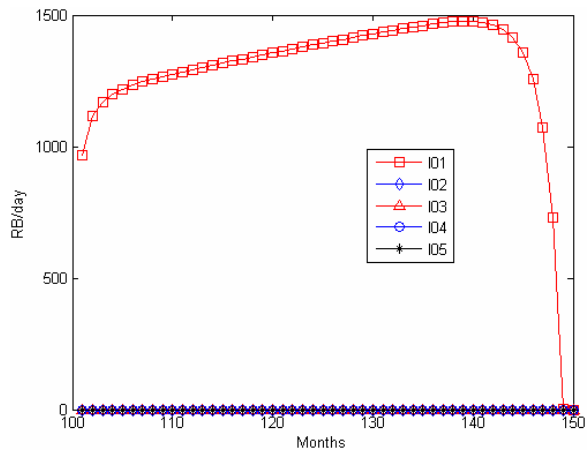


Figure 7a. Optimal injection rates at oil price \$20/RB and water injected price \$2/RB

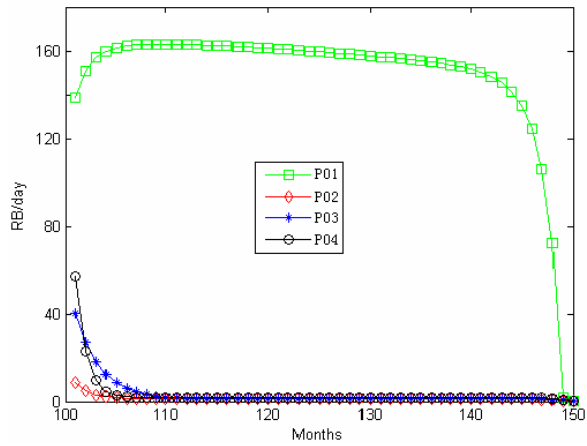


Figure 7b. Optimal oil production rates at oil price \$20/RB and water injected price \$2/RB

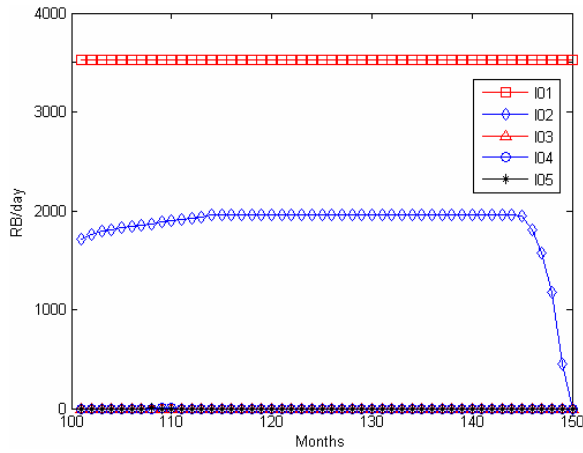


Figure 8a. Optimal injection rates at oil price \$60/ RB and water injected price \$2/RB

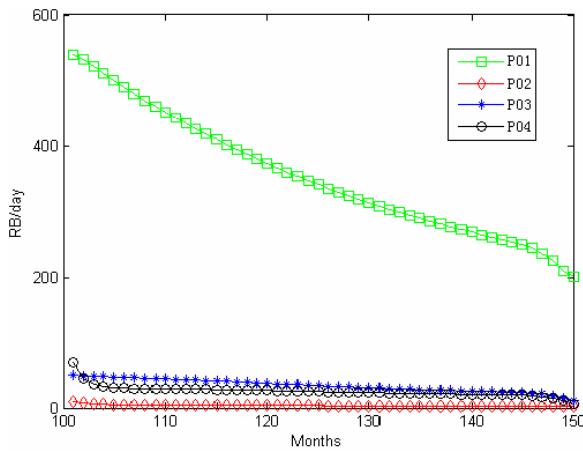


Figure 8b. Optimal oil production rates at oil price \$60/RB and water injected price \$2/RB

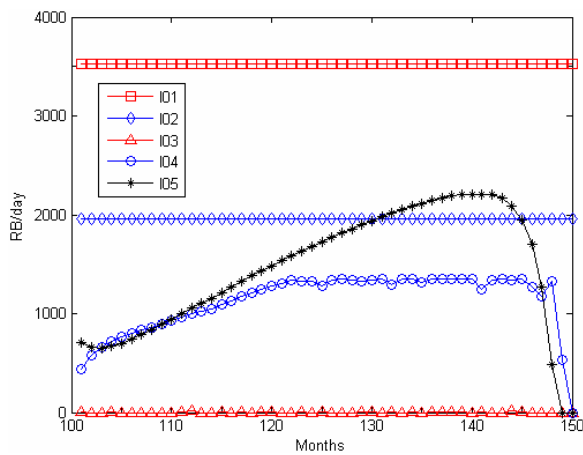


Figure 9a. Optimal injection rates at oil price \$180/RB and water injected price \$2/RB

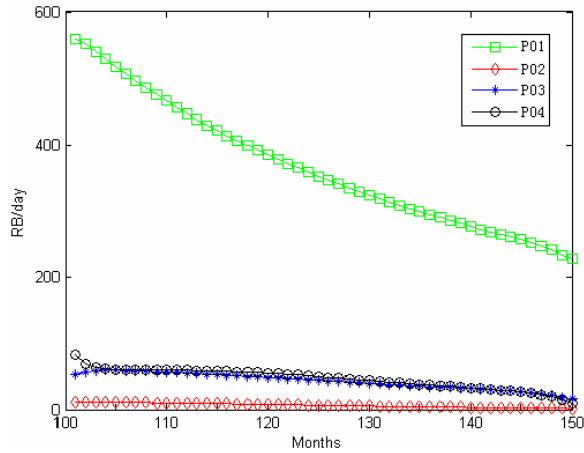


Figure 9b. Optimal oil production rates at oil price \$180/RB and water injected price \$2/RB

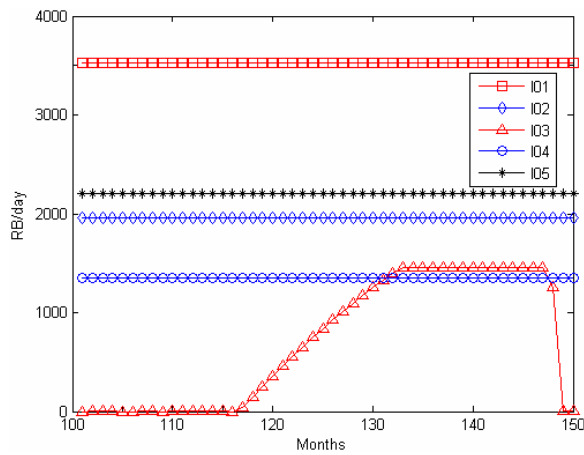


Figure 10a. Optimal injection rates at oil price \$400/RB and water injected price \$2/RB

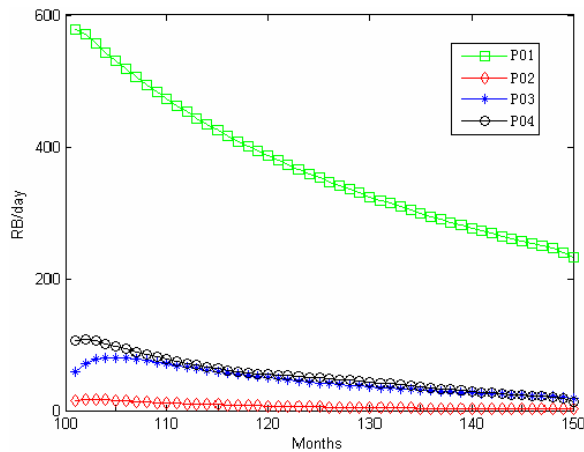


Figure 10b. Optimal oil production rates at oil price \$400/RB and water injected price \$2/RB

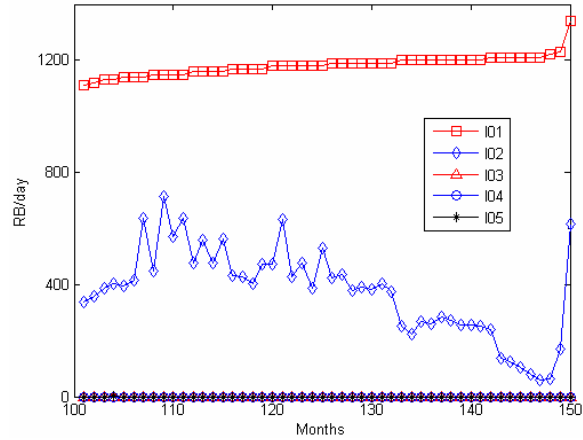


Figure 11a. Optimal injection rates at oil price \$20/RB and water disposed price \$1/RB

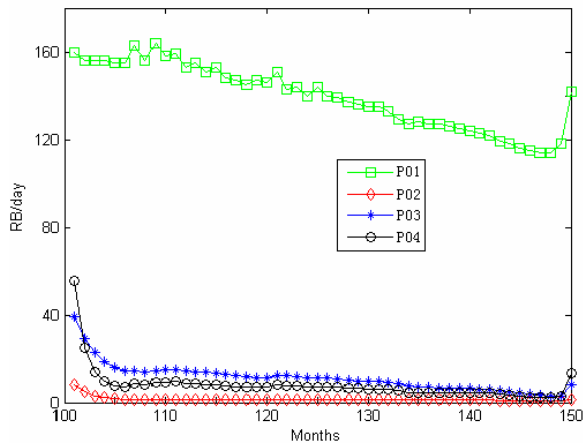


Figure 11b. Optimal oil production rates at oil price \$20/RB and water disposed price \$1/RB

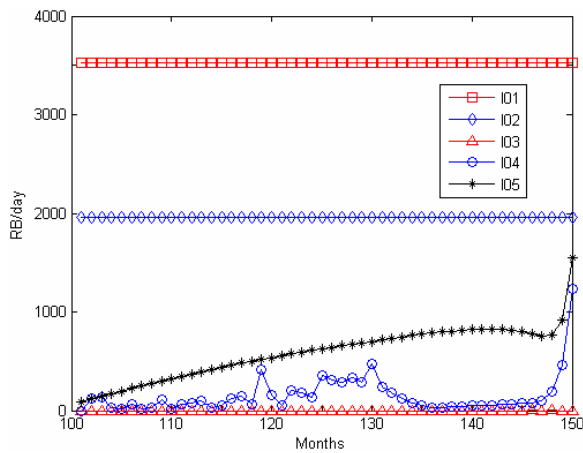


Figure 12a. Optimal injection rates at oil price \$60/RB and water disposed price \$1/RB

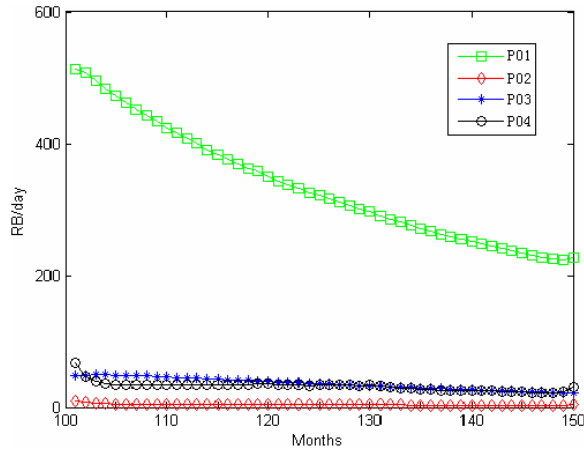


Figure 12b. Optimal oil production rates at oil price \$60/RB and water disposed price \$1/RB

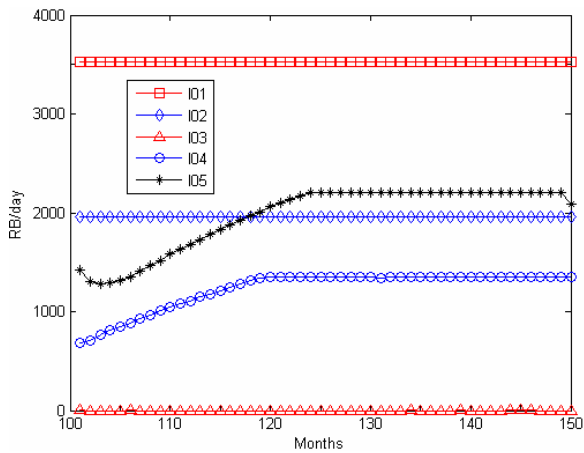


Figure 13a. Optimal injection rates at oil price \$120/RB and water disposed price \$1/RB

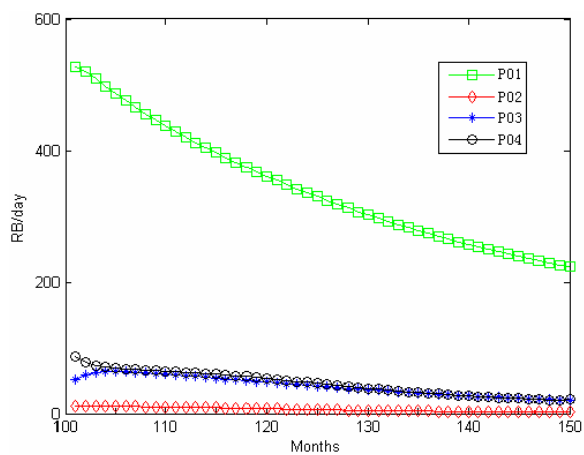


Figure 13b. Optimal oil production rates at oil price \$120/RB and water disposed price \$1/RB

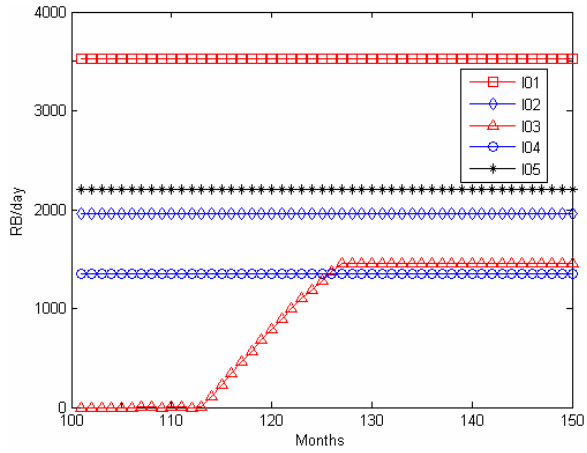


Figure 14a. Optimal injection rates at oil price \$240/RB and water disposed price \$1/RB

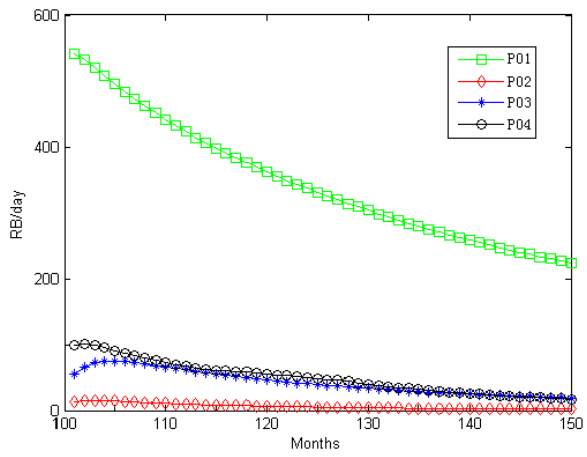


Figure 14b. Optimal oil production rates at oil price \$240/RB and water disposed price \$1/RB

RESULTS AND DISCUSSION

PART 4. IMPROVEMENTS TO CAPACITANCE MODEL ROBUSTNESS

One of the main restrictions of the capacitance model (CM) is the sensitivity of the weights (λ 's) to changes of the producing well bottom hole pressures (BHP's). If we have production wells with constant BHP's or if we have BHP data, then we are able to use the CM to correctly estimate the interwell connectivity coefficients. It is common, however, for production well BHP's to change, e.g. due to workovers or being shut-in, but there are no BHP measurements to monitor those changes. Here, a modification to the CM addresses this problem. Using this modification, we are able to apply the CM to field data where there are wells having unmeasured BHP's, provided that we have some information about the times when the BHP changes. These times, called segmentation times, can be estimated using some techniques discussed below. The segmented CM is a powerful tool to overcome the problem of unmeasured BHP fluctuations. If there are many times when the BHP changes in one or more wells, however, the performance of the method deteriorates.

4.1 Development of the Segmented Capacitance Model

We are starting with general form of the UCM (Eq. 9, Part 1.2.1.2 of this report; Yousef, 2006):

$$q_j(n) = \lambda_p q(n_0) e^{-\frac{(n-n_0)}{\tau_p}} + \sum_{i=1}^I \lambda_{ij} i'_{ij}(n) + \sum_{k=1}^{k=K} v_{kj} \left[p_{wfk}(n_0) e^{-\frac{(n-n_0)}{\tau_{kj}}} - p_{wfk}(n) + p'_{wfk}(n) \right] + \lambda_0 \quad (1)$$

where

$$i'_{ij}(n) = \sum_{m=n_0}^{m=n} \frac{\Delta n}{\tau_{ij}} e^{-\frac{(m-n)}{\tau_{ij}}} i_i(m) \quad (2)$$

and

$$p'_{wfk}(n) = \sum_{m=n_0}^{m=n} \frac{\Delta n}{\tau_{kj}} e^{-\frac{(m-n)}{\tau_{kj}}} p_{wfk}(m) \quad (3)$$

Since τ values for the BHP terms are generally large, by some modification the whole BHP term can be written as (Yousef, 2006):

$$\sum_{k=1}^{k=K} v_{kj} \left[p_{wfk}(n_0) e^{-\frac{(n-n_0)}{\tau_{kj}}} - p_{wfk}(n) + p'_{wfk}(n) \right] \approx \sum_{k=1}^{k=K} v_{kj} |p_{wfk}(n_0) - p_{wfk}(n)| \quad (4)$$

Using this model we are able to find the right interwell connectivity coefficients in the cases with fluctuating BHP's, provided that we have the BHP data. But in several field cases, we do not have any information about the BHP of the producing wells, and we need to develop a method to overcome this problem. Based on Eq. 1, if there are no BHP variations, the BHP term will be removed and we will have the simple UCM:

$$q_j(n) = \lambda_p q(n_0) e^{-\frac{(n-n_0)}{\tau_p}} + \sum_{i=1}^I \lambda_{ij} i'_{ij}(n) + \lambda_0 \quad (5)$$

Comparing this with Eq. 1, we can see that the interwell coefficients are the same in the constant BHP and fluctuating BHP cases, and the only difference is in the constant term, where it is λ_0 for constant BHP and it is $\lambda_0 + \text{BHP term}$, for the fluctuating BHP cases. Also based on Eq. 5

we can see that, for the constant BHP intervals, the BHP term is constant, or its change over a period of constant BHP is negligible. So, we can reformulate the model as:

$$q_j(n) = \lambda_p q(n_0) e^{-\frac{(n-n_0)}{\tau_p}} + \sum_{i=1}^I \lambda_{ij} i'_{ij}(n) + \lambda'_{0k} \quad (6)$$

where λ'_{0k} is the constant term of the model for the k-th interval of BHP (Fig. 1). In other words, instead of $\lambda_0 + \text{BHP}$ term, we have λ'_{0k} , which changes, whenever the BHP of one of the wells in the system changes.

4.2 Segmentation Procedure

In the conventional CM, by initializing the time constant (τ 's), the λ values are determined using MLR (multivariate linear regression). Based on the MSE (mean squared error) of the prediction of the production values, the time constants will be updated until the maximum number of iterations is met or the MSE of the prediction error decreases to a specified value. Here, since we need different values of λ'_0 , applying the simple MLR is not possible, and instead similar to the method suggested before to prevent negative weights (Jensen and others, 2006), all τ 's, λ 's and λ_0 's needs to be initialized. Below is the brief description of the method:

- Initialize all τ 's and λ 's. Interwell connectivity coefficients λ 's should be between zero and 1; τ 's should be positive. Also, for each period with constant BHP, a λ'_0 should be assigned.
- Find the convolved injection rates, for all injectors and the primary production term.
- For each time interval (constant BHP), estimate the production value.
- Find the error of the predicted production values, and update the τ 's, λ 's and λ_0 's.
- Repeat the procedure until either an acceptable error or the maximum number of the iterations is obtained.

Here, this algorithm was applied to some simulation cases and the results were compared to the conventional CM results.

4.2.1 Simulation cases

Case 1-1 (base case): Figure 2 shows the location of the wells for case 1. The injection rates are all sinusoidal and the simulation was run for 200 months (Fig. 3). At this case the bottomhole pressure of both production wells was assumed equal to 1,100 psi for all the production period. To find the interwell connectivity coefficients both BCM (Balanced CM) and UCM (Unbalanced CM) were applied (Table 1). It can be seen that, since the BHP of both wells are the same, and also the system is closed and balanced there is no need to the λ_0 term and the difference between the results of the BCM and UCM is very small.

Case 1-2: which is similar to case 1-1, but the BHP of producer 1 is 500 psi (BHP of well #2 is 1,100 psi similar to case 1-1). For this case, based on R^2 the performance of UCM is better than BCM (Table 2). Also, the interwell coefficients using UCM are very close to those of the base case besides the λ_0 . In fact, since the only difference between these two cases is the BHP of the producing wells, the interwell coefficients are similar and the effect of different BHP of the wells can be seen in the λ_0 of each well, where it is negative for well #1 (higher BHP, lower production) and positive for well #2 (lower BHP, higher production). This confirms that the change of the BHP has only effect on λ_0 and not on the other interwell connectivity coefficients.

Case 1-3: In this case, the BHP of both producers changes during production (Fig. 4). Applying the CM without considering the BHP fluctuations, the prediction was very poor. Both

CM considering BHP (Eq. 1) and also the segmented CM, however, gave us good results (Table 3). It can be seen that, the interwell connectivity coefficients using both methods are very similar to each other and also to the base case (Fig. 5). Also, the values of time constant for producers (τ_{pr}) are very large. Similar to the previous case, we can see that depending on the BHP of the wells at each interval the λ_0 at that interval may have positive or negative number.

To check the ability of the method on the cases with more number of producers, a case with four producers has been tried:

Case 2-1: Figure 6 shows the location of the wells. A similar injection profile to case 1-1 was used. At first, a case with constant BHP for all the wells was run (base case) and its corresponding coefficients was found. Then a case with fluctuating BHP (Fig. 7) with time has been run, and with use of CM+BHP and the segmented CM the interwell connectivity coefficients has been found. Based on the results, both models were able to find the interwell connectivity coefficients correctly (Fig. 8) and the R^2 for both methods was above 0.999.

Now, we are going to try a case with shut-in period of some wells.

Case 2-2: similar to the previous case, but here we have some shut-in period of each well. Since during the shut-in period of each well the BHP of that is not constant and fluctuates (Fig. 9), to apply segmented CM, a segmentation time is needed at every point, which gives us more free parameters than the number of the data. So, segmented CM cannot be used. Assuming constant BHP during the shut-in period of each well, using segmented CM the R^2 may seem high, but looking at the cross-plot we can see that the prediction is not good (Fig. 10). Applying CM+BHP a better prediction can be done, but the interwell connectivity coefficients are different from the base case.

4.2.2 Discussion of Simulation Results

In all the simulation cases, where we have a small number of BHP changes (in the shut-in case, the number of BHP changes is as long as the shut-in period) the segmented CM performs as good as CM+BHP. This confirms that the BHP term in CM+BHP can be substituted with the λ_0 term in the segmented CM. For example, the value of both BHP term and λ_0 for well 1 of case 2-1 are very close to each other and the difference between them is due to the small difference between their interwell connectivity coefficients (Fig. 11).

In the shut-in period cases, we saw that none of the CM and CM+BHP was able to calculate the right interwell connectivity coefficients. This is due to the inherent difference of the coefficients in the shut-in case with the other cases. In fact, by shutting-in a well the number of the active production wells in the system changes; thus the λ 's will change (Table 4). So finding the right coefficients using the data including shut-in period is impossible. Although, using CM+BHP we are able to predict the production of the producers with acceptable accuracy, but the obtained coefficients are not corresponding to the full system and by changing the period of shut-in these coefficients may change.

4.3 The use of segmented CM for stimulated wells

We have shown that the segmented CM could be applied in cases where the BHP of the production wells fluctuates provided that there are no shut-in periods. In field cases, another factor which violates the simple CM conditions is stimulation of the wells. In theory, the segmented CM is also not the right solution for stimulated production well cases; because stimulating the wells will change the near-well permeabilities, affecting the λ 's. If the change of

the λ 's is not large, using the segmented CM (or even simple CM) may solve the problem but, for high λ changes, it cannot be used. In general, it is better to divide the data at the stimulation times into different time periods and the problem solved for these different periods separately. In cases with short time of data; however, using the segmented CM could be the best choice, because there could be very few data in some time periods which may lead to overfitting the model to data and obtaining unstable and unrepresentative interwell connectivity coefficients.

Here, using some simple simulation cases, the changes of the λ after the stimulation will be shown, and then possible application of the segmented CM for the stimulated reservoirs without separating the data, will be shown.

Case 1-4- which is a 5x2 pattern similar to Case 1-1, with constant BHP equal to 1,100 psi. The only difference is the stimulation around well 1 (Fig. 12). It was assumed that, by acidizing well #1, the permeability of the surrounding cells within a radius of 200 ft has been increased from 40 md to 400 md. As expected, the λ 's for well #1 are increasing and those of well #2 are decreasing (Fig. 13).

Besides this case, some other stimulation cases with different performance of acidizing and also some hydraulic fracturing cases were tried, and for all the cases depending on the volume of the job, the λ 's for the stimulated wells has been increased and the λ 's for the other well(s) decreased. Based on this, stimulation of one or more wells in a field may change all the λ 's. Thus, it is not possible to find the interwell coefficients of a field using the data before and after the stimulation in one model and get the right coefficients. However, in some cases due to lack of information about the stimulations or the small number of data to divide, we may need to use all the data in one model. In the case of no information about the stimulations, the techniques which were used to recognize the segmentation times can be used (it will be explained in this report). For the case of the small number of data, the segmented CM may be useful. In fact, this model cannot describe the reservoir behavior perfectly. The interwell coefficients obtained by this method, however, can give us some information about the reservoir. They will be between the true coefficients of before and after stimulation coefficients, depending on the length of the data interval of pre- and post-stimulation.

To investigate the performance of the segmented CM on the stimulation cases, all the pre-and post-stimulation data case 1-4 was analyzed in one model. Applying the segmented CM, R^2 was more than 0.998 for both wells, but close inspection of the scatter plot of the wells revealed that the prediction was mediocre for well #1 (Fig. 14). The large increase in the production after stimulation caused the large R^2 . But, because of the inherent difference between the λ 's of the pre and post stimulation, the model is not able to predict the smaller changes in production due to the injection rates changes. The prediction error could not be decreased to zero and we can only reach to an optimum point. Applying the segmented CM considering prior injection data (It will be explained later in this report); however, the prediction was improved a little bit (Fig. 15). As expected, the interwell coefficients for the best predictors are not the correct ones either for before stimulation or after stimulation conditions. These weights, however, are very close to the average weights of the base case and case 1-4 (Fig. 16). This shows the ability of the predictor to estimate the right weights, because the length of the data from each period (pre- and post-stimulation) used for the model was the same, and the average value of the weights could be a good estimation of the λ 's of the system.

4.4 Recognizing the segmentation times

In part 4.1 it was shown that using the segmented CM, having the segmentation times, or the times where the BHP of the production wells of the field has been changed, we are able to use the CM in the cases with fluctuating BHP with no need to the BHP data. Here, some methods to recognize the segmentation times looking at injection and production is described.

The possible methods to recognize the segmentation times could be categorized into two general methods: the methods based on only production data and the methods based on both injection and production data. In the first set of the methods we are trying to recognize the BHP changes (or more generally any other changes in the reservoir conditions or around the wellbore which may change the production suddenly) only looking at production data based on sudden changes in the production data or in its derivative. But in the second set of the methods, we are looking at both injection and production data, trying to find out if a change in the production profile (even not very sharp) is due to the injection or it is because of changing the producer conditions. In other words, if the changes in the production data at one point cannot be explained by the injection data, a segmentation time is probably needed at this point. So, we are trying to minimize the error of the prediction of the producers by changing the segmentation times.

In the optimization procedure of the second sets of the method, since the objective function, which is the MSE of the predicted production, is not differentiable over the segmentation times, we need to use an heuristic method such as genetic algorithms, simulated annealing, and direct search, which do not require the gradient of the objective function. Here we have used *direct search*. Briefly, this method searches a set of points around the current point and looking for the point where the value of the objective function is lower than the value at the current point. So in the optimization procedure the segmentation time is optimized using direct search and the interwell connectivity coefficients for each set of segmentation time are optimized using the conventional optimization methods. It should be mentioned that in optimizing the segmentation times, the segmentation time could have value only from the production times, and having a value other than the production times for segmentation time is meaningless. The stages to use this method with the CM to find the optimum segmentation times are:

- Initialize all τ 's and λ 's and also the segmentation times. For interwell connectivity coefficients (λ 's which corresponded to inj-prod pairs), these values should be between zero and one. Also τ 's should be positive. The segmentation time should be selected from the production data times.
- Apply the segmented CM to find the τ 's and λ 's based on the initialized segmentation times.
- Find the error of the predicted production and update the segmentation times using the direct search algorithm until either an acceptable error or the maximum number of the iterations is obtained.

4.4.1 Tests of the segmentation method

Here, some examples of using this method to estimate the optimum segmentation times are shown. Two examples are production profiles from wells in the Monument Butte Field.

Example 1- A simulation case similar to case 2-1 has been tried. Assuming that we do not know the true time of the BHP changes, we use the direct search algorithm by initializing $t_{seg1} = 30$ and $t_{seg2} = 100$. After 30 iterations (Fig. 17), the optimum set of segmentation locations obtained was the same as the true segmentation times. The algorithm is able to find the true segmentation times based on injection and production data in a simulation case perfectly.

Example 2- well no. 1214 from MBU, at interval from 152 to 175 months after the first production (Fig. 18). Using simple CM, the prediction has a poor R^2 (Fig. 19). Visual inspection of the production profile, it appears that $t_{\text{seg}} = 165$ and 168 are good estimates of the segmentation times. Applying the segmented CM with these segmentation times improves the results, but the match remains poor (Fig. 20). Using direct search, the optimum segmentation times were found to be: $t_{\text{seg}} = 169$ and 171, which gives us a $R^2 = 97\%$ (Fig. 21). In fact by changing the λ_0 at the segmentation times (169 and 171) the model is able to predict the production with minimum error, while adding segmentation times at $t_{\text{seg}} = 165$ and 168 (which were visually estimated) was not much useful. In other words, the changes in production at 165 and 168 could be explained using injection data, but the changes at 169 and 171 could not be explained using injection data and a segmentation point is needed to fit the model.

Example 3- well no. 1250 from MBU, at interval from 171 to 206 month after the first production (Fig. 22). Using simple CM, the results was very poor (Fig. 23). But using direct search to find the optimum segmentation times, the results improved (Fig. 24). Based on the field report of this well, there was a workover at month 184 on this well, which was recognized by the direct search algorithm as a required segmentation time. This shows that the algorithm is able to recognize the workover times in a production profile.

4.4.2 Discussion

The algorithm works very well in the simple simulation cases, where only the BHP of the wells have been changed. For the field cases, the results were acceptable but not perfect. There might be some stimulation in the field conditions whose effect on production is not restricted to only BHP changes and, as it was seen in part 4.2 it cannot be explained perfectly using a single segmented CM. But because we may lack data, using the segmented CM may be the only available choice, and it could be seen that its performance is much better than the simple CM.

In spite of the good performance of this algorithm, there are two problems associated with the methods based on both injection and production data. First, these algorithms are very time-consuming. For example, for this simple simulation case (example 1) where there were only 185 data points with 5 injectors, it took about 20 minutes to run the procedure over one producer, and if we have more wells, this time will increase drastically. In fact, at each iteration, several runs of the segmented CM are required to update the segmentation time. If we were to try it with different numbers of segmentation times--in the real cases we do not know how many segmentation times are required--it will take much longer than this. Second, a problem associated with these methods is their sensitivity to the initial values of the interwell coefficients at each updating of the segmentation times using the direct search. In fact, there is no guarantee that the obtained τ 's and λ 's at each stage of the segmentation time optimization are the optimum ones, and a non-optimum set at some iterations can lead the algorithm to a non-optimum segmentation time, or at least make the optimization procedure slower. To overcome this problem, we may update the initial set of τ 's and λ 's after some direct search iterations based on the τ 's and λ 's obtained at previous stages; however, there is no guarantee that this set is optimum, and not a local minimum. Also, running the algorithms for several times to get a consistent set of segmentation times is computationally quite demanding. Since these problems are related to the procedure and not to the optimization method of the segmentation times, using other heuristic methods instead of direct search will give the same problems. These problems encourage us to look again at the first set of methods, where only the production data are used to find the optimum segmentation times, as in Example 2. As it was mentioned earlier regarding Example 2,

the segmentation time at first was found by visual inspection and no specific algorithm was used to find the segmentation time in production data based methods. So the poor performance of that does not show that the production data base methods are not useful and applying different algorithms to investigate that is required. Also, since changing the BHP of one well affects the production of the other wells, estimation of the segmentation time based on several wells instead of individual estimation might be useful. In addition, using some algorithms such as wavelet analysis, which has been used to find formation layer boundaries (Rivera 2003), could be useful.

4.5 CM on the low-permeability cases

As noted by Albertoni (2002), analysis of simulation cases having low permeability, large compressibility, or other factors which decreases the diffusivity constant, indicates that the performance of the CM and AL methods deteriorates. Also, Yousef (2006) shows in his results that the R^2 for a small permeability case (7 md) was slightly lower than the R^2 he has reported for other cases. Theoretically, the CM does not have any problem with the low diffusivity cases, and having large dissipation does not violate any of the CM's (or AL's) assumptions. A plausible explanation for this problem could be the fact that the correlation of the signals may change after convolution. For the small dissipation cases, τ is small so the correlation coefficient of the convolved injection signals will not change much from that of original signals. But for the high dissipation cases, τ is larger and it has a larger effect on the correlation coefficient of the injectors. A large correlation coefficient of injectors may lead to collinearity and non-reliable coefficients (Yousef 2006). This problem is discussed through the use of two simple examples.

Example 4- Here, the correlation coefficient of some sinusoidal injection signals (Fig. 25) after and before shifting with different τ 's was investigated. It can be seen that, after shifting the signals, the correlation coefficient of the signals will be different from the non-shifted signals, and having larger τ 's this problem will be more serious (Table 5). In fact, after shifting the signals, the early parts of the signals (Fig. 26) will have large correlation coefficients, and the correlation coefficient of the other parts will be constant (Table 6). For the large τ 's, the period with high correlation will be longer so the total correlation coefficient will be larger than small τ 's cases.

Case 1-5- has a lower permeability (8 md) than Case 1-1. The R^2 for this case is less than Case 1-1 (Table 7) and the summation of the weights for some of the injectors, e.g. injector #4 or #5, is more than one, which is not physically interpretable. The weights are also inconsistent with different runs giving different weights. Looking at the correlation coefficient of the injection signals after shifting (Table 8.a), we can see that the correlation coefficients of some injectors are very high, which could be a possible reason for the uninterpretable weights. To test the probable effect of the injection rates, another set of injection rates (Fig. 27) was used. Applying the CM, the new set of weights is different from the previous one (Table 8.b). Looking at the correlation coefficients of the shifted injections rates (Table 8.a), the correlation coefficient is smaller than the previous case, so we have fewer problems with the weights: for injector #5 using the first set of the injection data, the summation of the weights was around 1.27, but the summation of the weights for the second set is 1.09. In other words, we see that less collinearity makes the weights more plausible.

4.6 Conclusions

1. Using the methods based on both injection and production data to find the segmentation times, the optimum segmentation times could be determined. But because of their sensitivity

to initialization and CPU time, the methods based on only the production data are needed to be developed and investigated.

2. The use of the segmented CM for stimulated reservoirs could be useful. Although, it does not give the true interwell connectivity coefficients, the results are much better than those obtained using the simple CM.

3. The use of prior injection data could improve the results especially for large dissipation cases. However, it is unable to solve the problem completely, even for 1x1 case where there is no interaction between the injection signals.

4. For the low permeability cases, and more generally small diffusivity, the interaction of the injection signals after shifting by the τ 's is an important factor that decreases the performance of the CM. Applying ridge regression may be useful to overcome this problem.

4.7 Tables and Figures

Table 1- The interwell coefficients (λ 's) for case 1-1. The performance of both BCM and UCM is good. Also the λ_0 's for UCM are small, which shows that they are not required.

	UCM		BCM	
	Well #1	Well #2	Well #1	Well #2
τ_1	29.565	29.497	29.175	29.598
τ_2	30.086	36.864	29.970	36.916
τ_3	30.671	30.633	30.468	30.686
τ_4	37.084	28.298	36.677	28.343
τ_5	35.848	35.822	35.753	35.845
τ_p	13.718	11.239	14.082	11.085
λ_1	0.500	0.500	0.495	0.501
λ_2	0.589	0.422	0.587	0.422
λ_3	0.498	0.498	0.495	0.499
λ_4	0.427	0.575	0.423	0.576
λ_5	0.502	0.502	0.500	0.502
λ_p	0.916	0.906	0.902	0.908
λ_0	-30.43	7.28	-	-
R^2	1.000	1.000	1.000	1.000

Table 2- The interwell connectivity coefficients for case 1-2 (BHPwell#1=500, BHPwell#2=1,100psi), the coefficients of UCM and BCM are different. But UCM gives psi coefficients very close to the base case and its R^2 is higher.

	UCM		BCM	
	Well #1	Well #2	Well #1	Well #2
τ_1	29.692	29.347	25.917	33.471
τ_2	30.189	36.698	28.984	38.616
τ_3	30.624	30.656	28.671	32.749
τ_4	37.045	28.310	33.550	30.149
τ_5	35.900	35.756	34.889	36.594
τ_p	16.088	10.334	21.972	6.714
λ_1	0.500	0.500	0.445	0.552
λ_2	0.589	0.421	0.567	0.442
λ_3	0.497	0.498	0.472	0.525
λ_4	0.427	0.575	0.389	0.606
λ_5	0.502	0.502	0.486	0.515
λ_p	0.954	0.853	0.790	0.476
λ_0	-297.76	275.52	-	-
R^2	1.000	1.000	0.997	0.998

Table 3- The interwell coefficients (λ 's) for case 1-3. The λ 's and the performance of both methods are almost the same.

CM+BHP			Segmented CM		
	Well #1	Well #2		Well #1	Well #2
τ_1	22.117	21.846	τ_1	21.916116	21.806757
τ_2	29.854	36.424	τ_2	29.876121	36.562613
τ_3	32.545	32.389	τ_3	32.140047	32.446725
τ_4	38.390	29.130	τ_4	37.428808	29.108709
τ_5	37.083	37.231	τ_5	36.934947	37.360489
τ_p	8.078	7.713	τ_p	5.9530313	0.5966281
τ_{pr-1}	1000000	73643	λ_1	0.4687191	0.4754287
τ_{pr-2}	38858	1000000	λ_2	0.5881846	0.4254227
λ_1	0.468	0.467	λ_3	0.5097028	0.516238
λ_2	0.585	0.420	λ_4	0.4221343	0.5772009
λ_3	0.517	0.518	λ_5	0.500541	0.5037187
λ_4	0.438	0.582	λ_p	0.9935625	0.996569
λ_5	0.499	0.500	λ_{0-1}	31.810838	16.939973
λ_p	43	51.304	λ_{0-2}	-233.621	286.83583
v_{pr-1}	0.433	-0.451	λ_{0-3}	299.47527	-251.3693
v_{pr-2}	-0.448	0.450	λ_{0-4}	34.921519	20.21477
λ_0	0.275	39.184	R^2	0.9971938	0.9969357
R^2	0.996	0.996			

Table 4- λ 's of well #1 by shutting-in different wells. The λ 's are different for different cases.

Shut-in well	--	Well#2	Well#3	Well#4	Well#2,3	Well#2,4	Well#3,4	Well#2,3,4
λ_1	0.329	0.448	0.390	0.374	0.576	0.582	0.495	0.979
λ_2	0.330	0.393	0.452	0.376	0.583	0.502	0.587	0.998
λ_3	0.249	0.340	0.340	0.316	0.496	0.495	0.495	1.000
λ_4	0.171	0.294	0.234	0.262	0.427	0.508	0.422	1.000
λ_5	0.170	0.232	0.291	0.259	0.419	0.415	0.501	0.993

Table 5- The correlation coefficient of signals, a) before shifting b) after shifting with $\tau = 30$ and c) after shifting with $\tau = 150$. The correlation coefficients of the signals have been increased after shifting. The correlation coefficients greater than 0.4 are highlighted.

	inj 1	inj 2	inj 3	inj 4	inj 5
inj 1	1.0000	0.0033	-0.0019	0.0026	-0.0435
inj 2	0.0033	1.0000	0.0020	-0.0026	0.0229
inj 3	-0.0019	0.0020	1.0000	0.0068	0.0075
inj 4	0.0026	-0.0026	0.0068	1.0000	-0.0019
inj 5	-0.0435	0.0229	0.0075	-0.0019	1.0000

a)

	inj 1	inj 2	inj 3	inj 4	inj 5
inj 1	1.0000	0.4902	0.4744	0.5148	0.4771
inj 2	0.4902	1.0000	0.3508	0.3767	0.3802
inj 3	0.4744	0.3508	1.0000	0.3715	0.3603
inj 4	0.5148	0.3767	0.3715	1.0000	0.3839
inj 5	0.4771	0.3802	0.3603	0.3839	1.0000

b)

	inj 1	inj 2	inj 3	inj 4	inj 5
inj 1	1.0000	0.8468	0.9108	0.9338	0.8714
inj 2	0.8468	1.0000	0.8273	0.8478	0.8004
inj 3	0.9108	0.8273	1.0000	0.9127	0.8570
inj 4	0.9338	0.8478	0.9127	1.0000	0.8778
inj 5	0.8714	0.8004	0.8570	0.8778	1.0000

c)

Table 6- The correlation coefficient of the shifted injection signals for a) from month 1 to 20 b) from month 21 to 500. The increase in the correlation coefficient is only in the first few months. The correlation coefficients greater than 0.4 are highlighted.

	inj 1	inj 2	inj 3	inj 4	inj 5
inj 1	1.0000	0.9973	0.9921	0.9950	0.9983
inj 2	0.9973	1.0000	0.9845	0.9871	0.9966
inj 3	0.9921	0.9845	1.0000	0.9924	0.9864
inj 4	0.9950	0.9871	0.9924	1.0000	0.9911
inj 5	0.9983	0.9966	0.9864	0.9911	1.0000

a)

	inj 1	inj 2	inj 3	inj 4	inj 5
inj 1	1.0000	-0.0364	0.0082	0.0035	-0.0906
inj 2	-0.0364	1.0000	0.0072	0.0029	-0.0090
inj 3	0.0082	0.0072	1.0000	0.0166	0.0119
inj 4	0.0035	0.0029	0.0166	1.0000	-0.0058
inj 5	-0.0906	-0.0090	0.0119	-0.0058	1.0000

b)

Table 7- The interwell connectivity coefficients for case 1-9 using different sets of the injection rates.

	Injection rates set 1		Injection rates set 2	
	Well #1	Well #2	Well #1	Well #2
τ_1	84.19	84.01	91.42	88.53
τ_2	94.86	160.61	89.78	145.46
τ_3	112.18	118.61	113.47	110.64
τ_4	363.62	67.17	162.34	93.05
τ_5	171.45	170.38	162.32	168.53
τ_p	202.49	166.41	179.42	205.28
λ_1	0.4578	0.4560	0.4829	0.4826
λ_2	0.5576	0.5071	0.5604	0.4300
λ_3	0.5064	0.5181	0.5013	0.4949
λ_4	0.9878	0.4314	0.4505	0.5514
λ_5	0.6385	0.6349	0.5318	0.5570
λ_p	1.1894	0.8992	0.8268	0.8015
λ_0	-1259.46	-108.10	-19.95	3.20
R^2	0.9990	0.9986	0.9948	0.9932
MSE	8.21	9.03	7.99	8.05

Table 8- The correlation coefficients between the injectors and also the primary production component of the model for the first (a) and the second (b) set of the injection rates after shifting. The correlation coefficient for second set of the injection rates is closer to zero. The correlation coefficients with absolute value greater than 0.4 are highlighted.

a)

	inj 1	inj 2	inj 3	inj 4	inj 5	primary prod.
inj 1	1.0000	0.1867	0.4392	0.4944	0.3307	-0.4932
inj 2	0.1867	1.0000	0.4106	0.4628	0.2824	-0.4609
inj 3	0.4392	0.4106	1.0000	0.8971	0.5350	-0.9072
inj 4	0.4944	0.4628	0.8971	1.0000	0.6003	-0.9950
inj 5	0.3307	0.2824	0.5350	0.6003	1.0000	-0.5993
primary prod.	-0.4932	-0.4609	-0.9072	-0.9950	-0.5993	1.0000

b)

	inj 1	inj 2	inj 3	inj 4	inj 5	primary prod.
inj 1	1.0000	0.0344	0.2222	0.0278	0.0805	-0.2559
inj 2	0.0344	1.0000	0.1116	0.0440	-0.0872	-0.0452
inj 3	0.2222	0.1116	1.0000	0.0409	0.1961	-0.2917
inj 4	0.0278	0.0440	0.0409	1.0000	0.3224	-0.5445
inj 5	0.0805	-0.0872	0.1961	0.3224	1.0000	-0.6252
primary prod.	-0.2559	-0.0452	-0.2917	-0.5445	-0.6252	1.0000

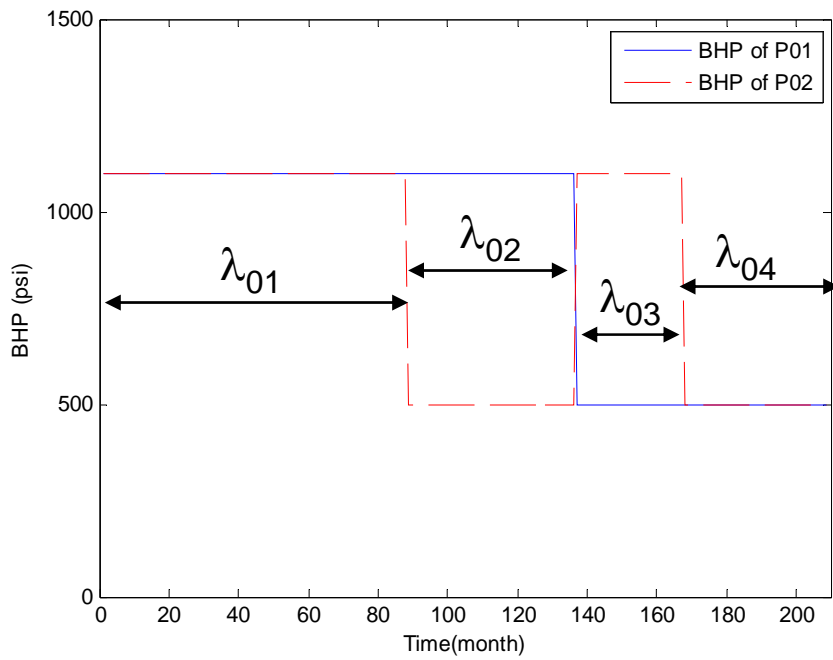


Figure 1- In the segmented CM different λ_0 's for different BHP's are used.

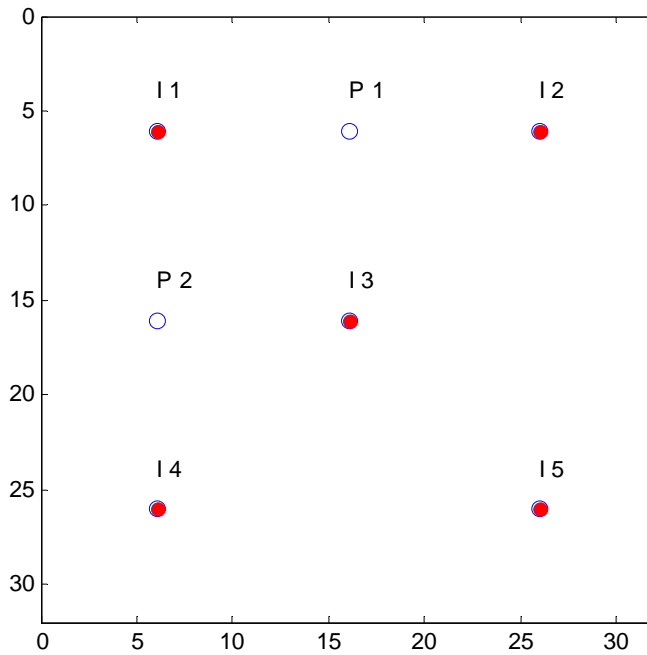


Figure 2- Location of the wells for case 1.

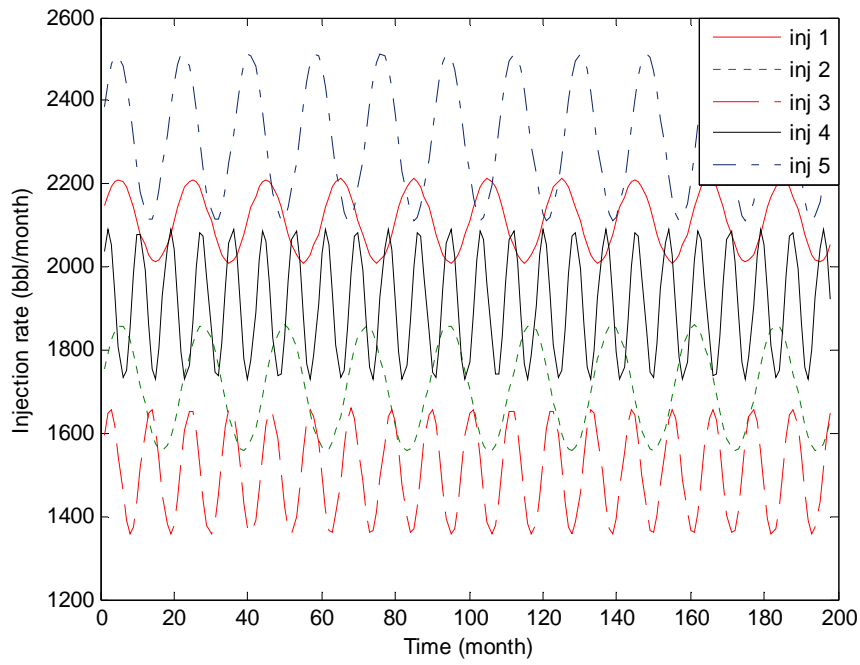


Figure 3- The injection rates in case 1 and case 2. The injection rates are fully uncorrelated.

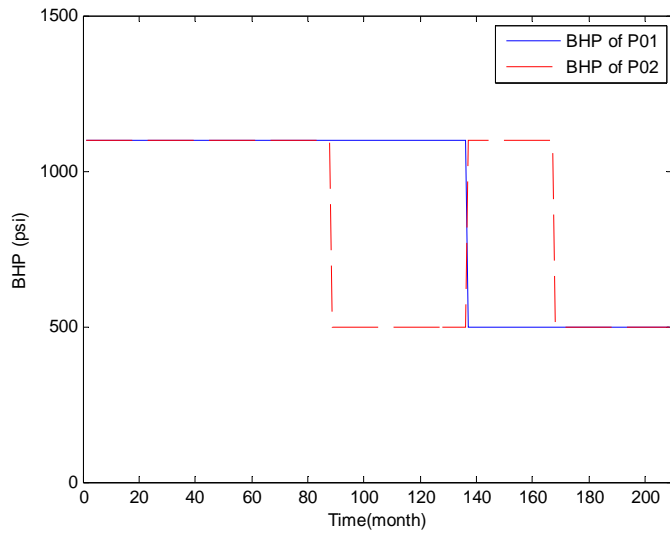


Figure 4- Bottom hole pressure changes of case 1-3.

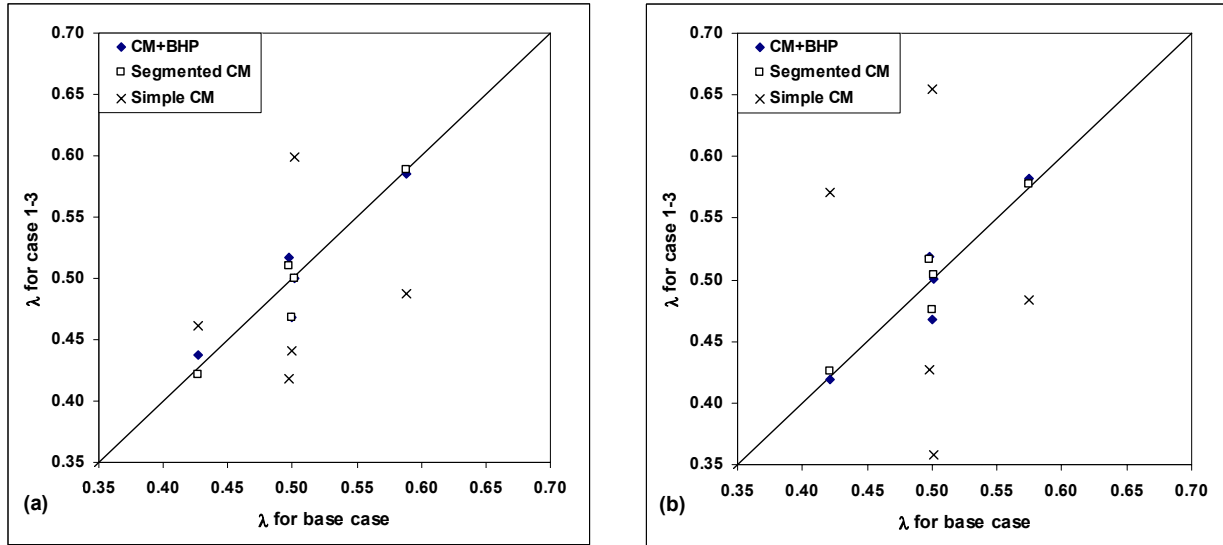


Figure 5- Comparison of the weights for case 1-3 with the base case: a) producer #1, b) producer #2. It can be seen that considering the BHP changes the weights are very close to the base case. Also the performance of the Segmented CM is as good as the CM+BHP.

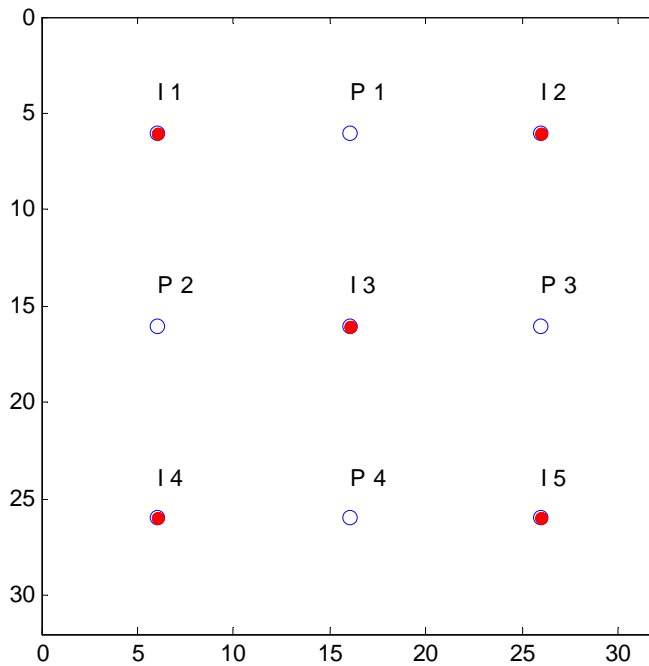


Figure 6-: Location of the wells for case 2.

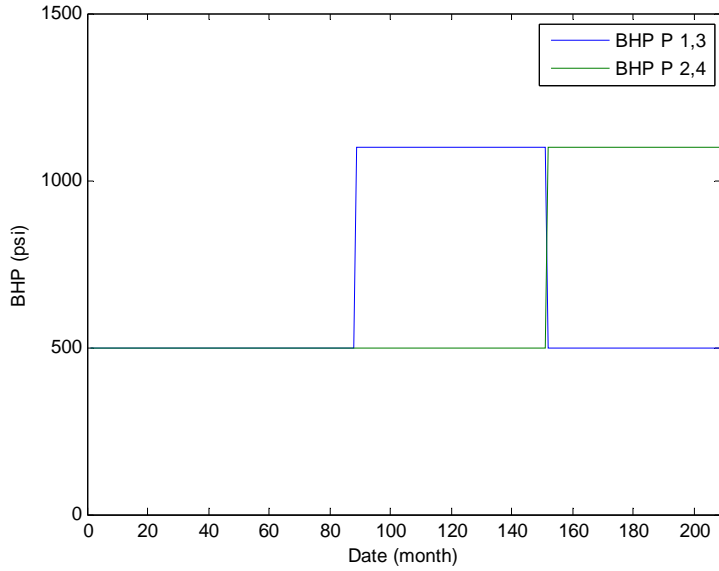


Figure 7- The BHP changes of the producing wells for case 2-1.

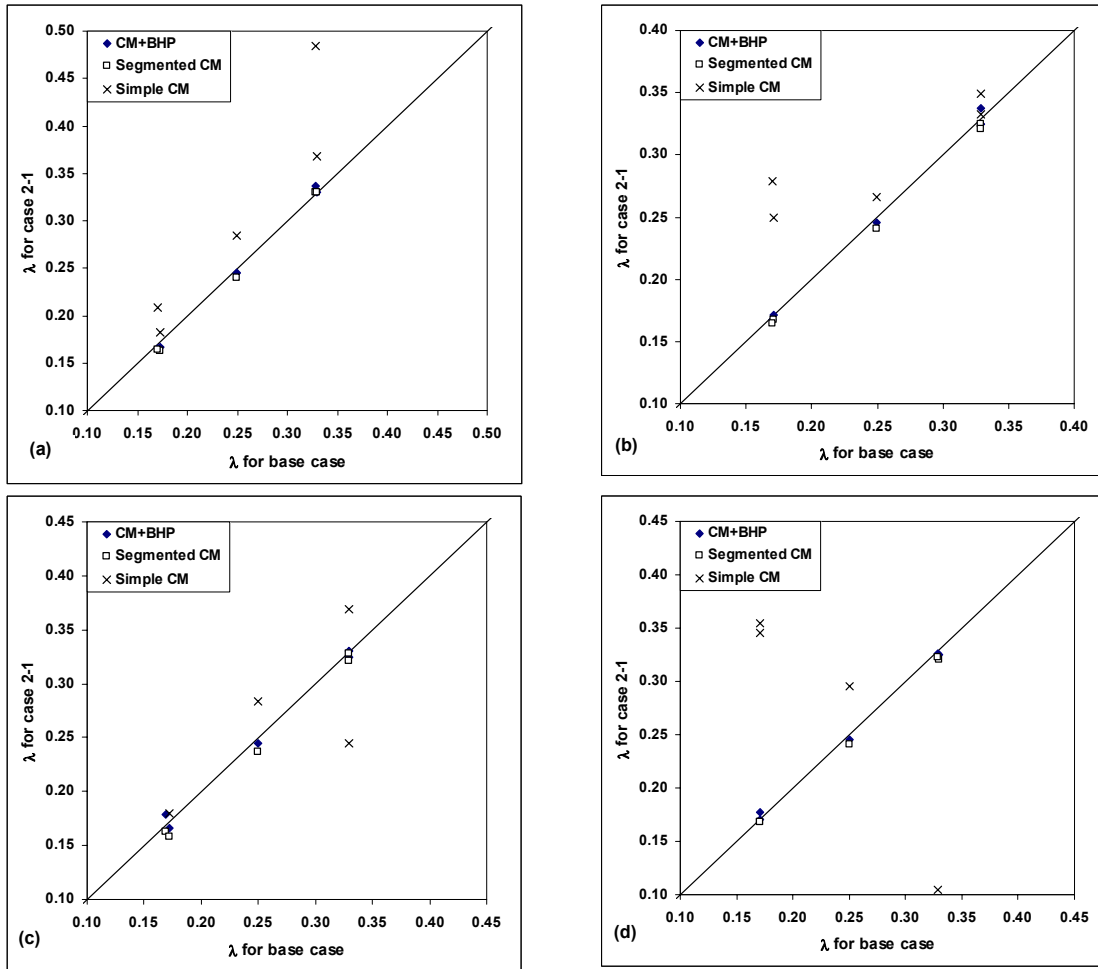


Figure 8- Comparison of weights for the fluctuating BHP and constant BHP, case 2-1 for producers 1-4 (a-d). Considering the BHP changes, the weights are very close to the base case.

The performance of the segmented CM is as good as the CM+BHP, even for a large number of producers.

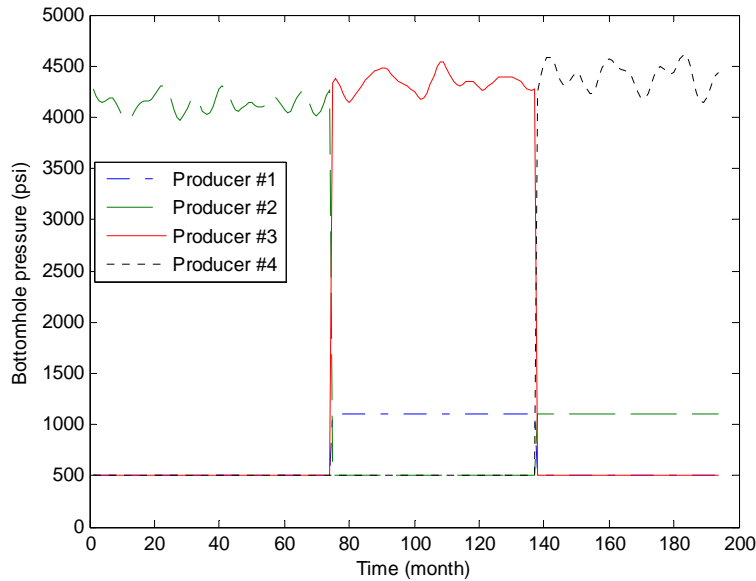


Figure 9- The BHP changes of the producing wells for case 2-2. In the shut-in period, the BHP 's are fluctuating.

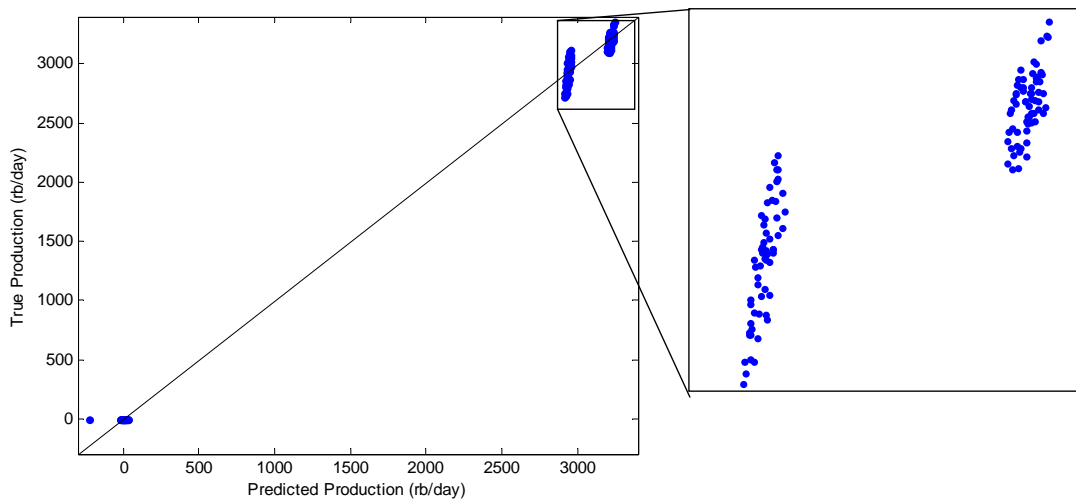


Figure 10- The R^2 of the prediction is very high (0.998) for the case of shut-in wells using the segmented CM, but the fit is poor.

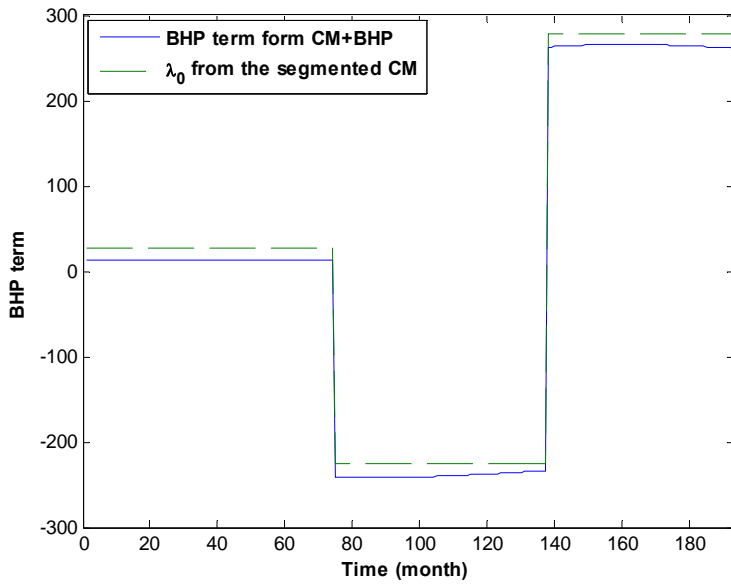


Figure 11- Comparison of the λ_0 from the segmented CM and the BHP term from the CM+BHP for case 2-1. The values of BHP term and λ_0 are very close to each other.

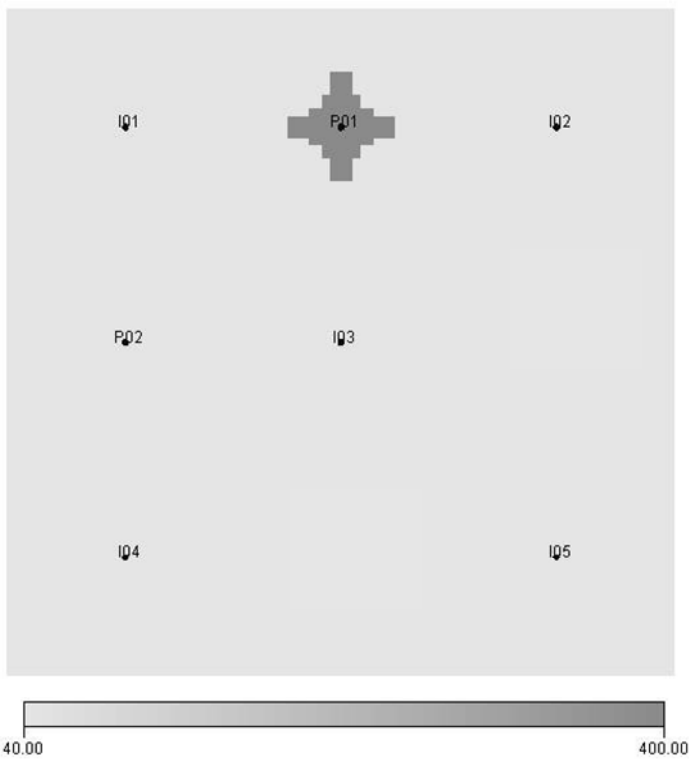


Figure 12- The permeability map of case 1-4, where producer 1 has been acidized around which the permeability is higher.

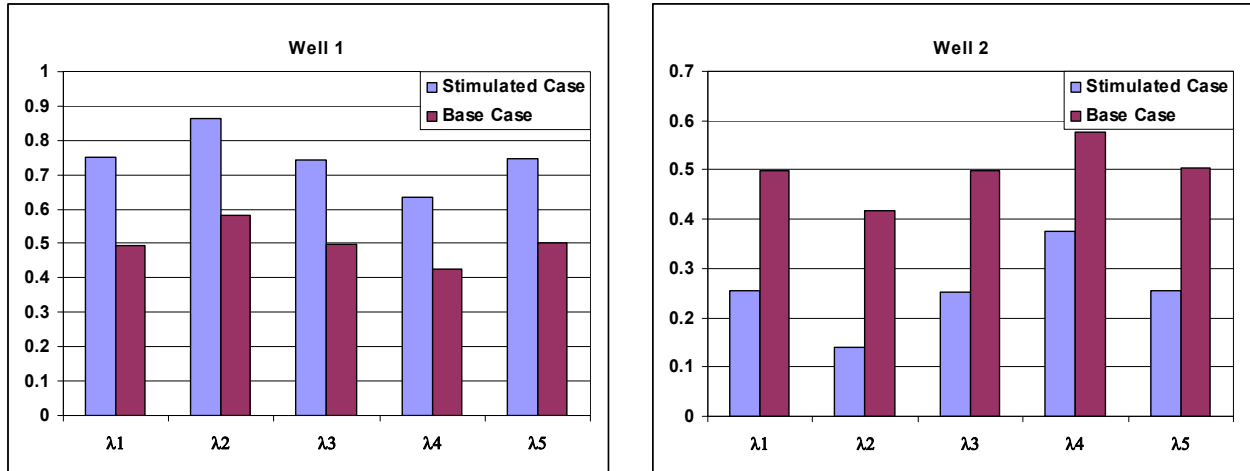


Figure 13: The interwell connectivity coefficients of the stimulated field (case 1-4) comparing with non-stimulated field (case 1-1). Aafter stimulation, the λ 's for stimulated well (well #1) increased and those of well #2 decreased.

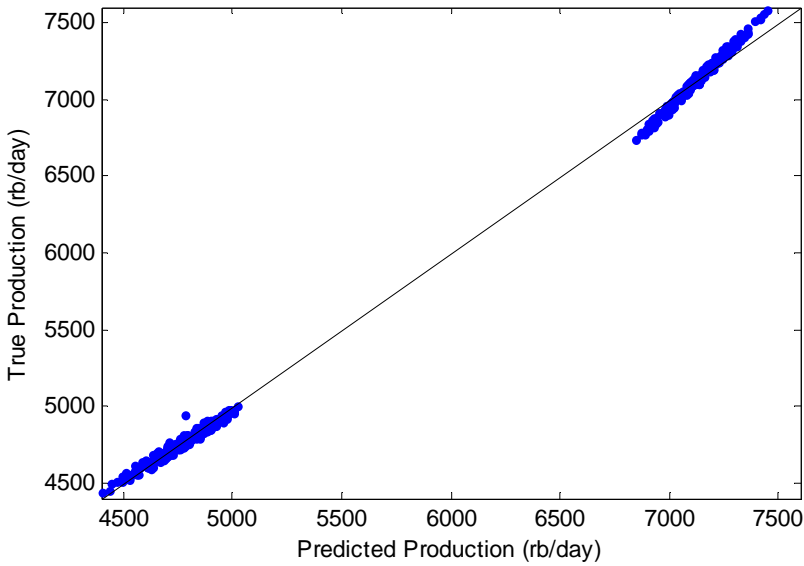
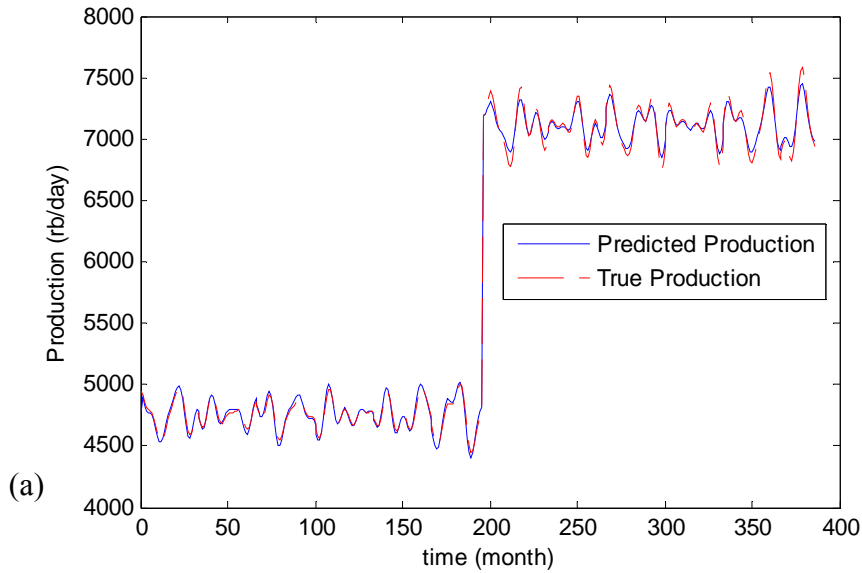


Figure 14- Using the segmented CM for combination of the base case and case 1-4 (modeling before and after stimulation data in one model), well #1: a) True and the predicted liquid production, b) True vs. the predicted liquid production. The prediction is good; the R^2 is 99.87% and the MSE is 42.16.

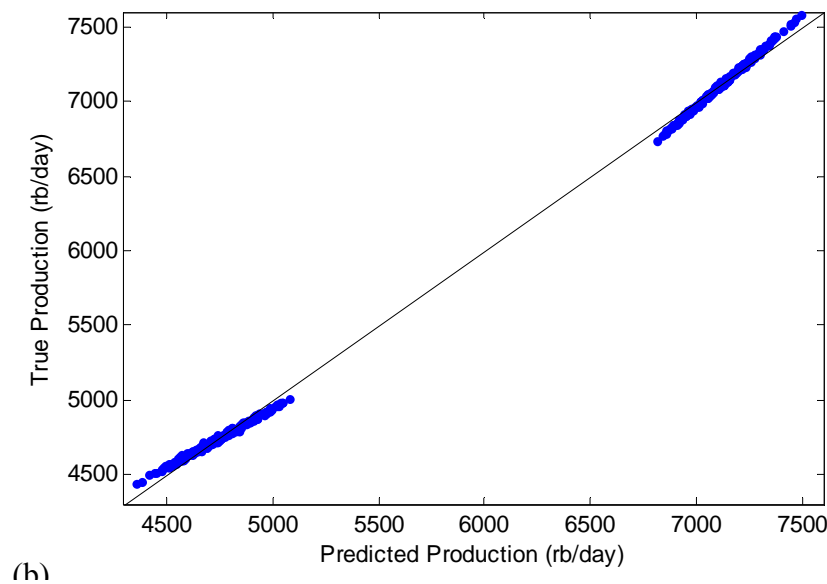
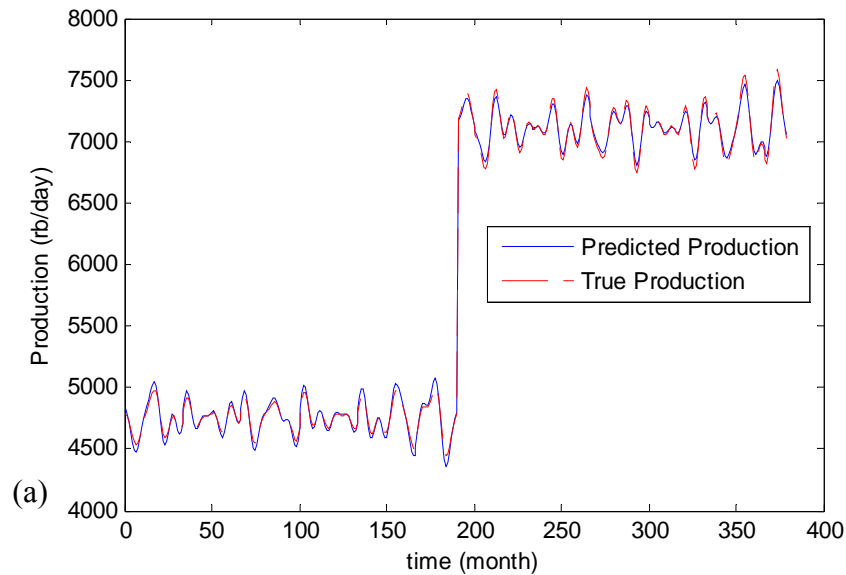


Figure 15- Using the segmented CM for combination of the base case and case 1-4 (modeling before and after stimulation data in one model), well #1: a) True and the predicted liquid production, b) True vs. the predicted liquid production. The prediction is good, the R^2 is 99.92%, and the MSE is 33.57. However, comparing the scatter of the points with the $y=x$ line, the weights are larger than the weights of the before stimulation period and smaller than the weights of the after stimulation period.

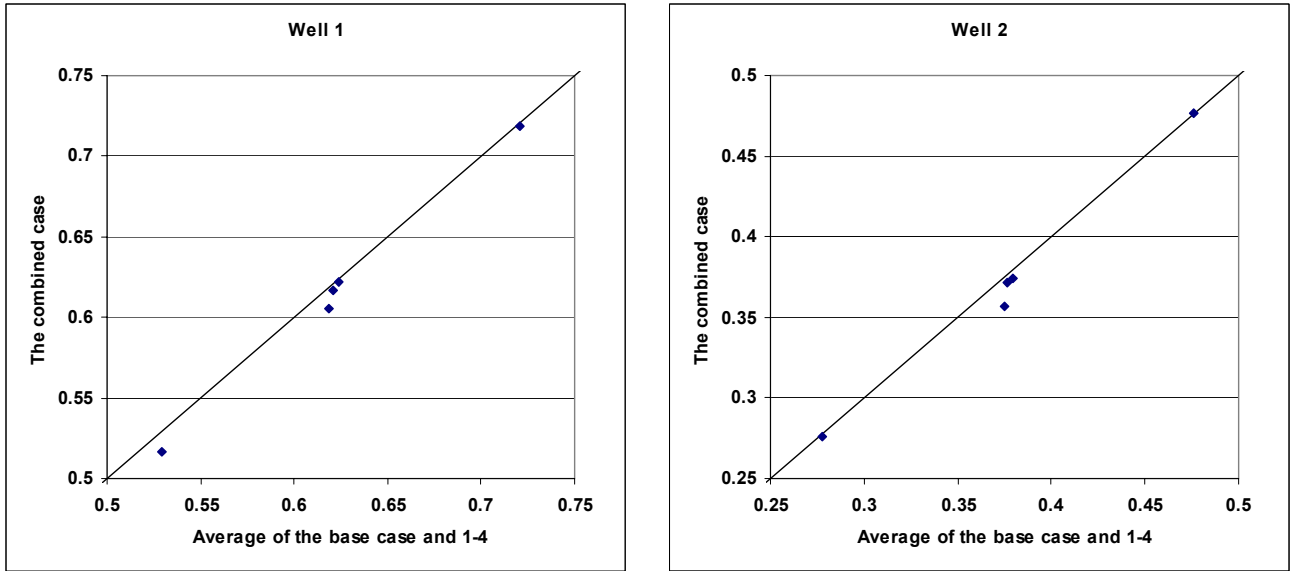


Figure 16: The λ 's for the combined case and the average λ 's of the base case and the stimulated Case (1-4). The weights of the combined case are very close to the average of the two cases.

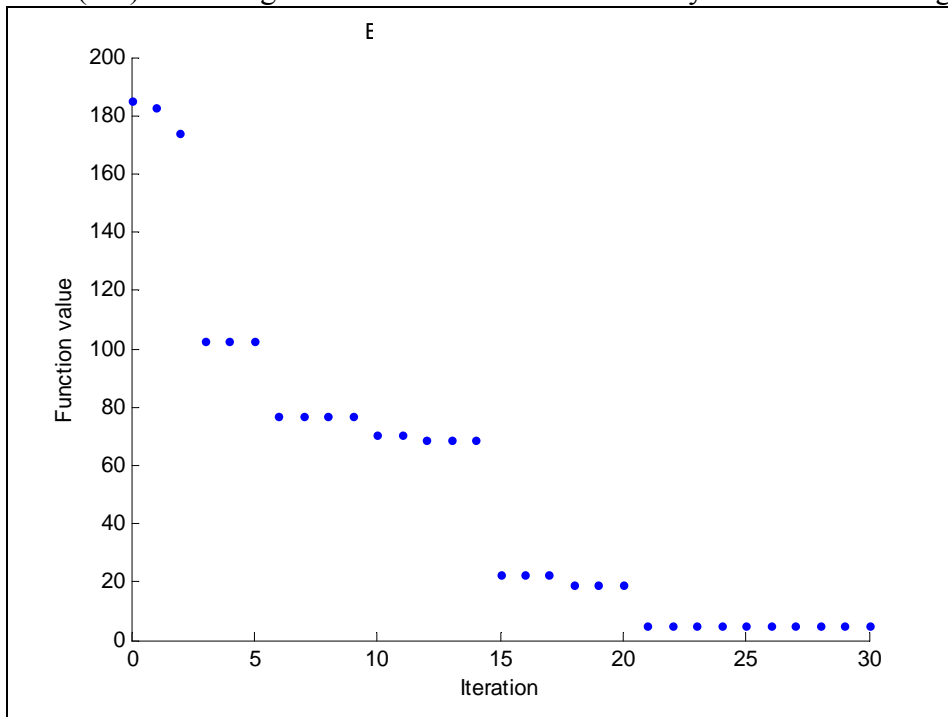


Figure 17- Decreasing the error of the prediction during optimization of the segmentation time for example 1 using direct search. The algorithm found the right segmentation times in 21 iterations.

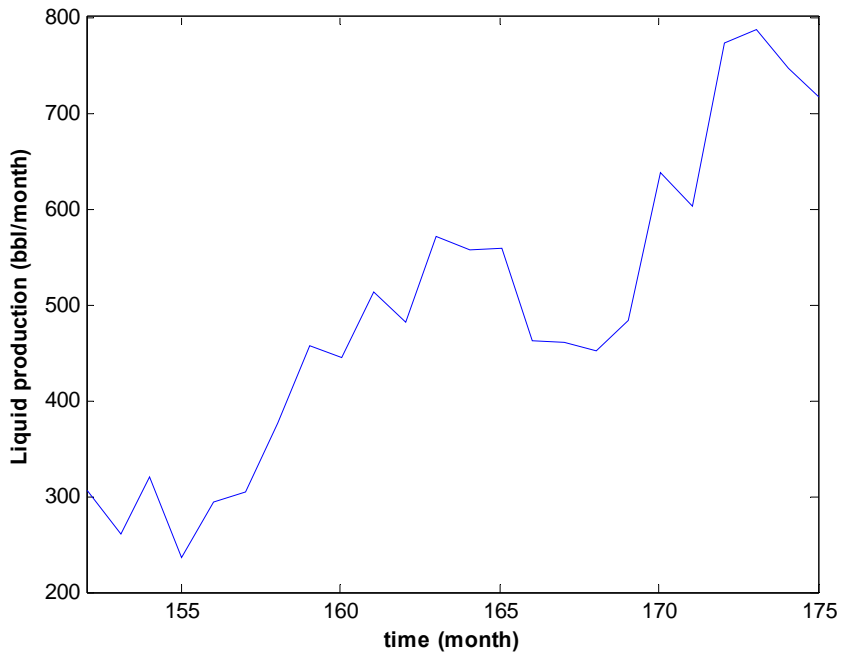


Figure 18- Production profile of well 1214 MBU, at interval 152-175 month, which is used for example 2

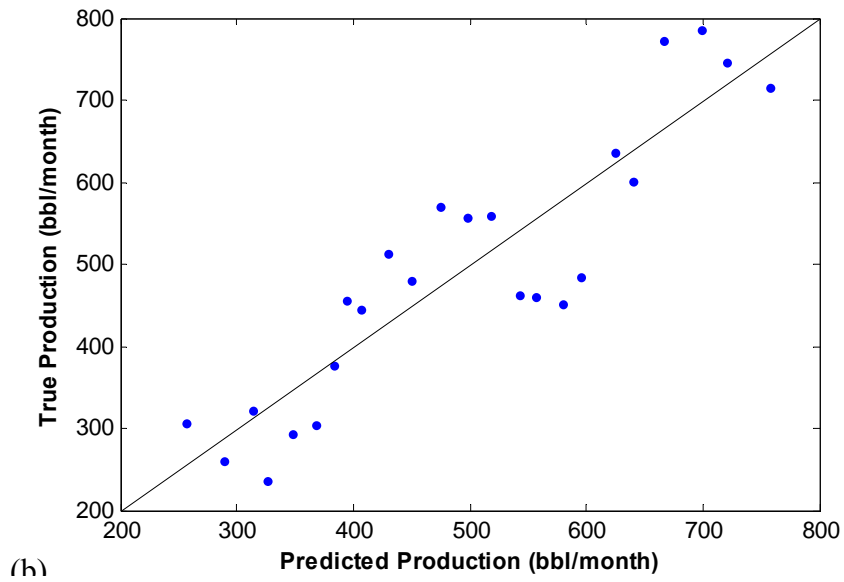
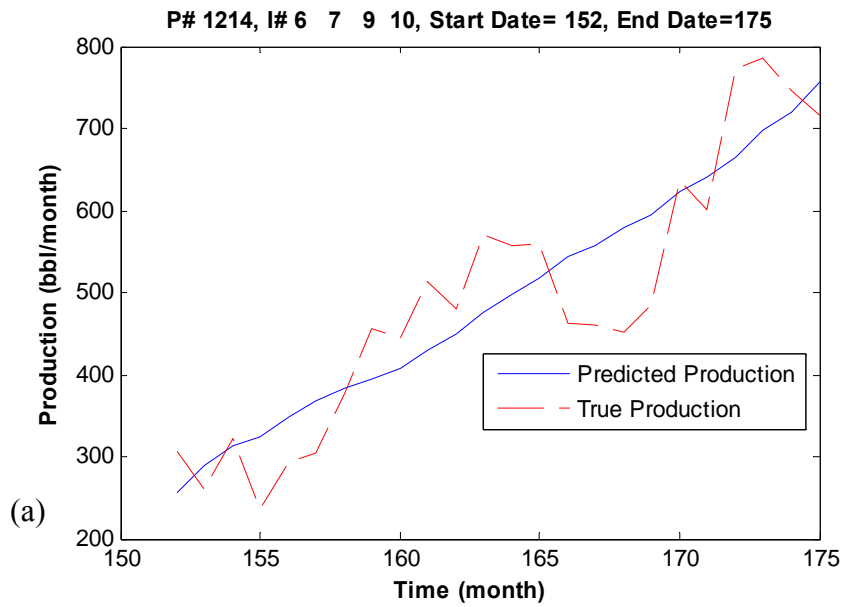


Figure 19- Using simple CM to find the interwell connectivity coefficients over the selected interval: a) True and the predicted liquid production, b) True vs. the predicted liquid production. The prediction is poor, and R^2 is 0.8117%.

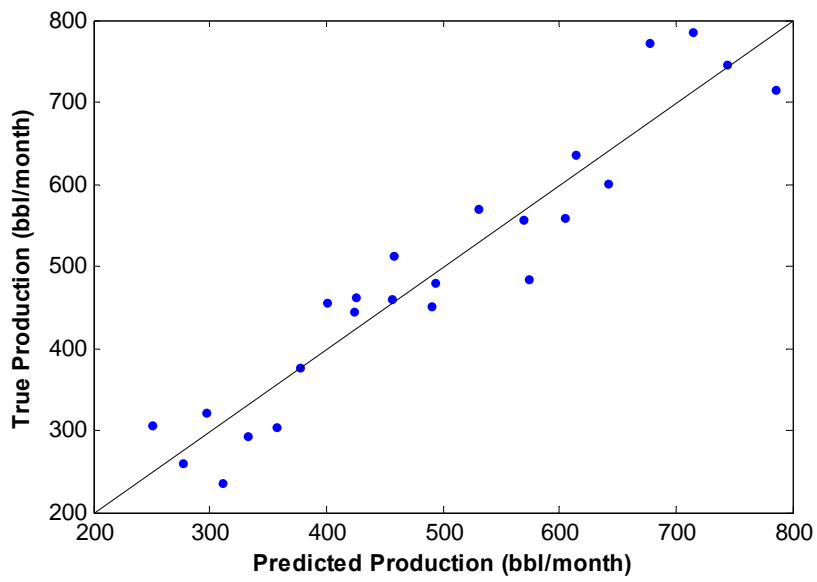
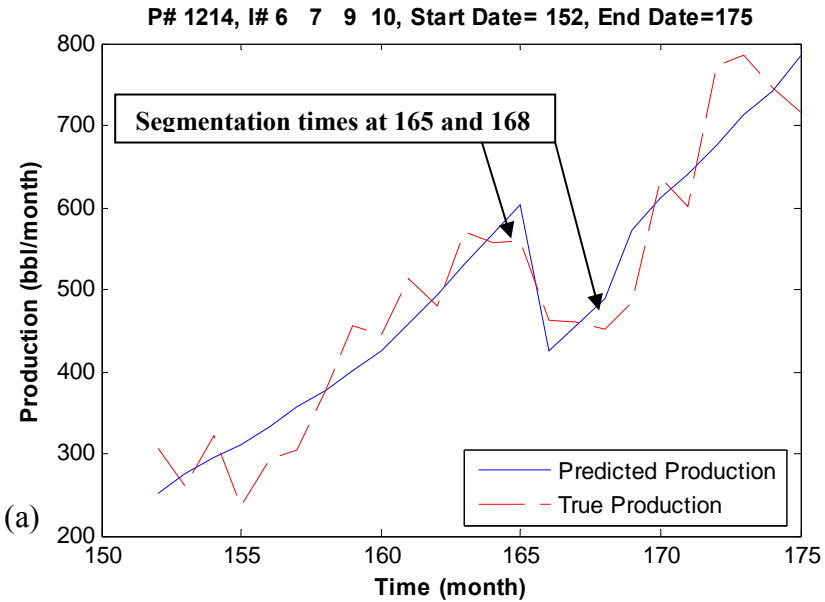


Figure 20- Using the segmented CM based on the visual estimation of the segmentation times: a) True and the predicted liquid production and the estimated segmentation times, b) True vs. the predicted liquid production. The prediction is better than the simple CM ($R^2=0.9066$), but it still has moderate error.

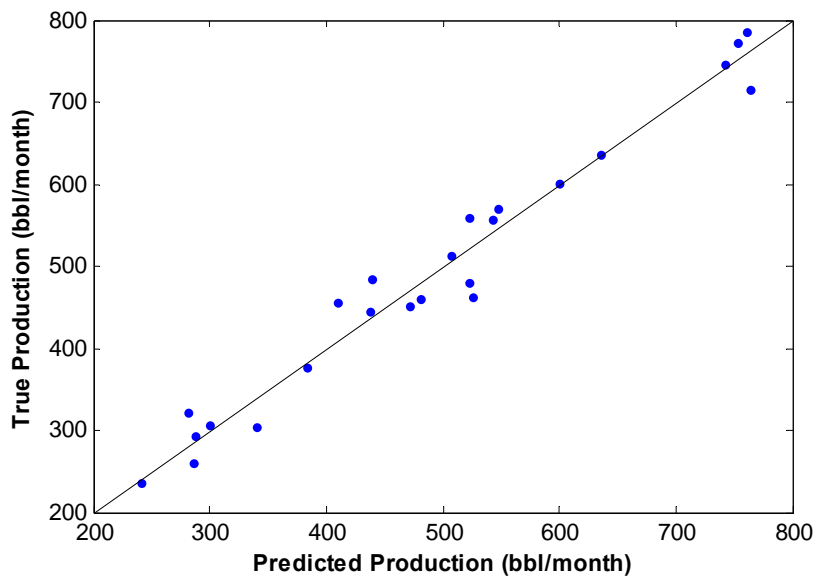
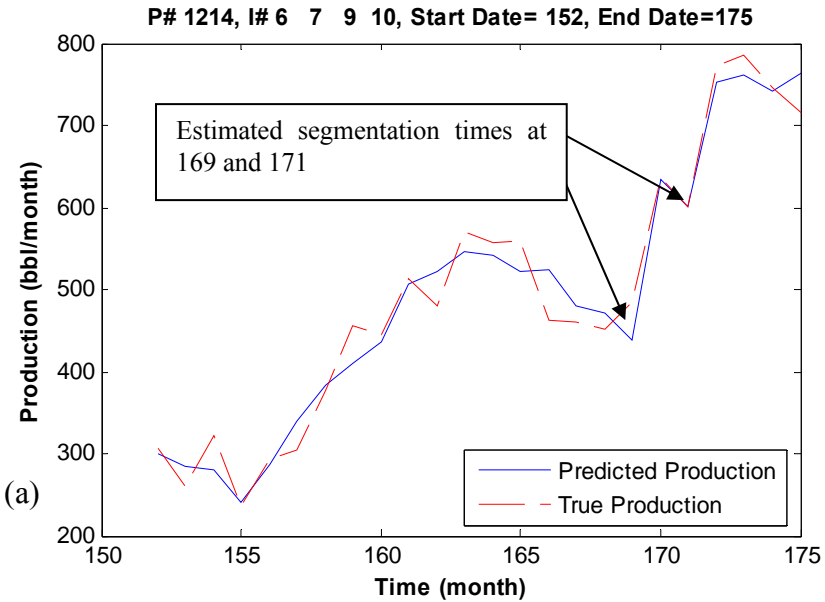


Figure 21- Using the segmented CM based on the direct search of the segmentation times: a) True and the predicted liquid production, b) True vs. the predicted liquid production. The prediction is quite good.

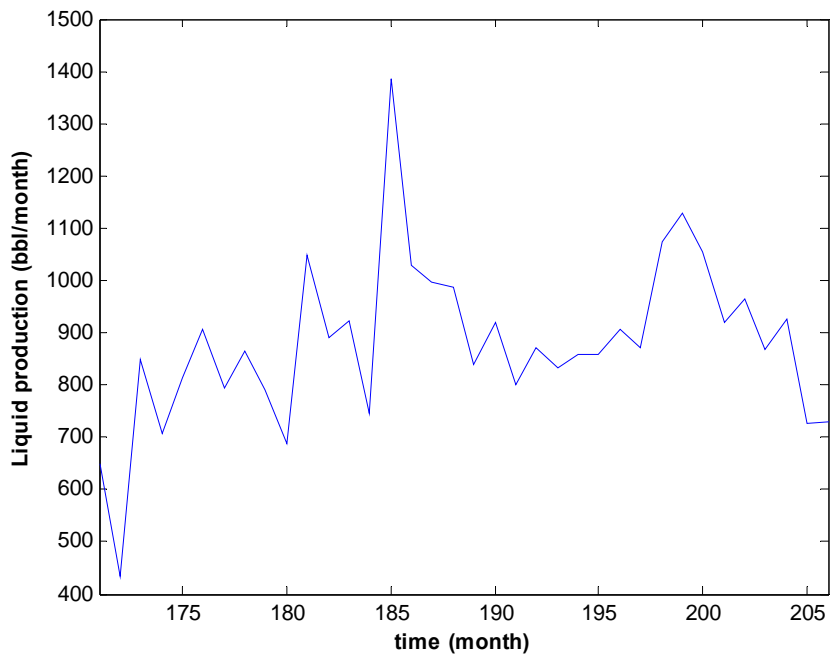


Figure 22- Production history of well 1250 MBU, at interval 171-206 month, which is used for Example 3

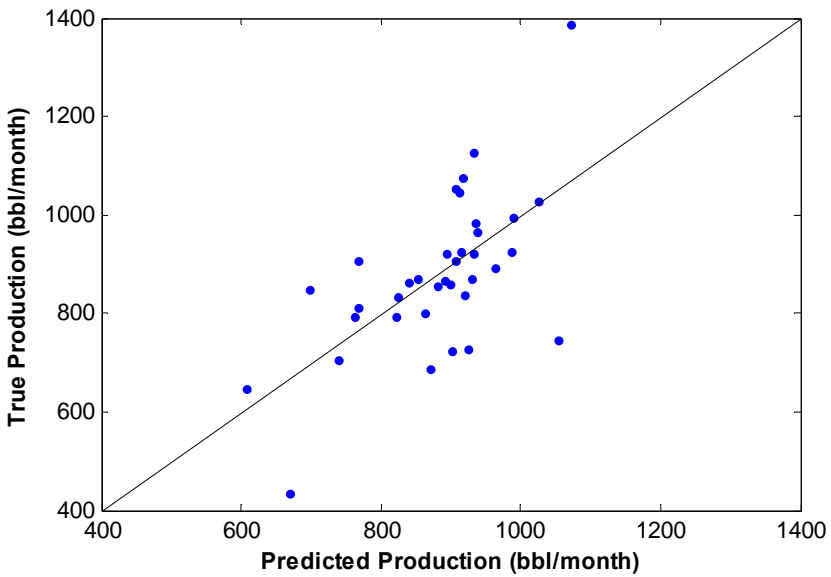
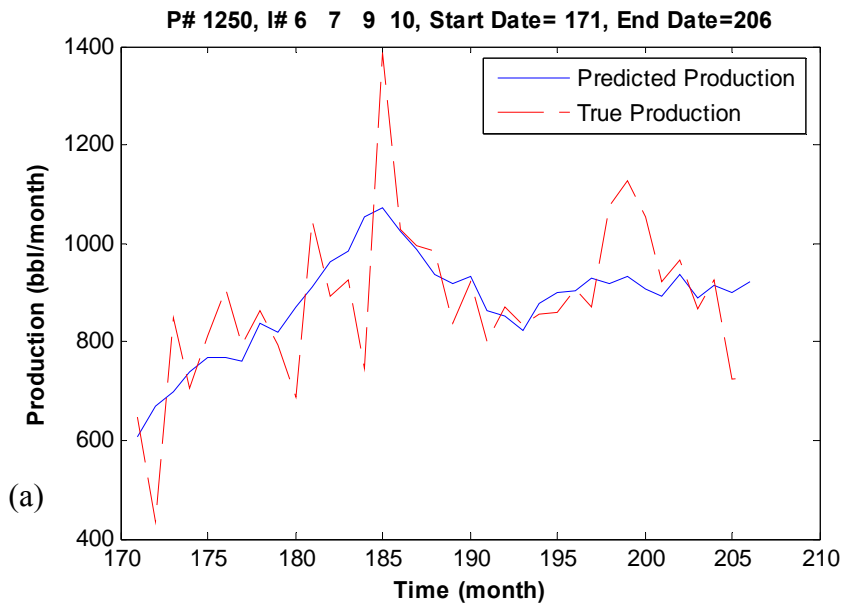


Figure 23- Using simple CM to find the interwell connectivity coefficients over the selected interval: a) True and predicted liquid production, b) True vs. the predicted liquid production. The prediction is not good ($R^2=.405$)

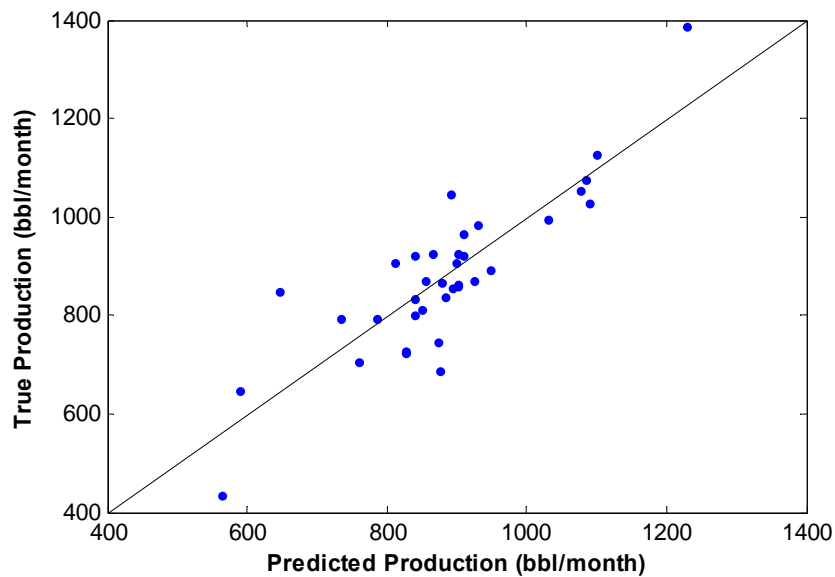
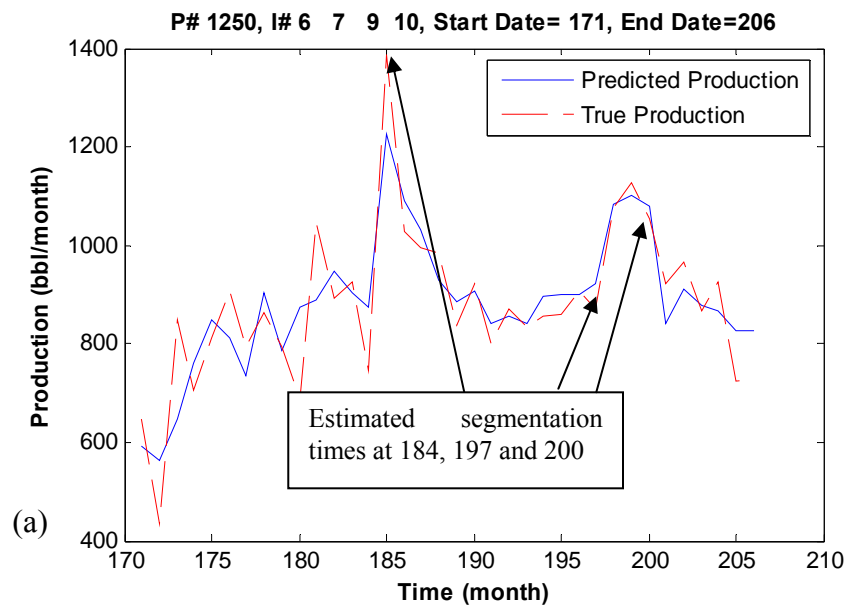


Figure 24- Using the segmented CM based on the direct search of the segmentation times to find the interwell connectivity coefficients over the selected interval: a) True and predicted liquid production, b) True vs. the predicted liquid production. The prediction is poor, but it is much better than the simple CM ($R^2 = 0.7368$)

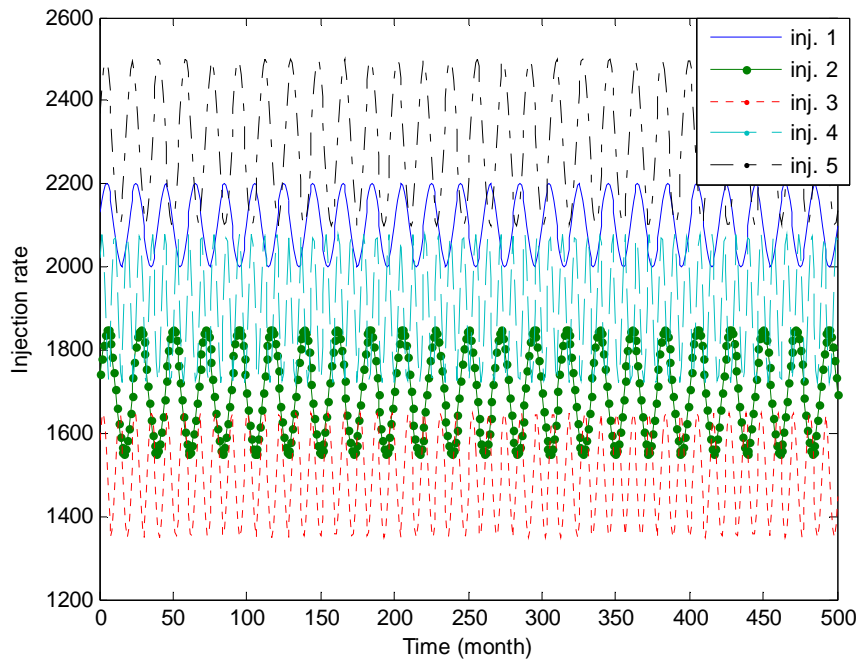


Figure 25-The injection signals with different frequency for example 4.

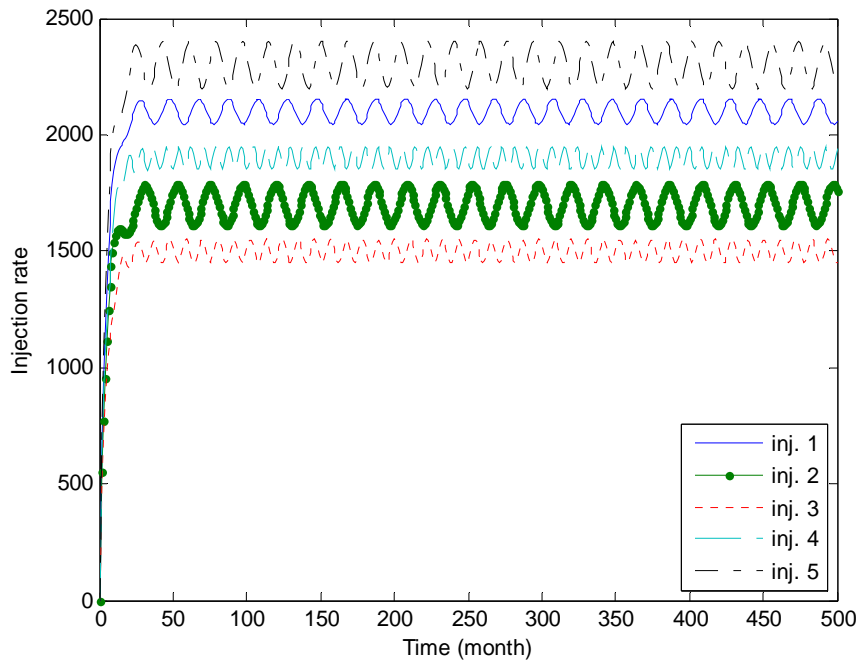


Figure 26- The injection signals for example 4 after shifting with $\tau=150$ days. The first 20 days have very similar signals.

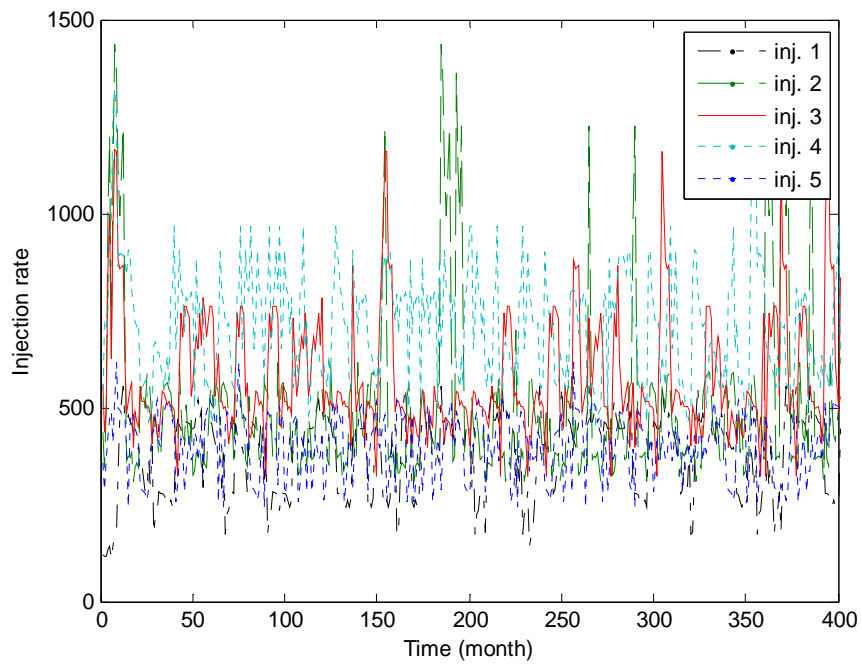


Figure 27- The second set of the injection rates for case 1-5.

RESULTS AND DISCUSSION

PART 5. SPECTRAL ANALYSIS OF INJECTION AND PRODUCTION DATA

5.1 Introduction

This project phase estimates interwell connectivity using the frequency spectra of the well rates. It tests the combination of Fourier transforms (FT's) of the flow rate data and analytical solutions from analog electrical circuits to infer the inverse diffusivity coefficient (IDC). We used the analytical solutions of the transmission line equations for 0D, 1D, and 2D resistance/capacitance (RC) networks to determine the interwell diffusivity parameters. We used the analogy between the electrical response of RC networks and the fluid response of permeable reservoirs on the basis of the similarities in their governing equations. Details of this method are described in Demiroren (2007) and Jensen and others (2006).

We conclude that the method works well in simple reservoirs, where the assumptions of an analytical solution are met, *i.e.* single-phase fluid and a homogeneous system. For two-phase liquid cases, we determined that the analogy remains applicable because we still could produce accurate interwell connectivity information. When we investigated cases with dissolved-gas production around the wellbore; however, the analogy broke down and the results were not as good as the liquid systems.

5.2 Method Description

Analytical solutions based on three RC network models (RC transfer functions) and reservoir transfer functions are put together in one common spectrum to compare the fluid flow with the analogous analytical solutions. The ultimate goal is to select the best RC network solution as the representative of the reservoir behavior. Finally, this analytical solution provides the interwell connectivity information in terms of the estimated diffusivity coefficient parameters, ϕ/k .

The other objective, besides inferring connectivity information, is to determine under which reservoir conditions this analogy between RC analog networks and reservoir works out through transfer functions.

Throughout the applications, homogenous reservoir models under various conditions are simulated in hypothetical cases. The RC transfer functions that are correspondent to the simulated reservoir models are used to identify high and low frequency components in frequency domain by spectral analysis. One of the RC transfer functions, which matches the reservoir transfer function of the simulated reservoir model, is selected to be the best approximation to the reservoir behavior. The RC coefficient, which is used to fit the analytical solution to the reservoir behavior, is assigned to the diffusivity coefficient due to the analogy between RC networks and reservoir. Finally, the estimated diffusivity coefficient via the analogous RC network provides the interwell connectivity information in terms of ϕ/k as it is tabulated at the end each application.

5.3 Reservoir Models Used in Simulation Analysis

Standard reservoir geometry will be used in the applications unless otherwise stated (Fig. 1). The standard geometry is a small and narrow reservoir with dimensions of 1500 ft x 150 ft x 20 ft. The grids are discretized by 150 x 50 x 5. This is a 5 layered model allowing fluid flow in y-direction. Flow in z-direction is not allowed by assigning a value of 1 md to the permeability in z-direction. The injector is located in gridblock at (1,1); the producer is located at (150, 50). The interwell distance is about 1508 ft (~460m). Waterflooding is performed in each simulation. 1%

random error is added to the injection rate, which is based on 30 frequencies. Simulated production rates given the reservoir parameters, which will be specified in each section, are modeled in Eclipse by E100. Demiroren (2007) gives details of the simulation model validation.

5.4 Results and Analysis of Cases

To test the spectral analysis procedure, several cases were analyzed. These cases cover single- and multi-phase fluids. The analysis seeks to identify which transmission line response best replicates the calculated transfer function and how the estimated diffusivity coefficient compares with the true value. Here, we present the results of three cases; the results and analyses of other cases are covered by Demiroren (2007).

5.4.1 Single Phase (Water Only) Production Case

Single phase production case forms a basis for the research because it is the case that involves the least amount of heterogeneity. This is the application of a simple reservoir where the assumptions of the analytical solutions are nearly met. Even though the reservoir is kept as a homogeneous model throughout the entire work, producing one more phase and including the relative permeability curves into the model creates heterogeneity in the system.

Reservoir parameters used for single phase production is stated in **Table 1**. Injection rate with main signal of 30 frequencies is utilized to simulate the standard reservoir geometry sketched in **Fig. 1**. According to the reservoir parameters, the diffusivity coefficient varies between $1.45e-1 \text{ sec/m}^2$ and $7.25e+0 \text{ sec/m}^2$. Reservoir transfer functions obtained from the simulations are shown in **Fig. 2**. In this figure, it is apparent that lower the compressibility effect, higher the transfer function amplitude. This implies the filtering ability of reservoir lessens as the compressibility effect gets smaller, which also allows for a smaller diffusivity coefficient. In the most compressible system, the high frequency values have ripples due to the stopband which occurs due to the filtering process in the reservoir.

Analytical solutions provided by three RC network models are calculated given the diffusivity coefficient parameters. First of all, three analytical solutions for an RC coefficient of $1.45e+0 \text{ sec/m}^2$ and the correspondent reservoir transfer function for $C_t = 1e-5 \text{ 1/psi}$ are compared in **Fig. 3** to select which one of the models describes the reservoir behavior most. It is obvious that 0-D lumped model represents the reservoir behavior better than the other two solutions. It is important to select the best representative model because interwell connectivity information is inferred from the analogy between the particular RC network and reservoir. In this case, 2-D and 1-D model solutions underestimate the reservoir transfer function, whereas 0-D solution fits the frequency cut-off and the transition region in high frequencies very well.

Figs. 4a to 4d display the results for the rest of the reservoir transfer functions. Each one of them is plotted with lumped RC transfer function to prove that lumped model provides the best approximation to the slightly compressible homogeneous systems. When total compressibility is between $1e-5 \text{ 1/psi}$ and $1e-6 \text{ 1/psi}$ as in **Figs 4a-c**, lumped RC solution is the answer to extract the interwell connectivity information from the analogy between two media. However, when system gets more compressible as in **Fig. 4d**, lumped model loses its ability to define the reservoir behavior and 2-D model fits the fluid flow behavior better.

It can be concluded from this analysis that compressible and slightly compressible systems should be interpreted differently because the type of solution that describes each system is different. Despite the fact that 2-D model solution seems to fit the reservoir better than the lumped model in **Fig. 4d**, it is still not an exact solution due to the ripples in high frequencies, which occurs due to the stopband. In cases where stopband appears in the spectrum, the ripples

are intended not to be included in the quantitative analysis. The reason is that the analytical solutions, which are RC transfer functions, include only the passband and the transition band of a low-pass filter. Since they are unable to identify the stopband, the ripples that appear in the stopband provide information only on a qualitative basis. Therefore, RC transfer functions are matched with only the passbands, the frequency cut-offs and the transition bands of the reservoir transfer functions.

As a result of the single phase production, the lumped model is selected as the best descriptive model for compressible systems that has a value between $1e-6$ and $1e-5$ 1/psi. Eventually, the analogy between RC network and reservoir provides valuable information to infer the interwell connectivity. The analogy between these two media ensures that corresponding RC coefficient should be equal to the estimated diffusivity coefficient as seen in **Table 2**. If the RC transfer functions do not match the reservoir transfer functions in the first place, then the RC coefficient of the analytical model is adjusted to approximate the reservoir behavior. In such a case, the modified RC coefficient is assigned to the estimated diffusivity coefficient, which yields the estimated ϕ/k values from the analogy between RC networks and reservoir. In single phase production, all reservoir transfer functions are matched with an analytical solution with no modification on the diffusivity coefficient. Representation of interwell connectivity in terms of estimated ϕ/k lets us make further interpretation for permeability. Since porosity is generally available through core samples and log analysis in reservoir engineering practices, permeability can be easily determined from such a relationship, which is classified in the last column.

5.4.2 Dry Gas and Water Case

Reservoir parameters and relative permeability curves used in the reservoir models are shown in **Table 3** and **Fig. 5**, respectively. In this application, the effect of free gas production on reservoir transfer functions is investigated. Injection rates are reduced by a factor of 10 and the standard reservoir geometry is simulated.

Fig. 6 illustrates the reservoir transfer functions produced from three total compressibility values. Basically, gas compressibility is kept constant around $1e-5$ 1/psi and water compressibility is changed to $1e-5$, $5e-6$ and $1e-6$ 1/psi. Water breakthrough takes place around 500 days out of 4096 days. The differences in total compressibility values appear by the change of the high frequency amplitudes, which is a result of attenuation in the reservoir. Ripples in high frequency components occur again when water compressibility at $1e-5$ 1/psi is used. The range of diffusivity coefficients applied in this case is $2.3e-1$ and $4.64e-1$ sec/m^2 .

Fig. 7a displays the three RC models for an RC coefficient of $2.03e-1$ sec/m^2 and the correspondent reservoir transfer function with C_t of $1.4e-6$ 1/psi. After adjusting the compressibility value to the water compressibility ($1e-6$ 1/psi) rather than the total value and decreasing the permeability down to 13 md results in an RC value of $1.16e+0$ sec/m^2 in **Fig. 7b**. Obviously, 0-D lumped model is the best choice to construct an analogy between RC network and reservoir fluid flow.

Figs. 8a and **8b** belong to the reservoir transfer function when the total compressibility in the system is $2.2e-6$ 1/psi. **Fig 8a** presents three RC analytical solutions when RC is set to the exact reservoir parameters, which are used to run the simulation. Analytical solutions overestimate the reservoir behavior. Therefore, in **Fig. 8b**, RC coefficient is modified to $3.15e+0$ sec/m^2 by increasing the compressibility value to the water compressibility value ($5e-6$ 1/psi) and decreasing the permeability value to the endpoint relative permeability to water (22.5 md). In this case, 0-D lumped model fits the reservoir behavior perfectly well. It should be noted that this

perfect match can't be considered unless the ripples that occur at the high frequencies are excluded from the evaluation.

Fig. 9 shows the reservoir transfer function of the most compressible reservoir model. Water compressibility is set to $1e-5$ 1/psi and total compressibility to $3.2e-6$ 1/psi. In **Fig. 9a**, exact reservoir parameters that are applied to run the reservoir simulation are used to calculate three RC transfer functions. However, the analytical solution needed an adjustment to fit the reservoir behavior. Hence, in **Fig. 9b** RC coefficient is increased to $5.58e+0$ sec/m² by replacing the total compressibility factor with the water compressibility factor and decreasing the permeability value down to 26md, as performed in the other two cases. Surprisingly, except for the ripples in high frequencies, lumped 0-D RC model is the one that matches the reservoir behavior.

As a result of the application in dry gas and water production, the lumped 0-D model approximated the fluid flow only in all reservoir models unlike it did in dead oil and water production case. The results are summarized in **Table 4**. This table points out which RC transfer function matched the reservoir behavior and shows if modifications on RC coefficients are applied. Once the RC coefficient is changed, due to the analogy between RC network and reservoir, diffusivity coefficient is also changed and represented as the estimated value as well as the estimated values for ϕ/k as displayed in the last column.

5.4.3 Dissolved Gas Production Around Wellbore

The effect of dissolved gas production on reservoir transfer functions is investigated with this application. Standard reservoir geometry and the injection rates reduced by a factor of 10 are simulated given the reservoir parameters in **Table 5** and relative permeability curves in **Fig. 10**. This case includes a sensitivity analysis that aims to indicate different varieties of oil and water compressibility factors. Basically, the water compressibility factors are applied when oil compressibility factor is set to $1e-6$ 1/psi. The oil compressibility factors are applied when water compressibility factor is set to $1e-6$ 1/psi (**Table 5**). In total, 6 simulation models are simulated under the conditions stated in **Table 6**.

Water breakthrough occurs around 345 day. Oil and dissolved gas production is performed up until breakthrough. After that day, water production dominates the total fluids production. Although free gas production is not included in the application, dissolved gas production around the wellbore is available at very small values from the gas saturation maps (not shown).

The effect of dissolved gas production is presented in terms of reservoir transfer functions in **Fig. 11**. The functions belong to different runs when oil and water compressibility factors are set to different values. Mainly, the runs are divided into two parts (**Table 6**). These are:

- *Part 1:* c_o is equal to $1e-6$ 1/psi. c_w is changed to $1e-6$, $5e-6$, $1e-6$ 1/psi.
- *Part 2:* c_w is equal to $1e-6$ 1/psi. c_o is changed to $1e-6$, $5e-6$, $1e-5$, $5e-5$ 1/psi.

Variations in attenuation of each simulation model exist due to the differences in total compressibility factors and the heterogeneity of the systems due to the dissolved gas production. The most compressible case is when oil compressibility is set to $5e-5$ 1/psi. Ripples at the stopband occur due to the strong filtering process in the reservoir at high frequency components. The least compressible system is when both oil and water compressibility values are set to $1e-6$ 1/psi.

The objective is to understand if dissolved gas production masks the spectrum where the reservoir transfer functions are presented. Obviously, dissolved gas production does not mask the main signal due to the useful presentation of the main signal, which consists of 30 frequencies. The heterogeneity of the system can be quantified only by the *RC* coefficient of the *RC* transfer function that fits the particular reservoir transfer function. As experienced from spectral analysis so far, higher the *RC* coefficient, more heterogeneous the system is.

Comparisons of the reservoir transfer functions with the correspondent *RC* transfer function are displayed in the following graphs in **Figs. 12-14**. As performed in previous applications, three *RC* transfer functions, which are calculated with the exact diffusivity parameters, are compared with the reservoir transfer function. If none of three *RC* models fits the reservoir transfer function, *RC* coefficient is adjusted to fit the reservoir behavior. Then, the adjusted *RC* coefficient is assigned to the diffusivity coefficient to compute the estimated values of interwell connectivity information, which is ϕ/k .

In **Fig. 12**, the least compressible systems with a total compressibility factor of $1.7e-6$ 1/psi are presented. In **Fig. 12a**, three *RC* transfer functions that don't match the reservoir behavior under current reservoir conditions with an *RC* of $2.47e-1$ sec/m² are shown. In **Fig. 12b**, reservoir transfer functions are shown to match with the lumped 0-D *RC* transfer function when *RC* is adjusted to $8.99e-1$ sec/m².

In **Fig. 13**, reservoir transfer functions with the same total compressibility factor of $3.1e-6$ 1/psi are presented. In **Fig. 13a**, three *RC* transfer functions that don't match the reservoir behavior under current reservoir conditions with an *RC* of $4.5e-1$ sec/m² are shown. In **Fig. 13b** is displayed to show that the best possible *RC* solution, which is lumped model, does not approximate these two reservoir transfer functions for even two different *RC* values.

In **Fig. 14**, two very compressible systems with the same total compressibility factor of $4.85e-6$ 1/psi are presented. In **Fig. 14a**, three *RC* transfer functions that don't match the reservoir behavior under current reservoir conditions with an *RC* of $7.03e-1$ sec/m² are shown. In **Fig. 14b**, there is also a poor fit for an *RC* value of $3.14e+0$ sec/m².

Figs. 15 present the most compressible system applied in this case. It is the most heterogeneous case of all applications and cases applied so far. It is already experienced that reservoir transfer functions represent heterogeneity by the degree of attenuation in high frequencies. In this case, stopband also exists by forming ripples and making it hard to fit an *RC* transfer function. As stated earlier, ripples of a stopband are not included in the quantitative analysis. In **Fig. 15a**, analytical solutions calculated by the exact *RC* value, which is imposed on the reservoir model, are compared with the reservoir transfer function. Although solutions are very close to the reservoir model, they are not perfect. Then, *RC* coefficient is adjusted to obtain a better match in **Fig 15b**, however it is not successful, either.

Finally, the results of the dissolved gas production around wellbore indicates that except for the least compressible system, none of the models fit the reservoir transfer function. This implies that the *RC* and diffusivity coefficients can not be quantified accurately when it comes to more complicated reservoir models. **Table 7** summarizes the results obtained from this application displaying the estimated diffusivity coefficient from the analogy and the interwell connectivity information in the last column.

5.5 Conclusions

1. Applications are performed only on single phase (water only) production and two phase production under various total compressibility factors including the application where dissolved gas evolution around wellbore.

2. Single phase production results applied on the reservoir models where total compressibility is $1\text{e-}6$, $5\text{e-}6$ and $1\text{e-}5$ 1/psi are successfully matched with the lumped RC transfer function for the following *RC* coefficients: $1.45\text{e-}1$, $7.25\text{e-}1$ and $1.45\text{e+}0$ sec/m^2 . Since no modification is applied on the coefficient of the RC transfer functions, estimated diffusivity coefficient is equal to the original diffusivity coefficient.
3. When total compressibility is increased to $5\text{e-}5$ 1/psi in single phase production, a stopband, besides a passband and a transition band, appears along with some ripples at high frequency values. The reservoir behavior can not be identified by the lumped RC model in this case. 2-D RC model is more descriptive when *RC* coefficient increases up to 7.25 sec/m^2 . No modification is performed on *RC* coefficient.
4. In two phase dead oil and water production, only accurate result is obtained from the least compressible reservoir model when water compressibility is set to $1\text{e-}6$ 1/psi. Lumped 0-D RC model fits perfectly to the reservoir transfer function when *RC* coefficient is modified due to the relative permeability to water and the water compressibility factor at a value of $5.8\text{e-}1$ sec/m^2 . In more compressible systems when water compressibility is set to $1\text{e-}5$ and $5\text{e-}6$ 1/psi, 2-D RC model captures the reservoir transfer function better; however the results are as accurate as the one in the least compressible reservoir model.
5. In two phase dry gas and water production, most reliable analogy is obtained again from the least compressible reservoir model when total compressibility factor is $1.4\text{e-}6$ 1/psi. 0-D lumped RC model captures the reservoir transfer function perfectly well at an *RC* value of $1.16\text{e+}0$ sec/m^2 . The difference of gas production in comparison to the dead oil production is apparently the amount of ripples appear in high frequencies when high compressibility values are applied. The effect of stopband and the reservoir filtering process is discerned much more in this case. Unlike the dead oil production case, very good matches in passband and transition bands are yielded with 0-D lumped models in all cases.
6. In the application, where dissolved gas production around wellbore is modeled, perfect analogy between RC models and reservoir transfer functions are obtained when total compressibility factor is set to $1.7\text{e-}6$ 1/psi. Lumped 0-D RC model captures the reservoir transfer function after a modification is done on RC value. It is increased from $2.47\text{e-}1$ to $8.99\text{e-}1$ sec/m^2 . Unfortunately, transfer functions do not work out at all in this application except for the least compressible system. RC transfer functions are unable to identify the exact transition band that of reservoir transfer functions.

5.6 Tables and Figures

Table 1—Reservoir parameters used for water only reservoir simulation.

Production phase	water
ϕ	0.1 d.less
k_x, k_y	100 md
k_z	1 md
μ_w	1 cp
B_w	1.01 RB/STB
C_w	5.00E-05 1/psi
	1.00E-05 1/psi
	5.00E-06 1/psi
	1.00E-06 1/psi
BHP @producer	250 psi
Initial pressure	1470 psi
Duration	4096 days

Table 2—Interwell connectivity estimates in single phase production case.

Total Compressibility 1/psi	Diffusion Coefficient s/m ²	RC Model matched	RC Modification	RC Coefficient s/m ²	Estimated Diffusion Coefficient s/m ²	Given ct. μ cp/psi	Estimated ϕ/k 1/md
1.00E-06	1.45E-01	0-D	-	1.45E-01	1.45E-01	1.00E-06	1.00E-03
5.00E-06	7.25E-01	0-D	-	7.25E-01	7.25E-01	5.00E-06	1.00E-03
1.00E-05	1.45E+00	0-D	-	1.45E+00	1.45E+00	1.00E-05	1.00E-03
5.00E-05	7.25E+00	2-D	-	7.25E+00	7.25E+00	5.00E-05	1.00E-03

Table 3—Reservoir parameters used for dry gas and water production.

Production phase	water, dry gas
ϕ	0.1 d.less
k_x, k_y	100 md
k_z	1 md
μ_w	1 cp
B_w	1.01 RB/STB
C_w	1.00E-05 1/psi
	5.00E-06 1/psi
	1.00E-06 1/psi
μ_g	0.01 cp
B_g	0.96 RCF/SCF
C_g	1.00E-05 1/psi
C_f	1.00E-08 1/psi
S_{gir}	0.12 fraction
S_{wc}	0.2 fraction
BHP @producer	250 psi
Initial pressure	1470 psi
Duration	4096 days

Table 4—Interwell connectivity inferred from dry gas and water production case.

Water Compressibility 1/psi	Total Compressibility 1/psi	Diffusion Coefficient s/m ²	RC Model matched	Modification	RC Coefficient s/m ²	Estimated Diffusion Coefficient s/m ²	Given ct.μ cp/psi	Estimated φ/k 1/md
1.00E-06	1.40E-06	2.03E-01	0-D	yes	1.16E+00	1.16E+00	1.40E-06	5.71E-03
5.00E-06	2.20E-06	3.19E-01	0-D	yes	3.15E+00	3.15E+00	2.20E-06	9.87E-03
1.00E-05	3.20E-06	4.64E-01	0-D	yes	5.58E+00	5.58E+00	3.20E-06	1.20E-02

Table 5—Reservoir parameters used in simulated reservoir model.

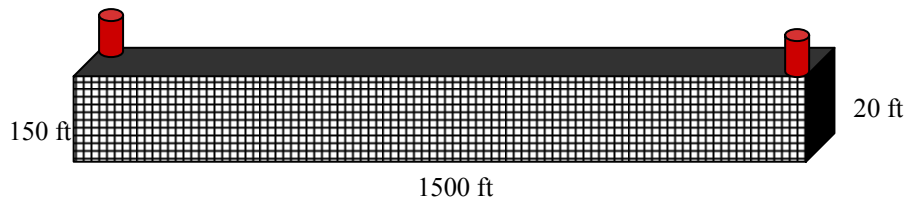
	Simulation Run #	Oil Compressibility 1/psi	Water Compressibility 1/psi	Total Compressibility 1/psi
Part 1	1	1.00E-06	1.00E-06	1.70E-06
	2	1.00E-06	5.00E-06	3.10E-06
	3	1.00E-06	1.00E-05	4.85E-06
Part 2	4	5.00E-06	1.00E-06	3.10E-06
	5	1.00E-05	1.00E-06	4.85E-06
	6	5.00E-05	1.00E-06	1.89E-05

Table 6—Reservoir parameters used in simulated reservoir model.

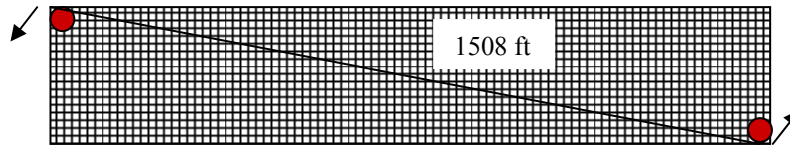
Production phase	water, live oil, dissolved gas
φ	0.1 fraction
k _x , k _y	100 md
k _z	1 md
μ _w	1 cp
B _w	1.01 RB/STB
c _w (when c _o undersaturated=1e-6 1/psi)	1.00E-06 1/psi
	1.00E-05 1/psi
	5.00E-06 1/psi
μ _o undersaturated	0.94 cp
c _o undersaturated (when c _w =1e-6 1/psi)	1.00E-06 1/psi
	5.00E-06 1/psi
	1.00E-05 1/psi
	5.00E-05 1/psi
c _f	1.00E-06 1/psi
S _{wc}	0.35 fraction
S _{or}	0.35 fraction
BHP @producer	3500 psi
Initial pressure	4100 psi
Saturation pressure	4000 psi
Duration	4096 days

Table 7—Interwell connectivity inferred from dissolved gas production case.

Sim Run #	Total Compressibility 1/psi	Diffusion Coefficient s/m ²	RC Model matched	Modification	RC Coefficient s/m ²	Estimated Diffusion Coefficient s/m ²	Given ct.μ cp/psi	Estimated φ/k 1/md
1	1.70E-06	2.47E-01	0-D	yes	8.99E-01	8.99E-01	1.70E-06	3.65E-03
2	3.10E-06	4.50E-01	-	-	-	-	-	-
3	4.85E-06	7.03E-01	-	-	-	-	-	-
4	3.10E-06	4.50E-01	-	-	-	-	-	-
5	4.85E-06	7.03E-01	-	-	-	-	-	-
6	1.89E-05	2.73E+00	-	-	-	-	-	-



(a) – cross sectional view



(b) – top view

Figure 1—Reservoir model used in numerical simulation.

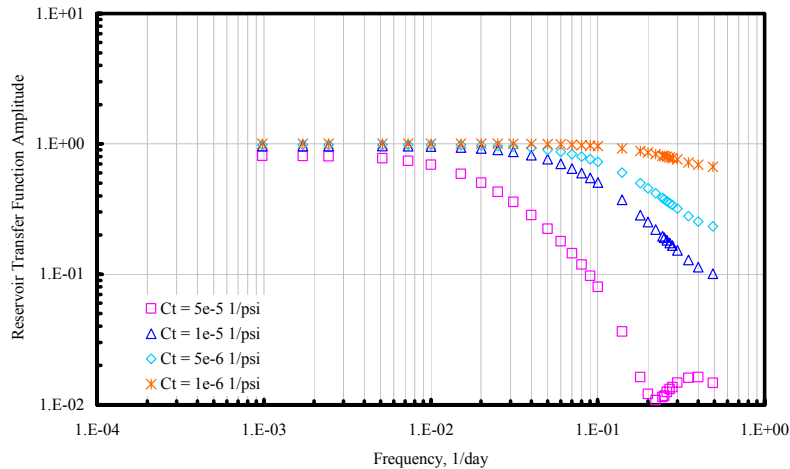


Figure 2—Reservoir transfer functions for single phase production for various total compressibility values.

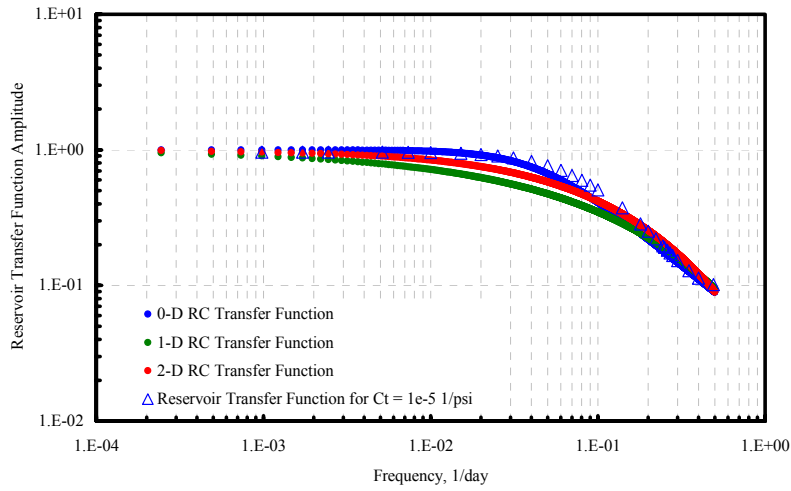


Figure 3—Comparison between three RC transfer functions ($RC=1.45e+0 \text{ s/m}^2$) and the reservoir transfer function for $c_t=1e-5 \text{ 1/psi}$.

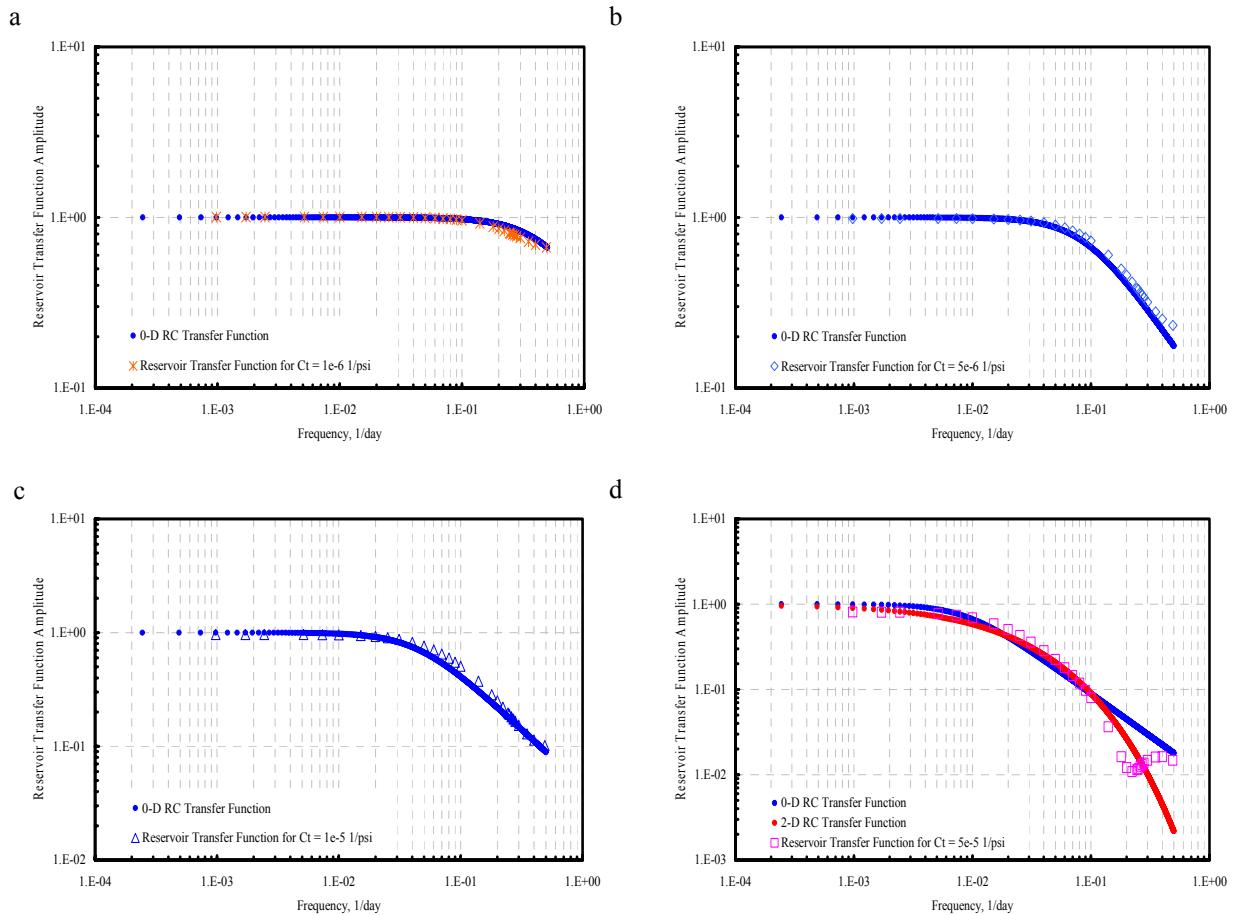


Figure 4—Comparison between lumped 0-D RC transfer function and the reservoir transfer functions for (a) $c_t=1e-6 \text{ 1/psi}$ (b) $c_t=5e-6 \text{ 1/psi}$ (c) $c_t=1e-5 \text{ 1/psi}$ (d) $c_t=5e-5 \text{ 1/psi}$.

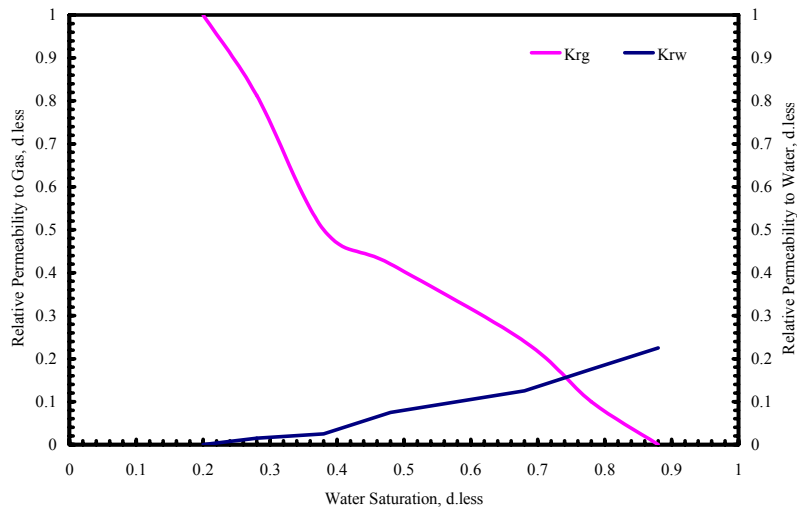


Figure 5—Relative permeability curves used in dry gas and water production.

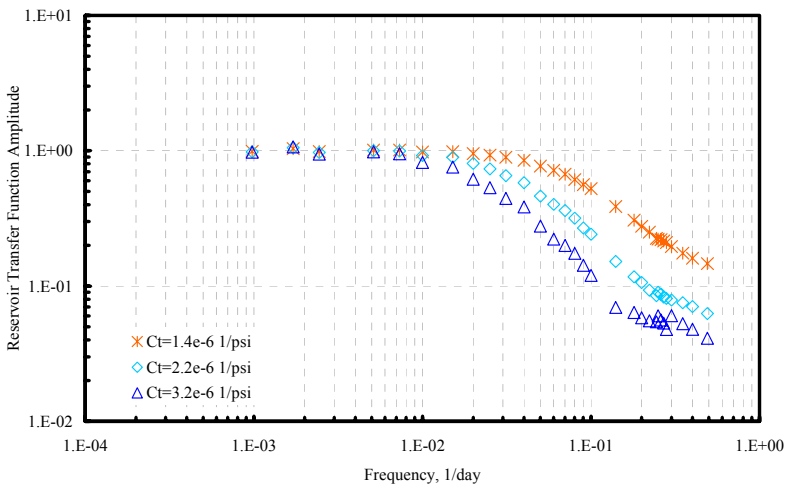


Figure 6— Reservoir transfer functions for dry gas and water production under various compressibility values.

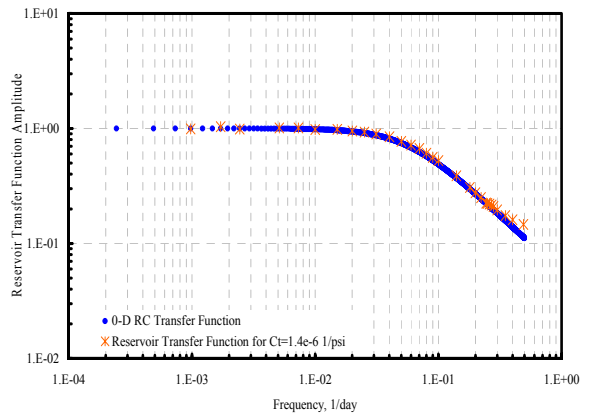
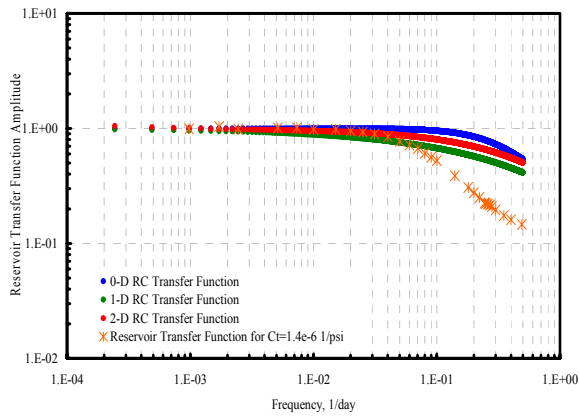


Figure 7— Comparison between three RC transfer functions and the reservoir transfer function for $c_t=1.4e-6$ 1/psi when (a) $RC=2.03e-1$ s/m² (b) $RC=1.16e+0$ s/m².

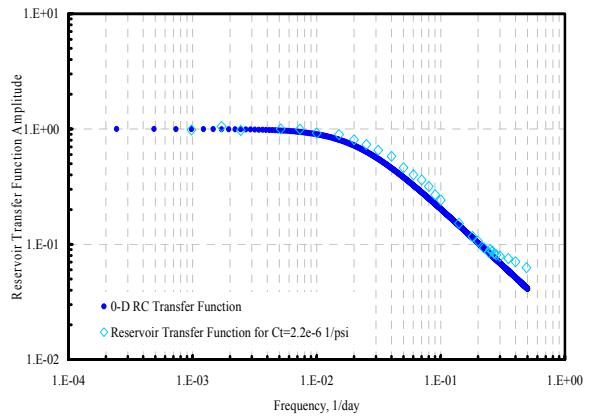
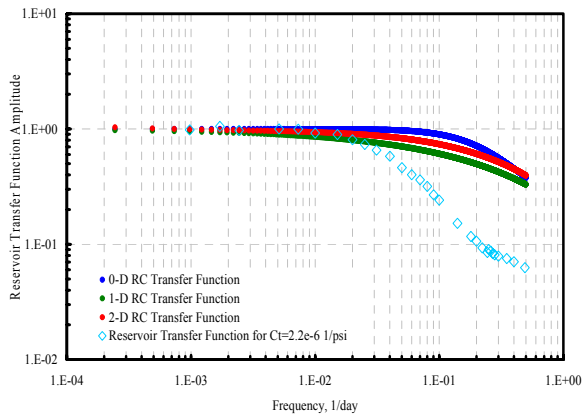


Figure 8— Comparison between the reservoir transfer function for $c_t=2.2e-6$ 1/psi and 0-D lumped RC transfer function when (a) $RC=3.19e-1$ s/m² (b) $RC=3.15e+0$ s/m².

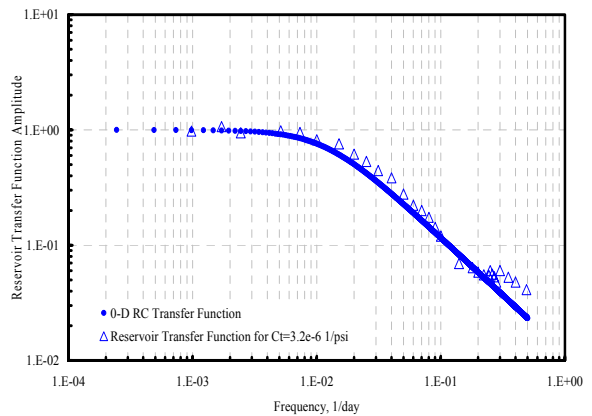
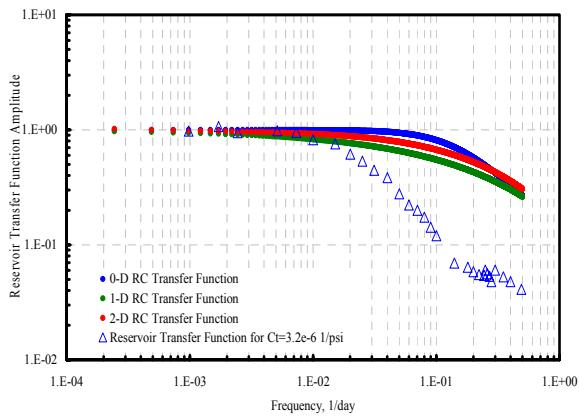


Figure 9— Comparison between the reservoir transfer function for $c_t=3.2e-6$ 1/psi and 0-D lumped RC transfer function when (a) $RC=4.64e-1$ s/m² (b) $RC=5.58e+0$ s/m².

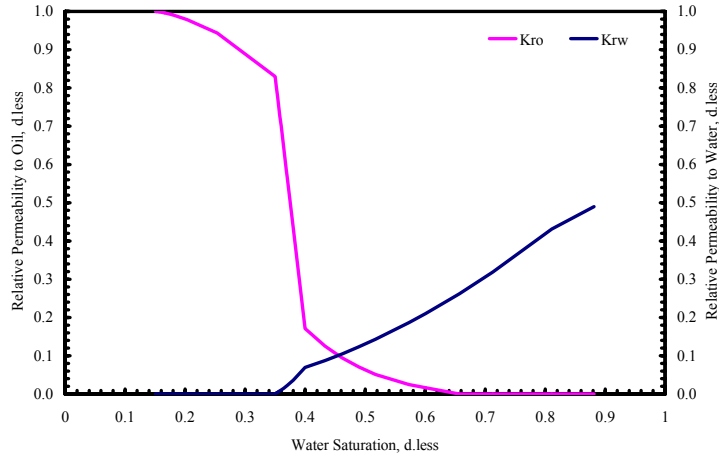


Figure 10—Relative permeability curves used in reservoir simulation.

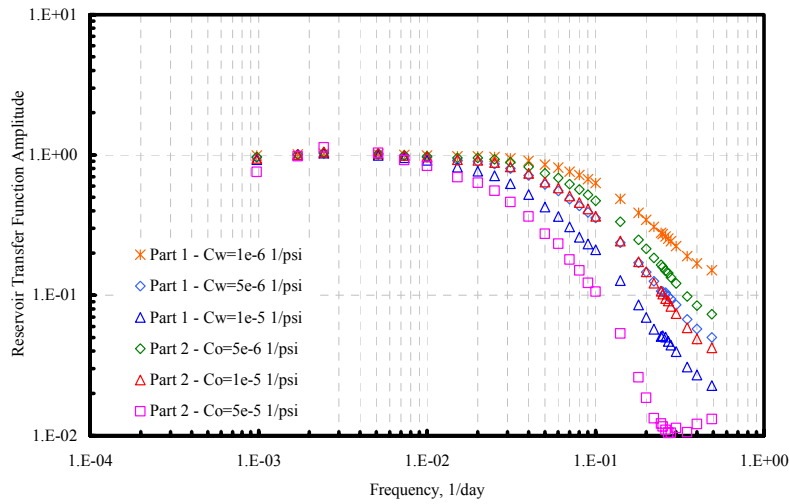


Figure 11— Reservoir transfer functions produced from live oil and water production simulation models for various compressibility values.

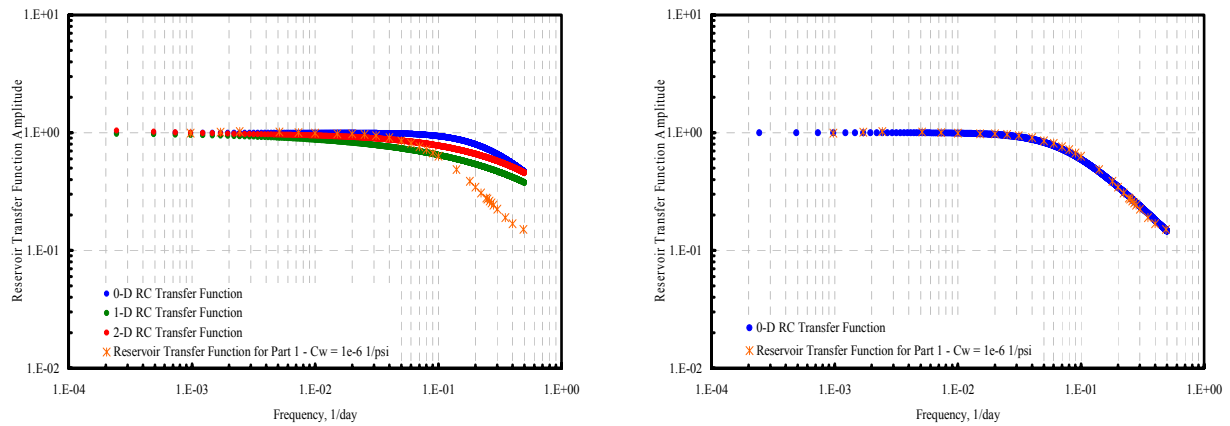


Figure 12— Comparison between the reservoir transfer function for $c_t=1.7e-6$ 1/psi and the RC transfer functions when (a) $RC=2.47e-1$ s/m² (b) $RC=8.99e-1$ s/m².

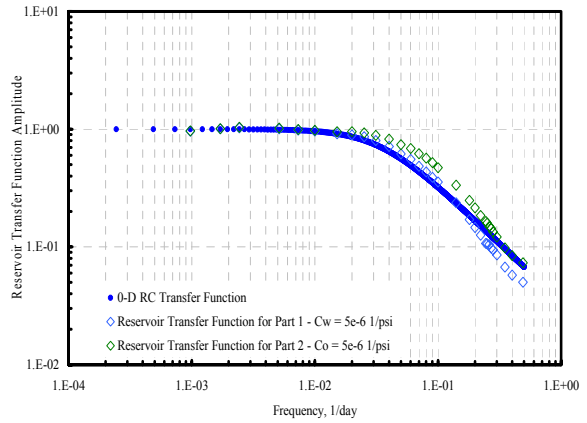
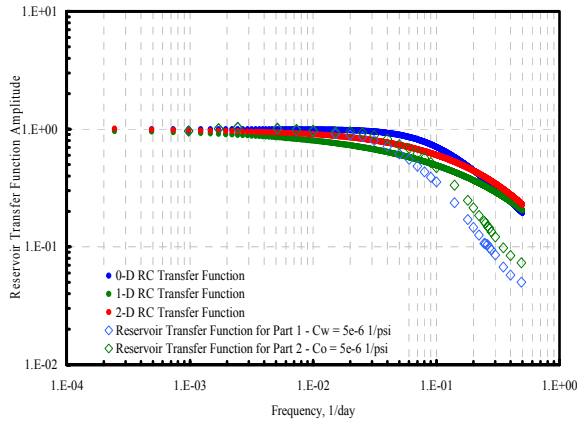


Figure 13— Comparison between the reservoir transfer function for $c_t=3.1e-6$ 1/psi and the RC transfer functions when (a) $RC=4.5e-1$ s/m² (b) $RC=1.92e+0$ s/m².

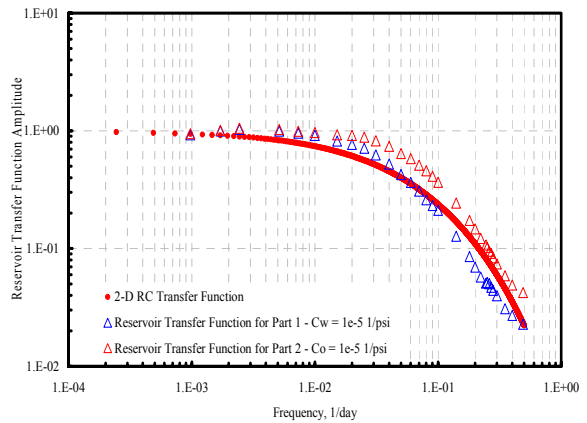
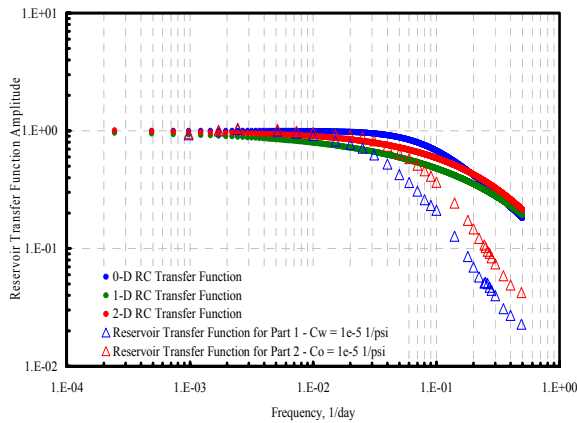


Figure 14— Comparison between the reservoir transfer function for $c_t=4.85e-6$ 1/psi and the RC transfer functions when (a) $RC=7.03e-1$ s/m² (b) $RC=3.14e+0$ s/m².

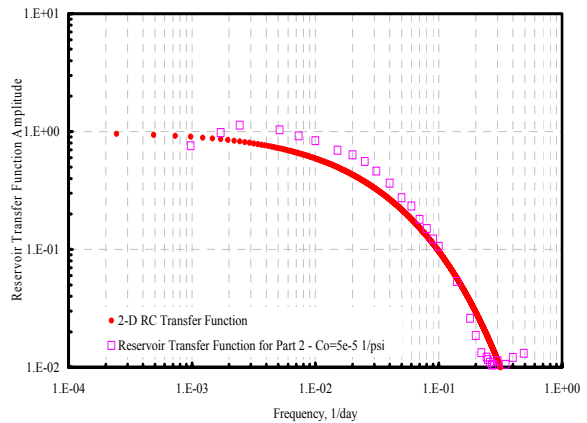
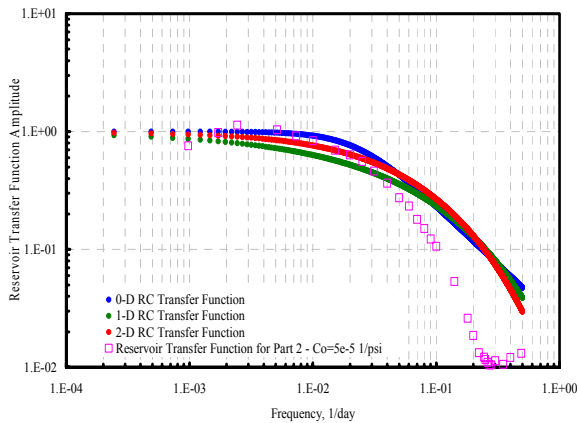


Figure 15— Comparison between the reservoir transfer function for $c_t=1.89e-5$ 1/psi and the RC transfer functions when (a) $RC = 2.74e+0$ s/m² (b) $RC = 6.89e+0$ s/m².

CONCLUSIONS

Building on the work of Albertoni and Lake (2003), an improved method to predict interwell connectivity has been developed. In testing with simulated and field data, the capacitance model (CM) outperformed the earlier version in several respects, including ability to incorporate bottom hole pressure data, when available, tolerance to injection well shut-in and reservoirs with large diffusivity, and fields still having a component of primary production. The CM represents a significant improvement to existing methods to estimate interwell connectivity in waterflooded reservoirs.

The CM assigns two parameters per well pair. While the value of each parameter can be individually interpreted for interwell connectivity, we have shown that there can be benefits to analyzing the parameters together. The analysis helps to identify high-connectivity regions and flow barriers in geologically complex systems.

By developing the CM, this project has successfully provided a tool for management of waterflooding reservoirs. In a proof-of-concept test, we showed that the CM can be used in to optimize well rates satisfying various constraints. Thus, operators can obtain guidance on the injection rates most suited to economic, water handling, or other conditions.

Interwell connectivity evaluation methods have always suffered problems with distinguishing reservoir influences from human interventions. Since the CM contains a specific term for bottom-hole pressure effects, we have explored ways to eliminate the influences of workovers and well treatments on the estimation process and have identified some promising methods. These methods are fallible, particularly in cases where the well has undergone numerous treatments, and will need further study to develop a robust estimator.

As an alternative to time domain analysis, such as used by the CM, we also investigated the use of frequency domain methods to estimate interwell connectivity. Our findings suggest that more sophisticated methods than the ones used here will be needed if spectral analysis is to replace the time-based approaches.

REFERENCES

- Albertoni, A. and Lake, L.W., 2003. Inferring connectivity only from well-rate fluctuations in waterfloods, *SPE Reservoir Evaluation and Engineering Journal*, 6, 6-16.
- Albertoni, A., "Inferring Interwell Connectivity From Well-Rate Fluctuations in Waterfloods," M.S. Thesis, The University of Texas at Austin, 2002.
- Araque-Martinez, A.N., "Estimation of Autocorrelation and Its Use in Sweep Efficiency Calculation," M.S. Thesis, The University of Texas at Austin, 1993.
- Barnes, D.A., Humphrey, K. and Mullenberg, L., 1990. A production optimization system for western Prudhoe Bay Field, Alaska, SPE 20653 presented at the 65th Annual Technical Conference and Exhibition held in New Orleans, Louisiana, U.S.A., 23-26 September.
- Barros-Griffiths, I., "The Extreme Spearman Rank Correlation Coefficient in the Characterization of the North Buck Draw field," M.S. Thesis, The University of Texas at Austin, 1998.
- Belsley, D., *Conditioning Diagnostics: Collinearity and Weak Data in Regression*, Wiley, New York, 1991.
- Bruce, W. A., "An Electrical Devices for Analyzing Oil Reservoir Behavior," *Trans, AIME*, p. 113-124, 1943.
- Buitrago, S., Rodriguez, E. and Espin, D., 1996. Global optimization techniques in gas allocation for continuous flow gas lift systems, SPE 35616 presented at the Gas Technology Symposium held in Calgary, Alberta, Canada, 28 April-1 May.
- Burbank, D., "Early CO₂ Flood Experience at the South Wasson Clearfork Unit," SPE 24160, presented at the SPE/DOE Eighth Symposium on Enhanced Oil Recovery, Tulsa, Oklahoma, 22-24 April, 1992.
- Cortez, O. D., and Corbett, P. M., "Time-Lapse Production Logging and the Concept of Flowing Units," SPE 94436, presented at the SPE Europec/EAGE Annual Conference held in Madrid, Spain, June 13-16, 2005.
- Craig, F. F., *The Reservoir Aspects of Waterflooding*, SPE Monograph Series, SPE, Richardson, Texas, 1971.
- Day, S., Griffin, T., and Martins, P., "Redevelopment and Management of the Magnus Field for Post-Plateau Production," SPE 49130, presented at the SPE Annual Technical Conference and Exhibition held in New Orleans, Louisiana, September 27-30, 1998.
- De Sant Anna Pizzaro, J.O.: "Estimating injectivity and lateral autocorrelation in heterogeneous media," PhD dissertation, U. of Texas at Austin, Austin, Texas (1998).
- Demiroren, N.: "Inferring Interwell Connectivity from Injection and Production Data Using Frequency Domain Analysis," M. S. Thesis, Texas A&M University, College Station (2007).
- Dutta-Roy K. and Kattapuram, J., 1997. A new approach to gas-lift allocation optimization, SPE 38333 presented at the SPE Western Regional Meeting held in Long Beach, California, U.S.A., 25-27 June.
- Edgar, T.F., Himmelblan, D.M. and Lasdon, L.S., 2001. *Optimization of chemical processes*, second edition, McGraw-Hill Co. Inc., New York.
- Everitt, W.L., and Anner, G. E.: *Communication Engineering*, third edition, McGraw Hill Inc., U.S.A. (1956).
- Fang, W.Y. and Lo, K.K., 1996. A generalized well-management scheme for reservoir simulation. *SPE Reservoir Engineering*, 11(2), 116-120.
- Gentil, P.H., 2005. The use of multilinear regression models in patterned waterfloods: physical meaning of the regression coefficients, M.S. Thesis, The University of Texas at Austin.

- Gunter, G. W., Finneran, J. M., Hartmann, D. J., and Miller, J. D., "Early Determination of Reservoir Flow Units Using an Integrated Petrophysical Method," SPE 38748, presented at the SPE Annual Technical Conference and Exhibition held in San Antonio, Texas, October 5-8, 1997.
- Harman, T.L. et.al.: *Advanced Engineering Mathematics with Matlab*, Brooks/Cole Inc., Pacific Grove, California (2000).
- Heffer, K.J., Fox, R.J., and McGill, C.A.: "Novel Techniques Show Links Between Reservoir Flow Directionality, Earth Stress, Fault Structure and Geomechanical Changes in Mature Waterfloods," paper SPE 30711 presented at the 1995 SPE Annual Technical Conference and Exhibition, Dallas, 22-25 October.
- Hocking R., "Development in Linear Regression Methodology," *Technometrics*, vol. 25, 219-230, 1983.
- Hoerl, A., and Kennard, R., "Ridge Regression: Application to Non-Orthogonal Problems," *Technometrics*, vol. 12, p 69-82, 1970b.
- Hoerl, A., and Kennard, R., "Ridge Regression: Biased Estimation for Non-Orthogonal Problems," *Technometrics*, vol. 12, p 55-63, 1970a.
- Hollaender F. et.al: "Harmonic Testing for Continuous Well and Reservoir Monitoring," paper SPE 77692 presented at the 2002 SPE Annual Technical Conference and Exhibition, San Antonio, Texas, 29 September -12 October.
- Ibragimov, A., Khalmanova, D., Valko, P., and Walton, J., "On a Mathematical Model of the Productivity Index of a Well from Reservoir Engineering," *Journal of Applied Mathematics*, Vol. 65, pp. 1952-1980, 2005.
- Jansen, F.E. and Kelkar, M.G.: "Application of Wavelets to Production Data in Describing Inter-Well Relationships," paper SPE 38876 presented at the 1997 SPE Annual Technical Conference and Exhibition, San Antonio, Texas, 5-8 October.
- Jensen, J. L., Lake, L.W., Corbett, P.W.M., and Goggin, D.J., *Statistics for Petroleum Engineers and Geoscientist*, Elsevier Science, Amsterdam, The Netherlands (2003).
- Jensen, J. L., Lake, L.W., Yousef, A.A., Gentil, P. and Demiroren, N.: "Interwell Connectivity and Diagnosis Using Correlation of Production and Injection Rate Data in Hydrocarbon Production," annual report, Contract No. DE-FC26-03NT15397, U.S. DOE, Washington, DC (August 2005).
- Jensen, J. L., Lake, L.W., Yousef, A.A., Gentil, P., Demiroren, N., and Kaviani, D.: "Interwell Connectivity and Diagnosis Using Correlation of Production and Injection Rate Data in Hydrocarbon Production," annual report, Contract No. DE-FC26-03NT15397, U.S. DOE, Washington, DC (August 2006).
- Johnson, C.R., et.al.: "Pulse-Testing: A New Method for Describing Reservoir Flow Properties Between Wells," paper SPE 1517 presented at 1966 SPE 41st Annual Fall Meeting, Dallas, Texas, 2-5 October.
- Kosmidis, V.D., Perkins, J.D. and Pistikopoulos, E.N., 2005. A mixed integer optimization formulation for the well scheduling problem on petroleum fields, *Computers and Chemical Engineering*, 29, 1523-1541.
- Kosmidis, V.D., Perkins, J.D., and Pistikopoulos, E.N., 2004. Optimization of well oil rate allocations in petroleum fields, *Industrial and Engineering Chemistry Research*, 43, 3513-3527.

- Kuo, C.H.: "Determination of Reservoir Properties from Sinusoidal and Multirate Flow Tests in One or More Wells," paper SPE 3265 presented at 1971 SPE 46th Annual Fall Meeting, New Orleans, Louisiana, 3-6 October.
- Lake, L. W., Enhanced Oil Recovery, Prentice-Hall, Inc., New York, pp. 195-196, 1989.
- Larsen, L., "General Productivity Models for Wells in Homogeneous and Layered Reservoirs," paper SPE 71613 presented at the SPE Annual Technical Conference and Exhibition, New Orleans, Louisiana, September 30-October 3, 2001.
- Lee, J. et.al.: Pressure Transient Testing, Textbook Series, SPE, Vol. 9, Richardson, Texas, (2003).
- Litvak, M.L., Clark, A.J., Fairchild, J.W., Fossum, M.P., MacDonald C.D. and Wood, A.R.O., 1997. Integration of Prudhoe Bay surface pipeline network and full field reservoir models, SPE 38885 presented at the SPE Annual Technical Conference and Exhibition held in San Antonio, Texas, U.S.A., 5-8 October.
- Marquardt, D. W., and Snee, R. D., "Ridge Regression in Practice," The American Statistician, vol. 29, p 3-19, 1975.
- Martinez, E.R., Moreno, W.J., Moreno, J.A. and Maggiolo, R., 1994. Application of genetic algorithm on the distribution of gas lift injection, SPE 26993 presented at the III Latin American/Caribbean Petroleum Engineering Conference held in Buenos Aires, Argentina, 27-29 April.
- Muskat, M.: Physical Principles of Oil Production, McGraw Hill Inc., U.S.A. (1949).
- Panda, M.N. and Chopra, A.K.: "An Integrated Approach to Estimate Well Interactions," paper SPE 39563 presented at the 1998 SPE India Oil and Gas Conference and Exhibition, New Delhi, 17-19 February.
- Raghavan, R., Well Test Analysis, Prentice-Hall, Englewood Cliffs, New Jersey, 1991.
- Refunjol, B.T., and Lake, L. W., "Reservoir Characterization Based on Tracer Response and Rank Analysis of Production and Injection Rates," paper presented at the Fourth International Reservoir Characterization Technical Conference, Houston, Texas, March 2-4, 1997.
- Refunjol, B.T.: "Reservoir characterization of North Buck Draw field based on tracer response and production/injection analysis," MS thesis, U. of Texas at Austin, Austin, Texas (1996).
- Rivera, N.: Reservoir characterization using wavelet transforms, PhD Dissertation, Texas A&M U., College Station, 2003.
- Rosa, A.J and Horne, R.N.: "Reservoir Description by Well-Test Analysis by Use of Cyclic Flow-Rate Variation," paper SPE 22698 presented at 1991 SPE Annual Technical Conference and Exhibition, Dallas, Texas, 6-9 October.
- Sabet, M. A., Well Test Analysis, Gulf Publishing Company, Houston, Texas (1991).
- Schmalz, J. P., and Rahme, H. S., "The Variation in Water Flood Performance with Variation in Permeability Profile," Producers Monthly, pp. 9-12, July, 1950.
- Sellers, R., and Hawkins, C., "Geology and Stratigraphic Aspects of the Buck Draw Field, Powder River Basin, Wyoming" Wyoming Geological Association 43rd Annual Field Conference Guidebook, pp. 97-110, 1992.
- Shook, G. M., "A Simple Fast Method of Estimating Fractured Reservoir Geometry from Tracer Tests," Transactions of the Geothermal Resources Council, Vol. 27, September 2003.
- Smith, Steven W.: The Scientist and Engineer's Guide to Digital Signal Processing, second edition, California Technical Publishing, California (1999).
- Snee R., "Development in Linear Regression Methodology," Technometrics, vol. 25, p 230-237, 1983.

- Soeriawinata, T. and Kelkar, M.: "Reservoir Management Using Production Data," paper SPE 52224 presented at the 1999 SPE MidContinent Operation Symposium, Oklahoma City, Oklahoma, 28-31 March.
- Stoitsits, R.F., Batesole, E.C., Champion J.H. and Park, D.H., 1992. Application of nonlinear adaptive modeling for rigorous representation of production facilities in reservoir simulation, In SPE 24898 presented at the 67th Annual Technical Conference and Exhibition held in Washington, D.C., U.S.A., 4-7 October.
- Walsh, M.P., and Lake, Larry W., A Generalized Approach to Primary Hydrocarbon Recovery, Elsevier Science, Amsterdam, The Netherlands (2003).
- Wang, P., Litvak, M.L. and Aziz, K., 2002a. Optimization of production operations in petroleum fields, SPE 77658 presented at the Annual Technical Conference and Exhibition held in San Antonio, Texas, U.S.A., 29 September-2 October.
- Wang, P., Litvak, M.L. and Aziz, K., 2002b. Optimization of production from mature fields, presented at the 17th World Petroleum Congress, Rio de Janeiro, Brazil, September 1-5.
- Yousef, A. A., Gentil, P., Jensen, J. L., and Lake, L. W., 2006b. A Capacitance Model to Infer Interwell Connectivity from Production and Injection Rate Fluctuations, SPE Reservoir Evaluation and Engineering Journal, 9, 630-646.
- Yousef, A. A., Lake, L.W. and Jensen J.L., 2006a. Analysis and Interpretation of Interwell Connectivity From Production and Injection Rate Fluctuations Using a Capacitance Model, paper SPE 99998 presented at the SPE/DOE Symposium on Improved Oil Recovery, Tulsa, Oklahoma, 22-26 April.
- Yousef, A.A., 2006. Investigating statistical techniques to infer interwell connectivity from production and injection rate fluctuations, PhD dissertation, The University of Texas at Austin.